Investigating B cell biology in CASPR2-antibody encephalitis

Dr Bo Sun
St. Cross College
University of Oxford

Thesis submitted for degree of

Doctor of Philosophy

March 2022

Abstract

CASPR2-antibody encephalitis is an increasingly recognised cause of autoimmune encephalitis and part of a growing body of neuroglial antibody-mediated diseases. At its core, B cells are responsible for all autoantibody production; however, their origin and the pathogenicity of their secreted CASPR2 autoantibodies remains poorly understood. By applying bulk and single-cell cultures, along with molecular approaches, I sought to characterise the underling B cell immunobiology of CASPR2-antibody encephalitis.

In a series of B cell culture experiments, CASPR2-antibody encephalitis patients were found to harbour CASPR2-reactive memory B cells, whereas healthy donors did not. Unexpectedly, both patients and healthy donors possessed circulating naïve B cells with CASPR2-reactivity. Further characterisation of naïve and memory B cell B cell receptor (BCR) reactivities, using recombinant monoclonal antibodies (mAbs), revealed that naïve B cell-derived mAbs could not bind as monovalent F(ab) fragments, but memory B cell-derived mAbs and their unmutated common ancestors (UCAs) could. Together, these observations support the contribution of peripheral B cell tolerance failure in the pathogenesis of CASPR2-antibody encephalitis.

Investigating the functional properties of mAbs generated from CASPR2-reactive memory B cells, reproduced epitope immunodominance of the Discoidin domain and confirmed their ability to internalise CASPR2. Additionally, for the first time, Laminin G-like 3 domain targeting mAbs are described and display favourable binding kinetics and modulated CASPR2 function *in vitro.* Interestingly, *in vitro* neuronal assays identify two distinct modes of antibody-mediated CASPR2 modulation; downregulation vs. upregulation of CASPR2 expression. Correspondingly, AMPA receptors may be downregulated and upregulated, respectively. However, both antibody-mediated mechanisms were capable of modulating neuronal synaptic signalling *in vitro,* supporting their net disruption of CASPR2 functionality. Finally, the identification of differential binding to rodent CASPR2 raises important questions and warrants future research to address their utility in current diagnostic assays and the informed use of murine models.

Acknowledgements

The work presented within this thesis could not have been possible without the support of many exceptional individuals. I would first like to extend my absolute thanks and gratitude to my supervisors Associate Professor Sarosh Irani, Dr Rachael Bashford-Rogers and Dr Patrick Waters. Their unwavering support and encouragement have helped me through the tribulations of research, and their enthusiasm for intellectual discussion have helped ground the triumphs. My sincerest thanks also go to my post-doctoral colleagues, Dr Mateusz Makuch and Dr Deniz Akdeniz, for their friendship, invaluable day-to-day guidance and support in the laboratory. A special mention must also be made to Dr Mark Woodhall, whose unconditional help maintaining cell lines, has helped rescue many experiments during the COVID19 pandemic.

I extend my gratitude to all members of the Oxford Autoimmune Neurology Group, the Bashford-Rogers group and our collaborators; their respective contributions are recognised at the end of each chapter. Additionally, I would like to express my appreciation to the COvid-19 Multi-omics Blood Atlas (COMBAT) consortium for the opportunity to contribute to an invaluable body of research during the COVID19 pandemic. A special thanks also goes to specific members within the consortium, Dr Fabiola Curion, Dr Kathrin Jansen and Dr Lucy Garner, for the rich and informative discussions that have aided my development in bioinformatics.

All of this work would not have been possible without the financial support of the Association of British Neurologist Clinical Research Training Fellowship and the Patrick Berthoud Charitable Trust. Nor would it have been possible without the generosity of the patients, to whom I extend a special thanks.

On a personal level, I want to acknowledge the unconditional love and support provided to me by my family and in particular, my wife Lucy, whose kindness, strength and resilience, I aspire to. Lastly, but not least, I thank my children, Millie and Milo, whose smiles lift me up even in my lowest lows.

Table of Contents

CHAPTER 1 INTRODUCTION 8

1.3 B CELL IMMUNOBIOLOGY 8
1.3.1 ANTIBODIES 8
1.3.2 ANTIBODY ISOTYPES 9
1.3.3 B CELL DEVELOPMENT 14
1.3.4 B CELL TOLERANCE 15
1.3.5 B CELLS IN THE ADAPTIVE IMMUNE RESPONSE 17
1.4.2 B CELL TOLERANCE IN NSAB-MEDIATED DISEASES 25
1.5 CASPR2 AUTOANTIBODY ENCEPHALITIS 27
1.6.1 IS B CELL TOLERANCE IMPAIRED IN CASPR2-ANTIBODY ENCEPHALITIS? 40
1.6.2 IS AUTOANTIBODY IMMUNODOMINANCE OF THE N-TERMINAL DOMAINS REPRODUCIBLE AT A SINGLE-B CELL LEVEL? 40
1.6.3 HOW DO CASPR2-SPECIFIC MABS FUNCTIONALLY MODULATE CASPR2 PROTEIN? 40

CHAPTER 2 THE B CELL RECEPTOR LANDSCAPE IN CASPR2-ANTIBODY ENCEPHALITIS 41

2.1 INTRODUCTION 41
2.2 HYPOTHESIS 44
2.2.1 CASPR2-REACTIVE B CELLS ARE EXCLUSIVE TO PATIENTS, AND BREAK BOTH PRE AND POST GERMINAL CENTRE TOLERANCE CHECKPOINTS. 44
2.2.2 STUDYING NUCLEOTIDE SEQUENCES OF CASPR2-REACTIVE MEMORY B CELL-DERIVED BCRS WILL REVEAL EVIDENCE OF SOMATIC HYPERMUTATION, AS A PROXY OF GERMINAL CENTRE SELECTION. 44
2.3 METHODS 44
2.3.1 STUDY APPROVAL, SUBJECTS AND SPECIMENS 44
2.3.2 LIVE CELL-BASED ASSAY 45
2.3.3 CELL LABELLING AND FLUORESCENCE ACTIVATED CELL SORTING 45
2.3.4 CELL CULTURE 46
2.3.5 DETERMINATION OF TOTAL AND CASPR2-REACTIVE IMMUNOGLOBULINS 47
2.3.6 CDNA SYNTHESIS AND AMPLIFICATION OF VH AND VL SEQUENCES 48
2.3.7 IMMUNOGLOBULIN SEQUENCE ANNOTATION 48
2.3.8 CLONAL ASSIGNMENT 49
2.3.9 STATISTICAL ANALYSIS AND VISUALISATION 50
2.3.10 CLONING 50
2.3.11 RECOMBINANT EXPRESSION OF MONOCLONAL ANTIBODIES 51
2.3.12 ANTIBODY PURIFICATION 52

2.4 Results **52**
2.4.1 Bulk culture of naïve and memory B cells in CASPR2 patients and healthy donors 52
2.4.2 *Ex vivo* frequency of CASPR2-reactive B cells within naïve and memory compartments. 55
2.4.3 An optimised clonal assignment 58
2.4.4 Clonality and variable domain features of CASPR2-reactive BCRs 61
2.5 Discussion **66**
2.6 Conclusion **69**
2.7 Acknowledgements **70**

CHAPTER 3, BINDING PROPERTIES OF CASPR2-SPECIFIC MONOCLONAL ANTIBODIES **71**

3.1 Introduction **71**
3.2.1 Patient-derived CASPR2-reactive mAbs recapitulate epitope dominance observed in studies of patient sera 73
3.2.2 CASPR2-reactive mAbs binding is dependent on tertiary structure and correct glycosylation. 73
3.2.3 Murine CASPR2 will not recapitulate CASPR2-reactive mAb binding to human CASPR2. 73
3.3 Methods **73**
3.3.1 mAb cloning and expression 73
3.3.2 F(ab) fragment generation 73
3.3.3 CASPR2-CASPR4 domain swaps 74
3.3.4 Surface quantification of protein expression 75
3.3.5 Protein expression and purification 75
3.3.6 De-glycosylation and denaturation of CASPR2-ECD 76
3.3.7 Indirect ELISA 76
3.3.8 Immunohistochemistry staining 77
3.3.9 Neuronal cultures 78
3.3.10 Surface plasmon resonance 78
3.3.11 Epitope binning 79
3.3.12 Mouse CASPR2 cloning 80
3.4 Results **80**
3.4.1 The influence of valency on CASPR2 binding 80
3.4.2 The epitope landscape of CASPR2-reactive B cells 83
3.4.3 The influence of CASPR2 conformation and glycosylation on mAb binding 90
3.4.4 Tissue detection of CASPR2 protein 92
3.4.5 Characterising affinities 95

3.4.6 mAb binding across species 97
3.5 Discussion 100
3.6 Conclusion 104
3.7 Acknowledgements 104

CHAPTER 4 ASSESSING MECHANISMS OF ANTIBODY-MEDIATED DISRUPTION OF CASPR2 PROTEIN 106

4.1 Introduction 106
4.2 Hypothesis 108
4.2.1 Patient derived mAbs block CASPR2 CNTN2 ligand interaction 108
4.2.2 Patient derived mAbs internalise surface CASPR2 108
4.2.3 Patient derived mAbs disrupt neuronal homeostasis 108
4.3 Methods 108
4.3.1 Contactin-2 and Contactin-1 constructs 108
4.3.2 Protein expression and purification 109
4.3.3 F(ab) fragment generation 110
4.3.4 Direct pHrodo™ conjugation of mAbs 110
4.3.5 Indirect labelling of mAbs with Zenon™ pHrodo™ 111
4.3.6 pHrodo™ internalisation live cell-based assay 111
4.3.7 pHrodo™ image quantification 112
4.3.8 Bispecific mAb expression vectors 112
4.3.9 Expression and purification of bispecific antibody 113
4.3.10 Cortical neuron culture- Coimbra University 114
4.4 Results 115
4.4.1 Validating CASPR2 interactions with CNTN2 and CNTN1 115
4.4.2 Autoantibody-induced internalisation of CASPR2 118
4.4.3 Dynamin dependent CASPR2 autoantibody-mediated internalisation 122
4.4.4 Internalisation capacity of monovalent mAb species 123
4.4.5 Autoantibody internalisation in primary neuronal cultures 126
4.4.6 Data from Carvalho group, generated by Dr. Dominique Fernandes PhD 129
4.5. Discussion 132
4.6 Conclusion 134
4.7 Acknowledgements 135

CHAPTER 5 CHARACTERISING UNMUTATED COMMON ANCESTORS OF CASPR2 MEMORY B CELLS 136

5.1 Introduction 136
5.2 Hypothesis 139

5.2.1 CASPR2-reactive memory B cell-derived mAbs bivalently bind CASPR2 as germline UCAs, inferring that they derive from high affinity naïve B cell precursors. 139
5.2.2 UCAs of CASPR2-reactive memory B cells have pathogenic potential *in vitro*. 139
5.3 Methods 139
5.3.1 UCA reversion method 139
5.3.2 Domain specificity characterisation 140
5.3.3 Immunohistochemistry staining 140
5.3.4 Neuronal culture 141
5.3.5 Surface plasmon resonance 141
5.3.6 pHrodo™ internalisation live cell-based assay 142
5.3.7 Cortical neuron culture- Coimbra University 142
5.4 Results 143
5.4.1 Inferring unmutated common ancestors 143
5.4.2 Affinities of UCAs 145
5.4.3 Tissue binding of UCAs 147
5.4.4 Internalisation capacity of UCAs 149
5.4.5 Data from Carvalho group, generated by Dr. Dominique Fernandes PhD 152
5.5 Discussion 154
5.6 Conclusions 156
5.7 Acknowledgements 157

CHAPTER 6 SUMMARY AND FUTURE WORK 158

6.1 Overall summary 158
6.2 Is B cell tolerance impaired in CASPR2-antibody encephalitis? 158
6.3 Is autoantibody immunodominance of N-terminal domains reproducible at the single-B cell level? 160
6.4 How do CASPR2-specific mAbs functionally modulate CASPR2 protein? 162
6.7 Final thoughts 165

APPENDIX 167

REFERENCES 171

Chapter 1 Introduction

1.3 B cell immunobiology

1.3.1 Antibodies

Antibodies, also known as Immunoglobulins (Ig), are glycoproteins secreted by B cells that have undergone differentiation into plasma cells. Typically, antibodies bind foreign antigens with high specificity. Once bound, they may have direct or indirect effector mechanisms that facilitate the clearance or inactivation of antigen. Antibodies exist in various isotypes (summarised in **section 1.3.2**), but have structures that are largely homologous. All antibodies consist of two heavy chains (IgH) and two light chains, linked by disulphide bridges (**figure 1**). The fragments of antigen binding (F(ab)) are formed from paired IgH and IgL variable domains and are highly diverse as a result of B cell receptor (BCR) gene rearrangements, described in **section 1.3.3**[1–3]. The heavy chain constant regions (C_H 1-4), residing distal to the F(ab) arms, form the Fc fragment and have distinct biological activities that are dependent on antibody isotype. When expressed as a transmembrane protein, a result of alternative splicing[4], an antibody is referred to as a surface immunoglobulin (sIg) and forms the B cell receptor (BCR) when associated with CD79. The BCR is responsible for antigen recognition and activation of B cells[5].

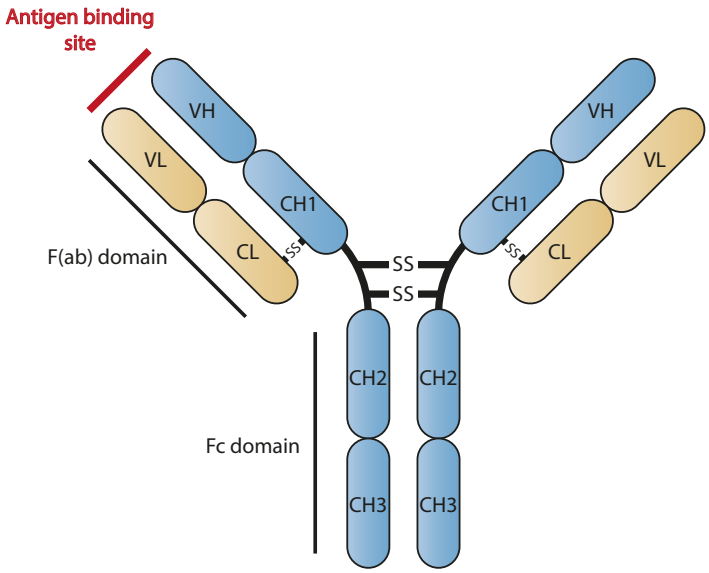

Figure 1. Representative antibody structure. VH denotes the variable region of the heavy chain and CH1-3 denotes the constant regions. IgM and IgE may have an additional CH4 region downstream of CH3 (not shown). VL and CL denote the variably region and constant region of the light chain respectively. Disulphide bonds are represented as -SS-. The F(ab) domain, antigen binding site and Fc domain are labelled respectively.

1.3.2 Antibody isotypes

There are five immunoglobulin isotypes, IgA, IgG, IgD, IgE and IgM, encoded by the α, γ, δ, ε and μ chains in the IgH gene locus. Each have distinct effector functions that vary based on their ability to fix complement and associate with different Fc receptors (FcRs)[6]. **Table 1** summarises these properties.

Table 1. Functional properties of immunoglobulin isotypes.

Immunoglobulin isotype	Structure	Serum concentration (mg mL^{-1})	Serum half-life (days)	Complement activation	Fc receptor
IgM	Pentamer/ hexamer	0.2-2.8	5	+++	FcμR
IgG1	Monomer	5-9.5	21	++	FcγRI, FcγRII, FcγRIII
IgG2	Monomer	2.2-4.8	21	+	FcγRII
IgG3	Monomer	0.4-1.0	7	+++	FcγRI, FcγRII, FcγRIII
IgG4	Monomer	0.1-0.6	21	-	FcγRI, FcγRII
IgA1	Monomer/ dimer	0.5-3.4	6	+	FcαR (CD89)
IgA2	Monomer/ dimer	0.5	6	+	FcαR (CD89)
IgD	Monomer	0.04	3	-	FcδR
IgE	Monomer	0.0003	0.5	-	FcεR I, II

Data is adapted from; Mankarious et al., 1988[7]; Lobo et al., 2004[8]; Schroeder et al.; 2010[9] and Vidarsson et al., 2014[6]. Effector functions are graded as +++, ++ and + in order of reported magnitude, with – representing no effector function.

IgM

IgM is expressed as the surface BCR of naïve B cells, but may be secreted as a soluble pentamer that is linked to a joining chain (J chain) by plasma cells. When bound to antigens, soluble IgM serves as a potent activator of complement and facilitates opsonisation and destruction of invading pathogens[10]. Typically, surface IgM on naïve B cells are anticipated to have low affinity for antigen since the variable, diversity and joining (V(D)J) genes have not undergone somatic hypermutation. While this is mostly true, some high affinity germline receptors exist and preferentially facilitate their B cells to undergo extrafollicular differentiation

into short lived plasma cells[11–13], which are responsible for the initial antibody response.

IgD

IgD, similar to IgM, is predominantly found as a surface receptor on naïve B cells and is thought to play a role in B cell modulation and selection[14]. Although it may be detectable at low levels in circulation, its effector functions remain unclear. Soluble IgD have been shown to bind some surface antigens of E coli[15] and Moraxella catarrhalis[16] and may modulate basophil responses[17].

IgG

IgG represents the most abundant immunoglobulin isotype in circulation, of which four subclasses exist; IgG1, IgG2, IgG3 and IgG4. Each subclass has distinct structural properties, varying affinities for different FcRs and differential ability to fix complement (summarised in **table 1**). Antibody responses to soluble protein antigens and membrane proteins primarily induce IgG1 responses with lower levels of IgG3 and IgG4[18], whereas IgG2 tend to be generated in response to bacterial capsular polysaccharide antigens[19]. IgG4 represents the least common, but most enigmatic subclass of IgG. IgG4 antibodies are unable to fix complement and are

often described in the context of long-term exposure to antigens in a non-infectious setting. Examples include long-term bee keepers and allergy patients undergoing oral immunotherapy[20,21]. The exchange of a proline for a serine in the IgG4 hinge region (P228S) leads to greater stereometrics flexibility which facilitates intra-chain disulphide bonds within the same heavy chain[22]. Under reducing conditions, this results in the dynamic dissociation and alternative re-association of paired heavy and light chains. This process is termed F(ab)-arm exchange and the resulting antibodies are functionally monovalent with bispecificity[23,24]. Although IgG4 are considered immunologically inert and are thought to have an anti-inflammatory function[25], their serum elevation and tissue infiltration by IgG4-positive plasma cells are coined as IgG4-related disease (IgG4RD)[26]. The spectrum of IgG4RD is wide and includes patients with autoimmune pancreatitis, thyroiditis, interstitial pneumonitis, interstitial nephritis, prostatitis, inflammatory pseudotumour and pertinent to this body of research, autoimmune neurological disease[27,28].

IgA

IgA is predominantly observed on mucosal surfaces and secreted fluids[29,30]. There are two isotypes of IgA (IgA1 and IgA2), of which IgA1 is most predominant in serum, with a ratio of 9:1; in serum, IgA predominantly exists as a monomer. In mucosal

tissue IgA1 and IgA2 are more evenly distributed and are secreted as dimers formed by its association with a J chain and a polymeric Ig-receptor ectodomain, called secretory component[31]. In recent times, serum IgA has been thought to have distinct immunological functions from secretory IgA in the gut[32]. In the absence of the secretory component, serum monomeric IgA can bind Fcα-receptor-I expressed on myeloid cells[33] and may induce pro-inflammatory responses[34]. Conversely, secreted dimeric IgA are thought to have a more nuanced role in maintaining balance between tolerance and immunity for commensal bacteria and pathogens[35].

IgE

IgE is the least abundant isotype in serum with the shortest half-life. Memory IgE responses constitute the first line of defence against parasitic infections, however, IgE-mediated immune responses to environmental antigens can lead to development of allergic disease such as asthma, allergic rhinitis and atopic dermatitis, and severe anaphylaxis [36].

1.3.3 B cell development

B cells are a crucial component of the adaptive immune system, and some ultimately differentiate into plasmablasts or plasma cells, collectively referred to as antibody-secreting cells (ASCs). ASCs are responsible for all antibody production *in vivo*. B cells arise from pluripotent haemopoietic stem cells and undergo staged maturation in the bone marrow that are defined by sequential rearrangement and expression of heavy and light chain immunoglobulin genes (**figure 2**). At the earliest stage of differentiation, progenitor B cells (pro-B) rearrangement of the variable (V), diversity (D), joining (J) genes of the heavy chain locus occurs via recombination activating genes 1 (RAG1) and 2 (RAG2), to generate a unique $V(D)J_H$ sequence[3]. Here, additional diversity is generated from alternative IGHD reading frames, D_H-D_H fusions and non-template insertions at D_H-J_H and V_H-D_H junctions[2,37]. If productive, this leads to the expression of an intact μ chain and progression to the next stage of development, the pre-B cell. When paired with a surrogate light chain (Igα/Igβ)[38,39], a pre-BCR is surface expressed and signals the pre-B cell to proliferate[40]. At this stage, light chain recombination occurs. Each locus of the light chain (κ and λ) contains multiple copies of variable and joining gene segments[41]. First, rearrangement occurs within the κ locus through joining of Vκ and Jκ genes. If this is not successful at producing a functional κ light chain, then rearrangement

of the λ locus occurs. Once a functional chain is achieved, a complete surface IgM BCR may then be expressed, a hallmark of an immature B cell. All development up to this point has been antigen independent.

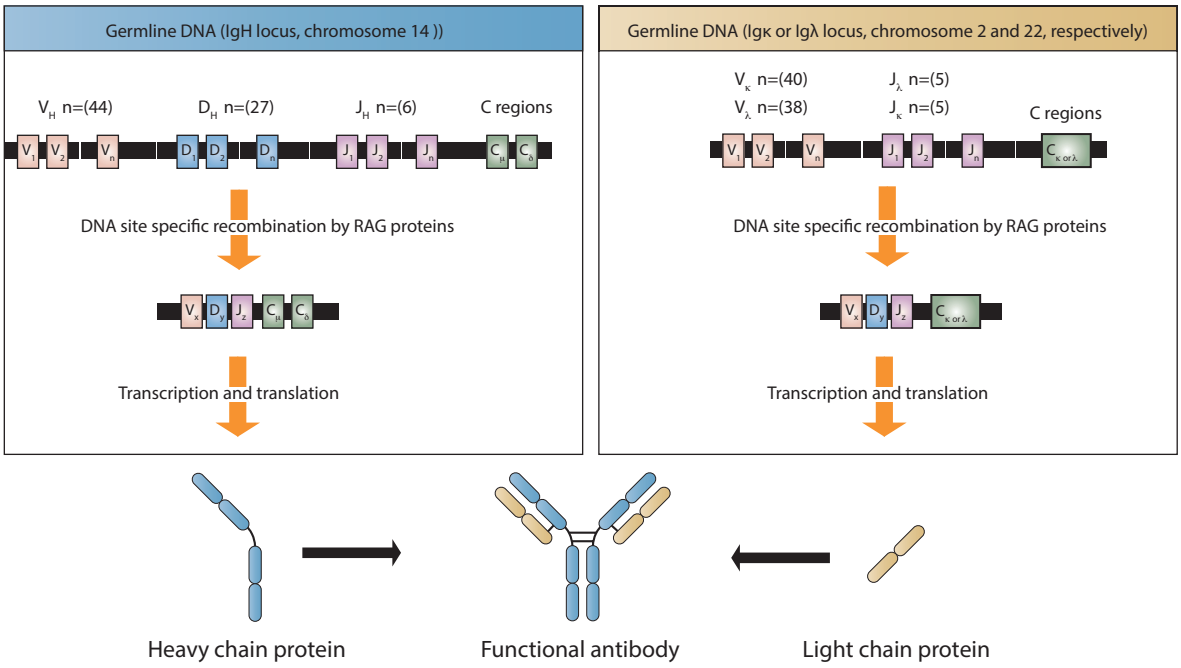

Figure 2. Immunoglobulin gene rearrangement. Cartoon representation of gene rearrangements and assembly for the heavy and light chain proteins to form a functional antibody. V_H, D_H and J_H denote IGHV, IGHD and IGHJ genes. Cμ and Cδ denote the μ and δ constant chains respectively. Cλ or κ denotes the λ or κ chains constant chain. V_x, V_y and V_z represent hypothetical orders of recombination.

1.3.4 B cell tolerance

In health, autoreactive BCRs are minimized by at least three proposed checkpoints along the developmental pathway[42–44] (**figure 3**). In the bone marrow, a substantial proportion of polyreactive and autoreactive early immature B cells (CD34−CD19+CD10+CD38+IgM+) are removed or modified via mechanisms of

central tolerance; apoptosis, induction of anergy and receptor editing[45]. This counter-selection is believed to depend on exposure of BCRs to autoantigens, with BCR signalling strength key to B cell fate[46].

Upon entry into the periphery, new emigrant B cells are exposed to a yet undefined peripheral tolerance checkpoint (**figure 3**) that further reduces the numbers of autoreactive B cells and is thought to depend not only on intrinsic properties of BCR signalling strength but also extrinsic factors, such as T regulatory (Treg) cells[47] and cytokines, including B cell-activating factor (BAFF)[48,49]. Subsequently, upon encounter with cognate antigens, autoreactivity can be acquired or increased as a result of somatic hypermutation (SMH)[44]. Indeed, up to 20% of post-germinal centre immunoglobulin class-switched IgG+ memory B cells have been found to express auto/polyreactive BCRs[44]. However, if the target autoantigen is expressed within the germinal centre microenvironment (**figure 3**), these autoreactive B cells fail to survive[50]. Therefore, germinal centre B cells that recognize rare or tissue-specific autoantigens may be less likely to be eliminated.

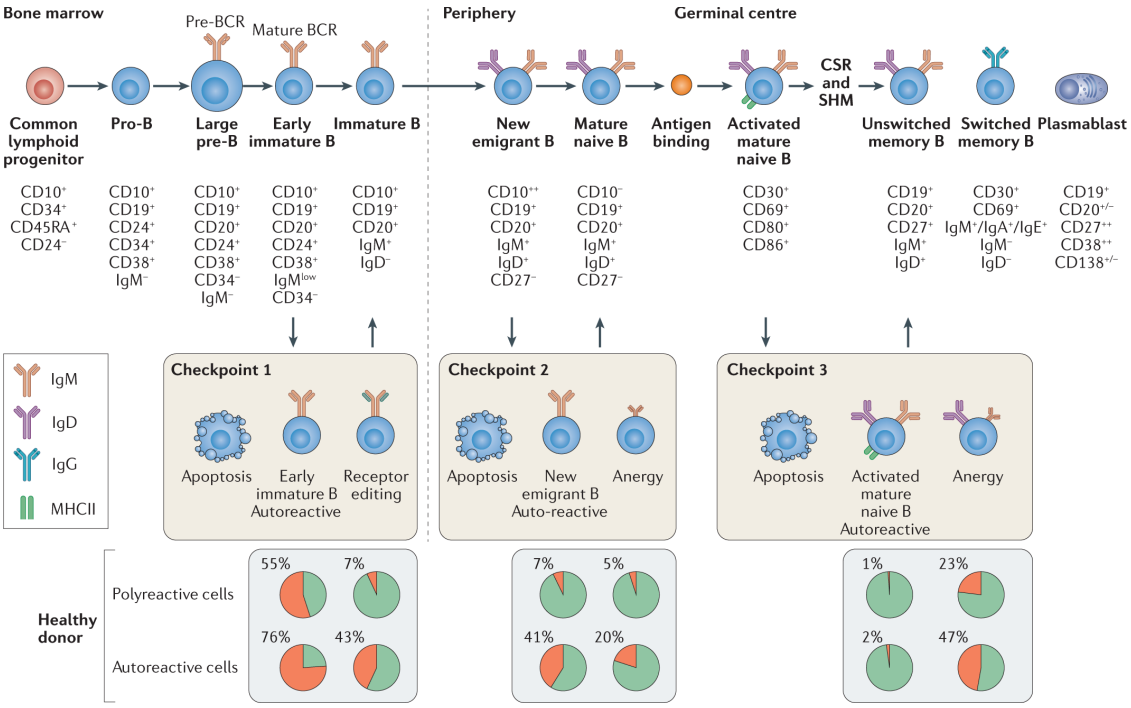

Figure 3. B cell tolerance checkpoints in humans. Pro-B cells in the bone marrow, which derive from common lymphoid progenitor cells, undergo B cell receptor heavy chain gene rearrangement. Newly rearranged heavy chains on pre-B cells acquire a surrogate invariant light chain to form a pre-B cell receptor (BCR). The surrogate invariant light chain is exchanged for a fully recombined, paired light chain in the early immature B cell so that immunoglobulin M (IgM) is expressed on the B cell membrane. At this point (Checkpoint 1), autoreactive BCRs are negatively selected through apoptosis or rescued via receptor editing of paired functional light chains. Positively selected or rescued B cells then exit the bone marrow as new emigrant B cells. Further negative selection occurs at the transition between new emigrant and mature naive B cells (Checkpoint 2) in the periphery. Upon encountering their cognate antigen, mature naive B cells can enter germinal centre reactions, where T cell-dependent immunoglobulin class switch recombination (CSR) and somatic hypermutation (SHM) occur, and they upregulate MHC class II. Within germinal centres, SHM can lead IgG^+ switched memory B cells to inadvertently acquire autoreactive BCRs with pathogenic potential. IgM^+ unswitched memory B cells can be further negatively selected (Checkpoint 3). The relative proportions of polyreactive and autoreactive B cells at each checkpoint are shown as the pie charts. MHCII, major histocompatibility complex class II. Image is replicated from (Sun et al, 2020[51], reproduced under CC BY 4.0).

1.3.5 B cells in the adaptive immune response

Upon encounter with antigens, IgMs cross-link and cluster on the surface of naïve B cells to provide intracellular signalling[52]. Antigens bound by B cell receptors (BCRs)

are then internalised and brought into MHCII-rich compartments through endocytic pathways. Proteolytic degradation of antigens internalised through the BCR are loaded onto MHCII and presented to T cell receptors (TCR) on CD4 T-helper cells. T-helper cells, recognising major histocompatibility complex II (MHCII)-presented peptides of the same antigen, then provide a second signal of activation through surface CD40 interaction with CD40 ligand (CD40L) on B cells[53]. Antigens inducing this pathway of B cell activation are termed T-cell dependent antigens and typically undergo further affinity maturation in germinal centres. T-cell independent antigens, such as bacterial polysaccharides, contain repetitive epitope units that facilitate cross-linking of multiple BCRs and provide the first signal for activation. As T cells are not involved, a second signal of activation may come from Toll-like receptors or interactions with the complement system through recruitment of CD21[54].

1.3.5.1 T cell priming

During an immunising event, CD4+ T-helper cells are activated by professional antigen presenting cells (macrophages, B cells and dendritic cells). These armed T cells are then trapped and proliferate within T cell zones of local lymphoid tissue[55]. Activated B cells first migrate into these T cell zones through high endothelial venules of lymphoid tissue. The interaction of antigen-active B cells and armed T-

helper cells creates a primary focus which may further migrate to a primary lymphoid follicle to form a germinal centre, or perpetuate local "extrafollicular" responses[11].

1.3.5.2 Extrafollicular responses

Within 2 days of an immunising events, B and T cell blasts have been observed at the T cell border. B cells that migrate to these extrafollicular regions then begin plasmablast (PB) differentiation[56]. These extrafollicular PBs then undergo transient proliferative expansion into short-lived plasma cells (PCs) (**figure 4**). These short-lived PCs are responsible for the first phase of the adaptive immune response and their response is characterised by early serological peaks in IgM. These early, usually unmutated, antibodies can be critical for the neutralisation of pathogens[10,57,58].

1.3.5.3 Germinal centres

T cell-dependent antigen-activated naïve B cells typically undergo further affinity maturation and selection in germinal centre reactions (**figure 4**). Germinal centres are sites of antigen-driven selection where B cells undergo clonal expansion, class-switch recombination and clonal diversification by somatic hypermutation (SMH)[59]. SMH of immunoglobulin genes plays a fundamental role in antibody-mediated immunity. SHM provides the molecular basis for affinity maturation of antibodies

and optimises antibody responses to target antigens. SHM is initiated by targeting Activation-Induced Cytidine Deaminase (AID) to rearranged V(D)J and switch regions of *Ig* genes. AID is an enzyme that deaminates cytosines to the highly mutagenic deoxy-uracil (U). Mutagenic processing of the U, via error-prone DNA repair, then generates an entire spectrum of point mutations. Functional BCRs encoded by mutated Ig genes are then re-challenged with antigen, presented by follicular dendritic cells within the light zone of the germinal centre, and positively selected for higher affinity binding[60–62]. Affinity matured B cells then undergo rapid proliferation within the dark zone and differentiate into either long-lived plasma cells or memory B cells.

1.3.5.4 Pathways of immune memory and recall

B cell immune memory may arise from multiple sources, but long-lived plasma cells and memory B cells are predominant[63] (**figure 4**). Typically, naïve B cells differentiate and give rise to long-lived PCs and memory B cells through germinal centre reactions. However, naïve B cells may also give rise to memory B cells independently of GCs; this is evidenced by the ability of BCL-6 deficient mice, incapable of developing GCs, to generate IgM+ and IgG+ memory B cells[64]. GC-independent memory B cells were further shown to be mainly IgM+ and derived

from the same precursor B cells as those that give rise to GCs, supporting their generation early in the immune response[65].

Current paradigms of B cell memory suggest that high-affinity antibodies produced by long-lived PCs form a background level of defence against the same pathogen(s). Memory B cells provide a second line of defence and may undergo new germinal centre reactions to generate further diverse antibody responses against variant pathogens that escape antibodies produced by long-lived PCs[66]. In this paradigm, the perpetual competition and repopulation of bone marrow resident long-lived plasma cells is expected to occur following pathogen re-challenge[67]; therefore, *de novo* naïve B cell recruitment to GCs also serves as a dynamic source of new long-lived PCs and memory B cells.

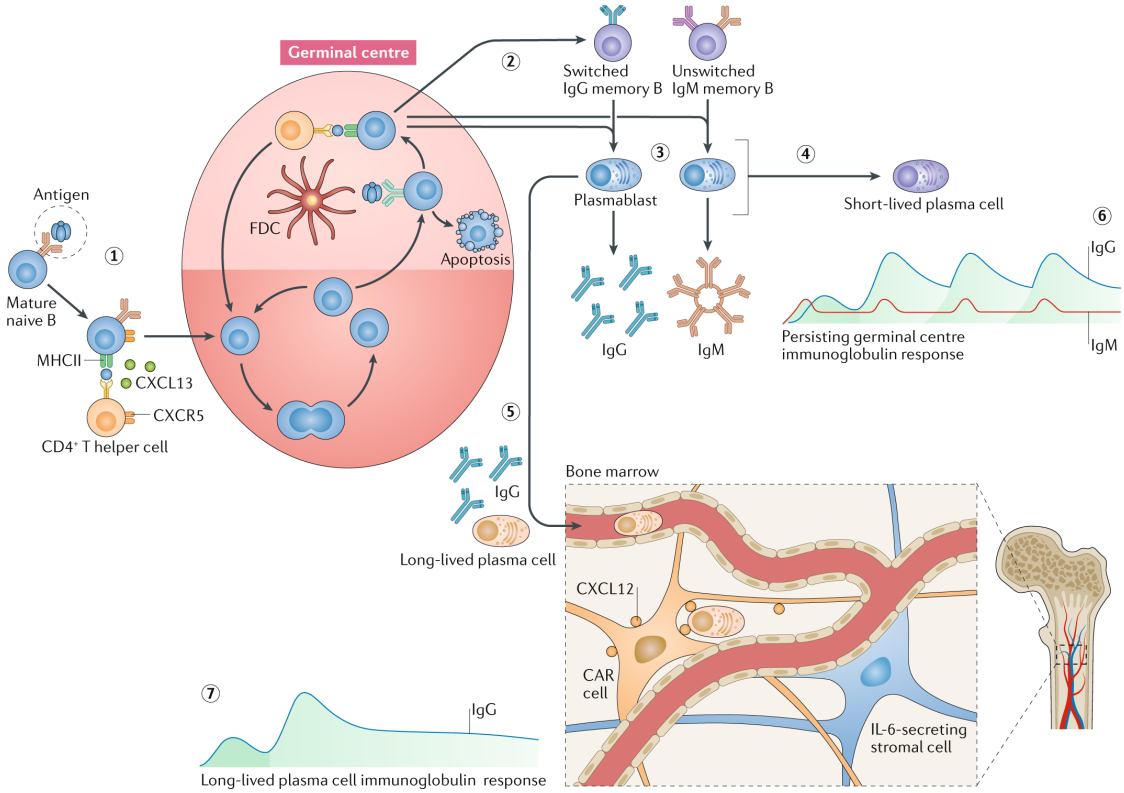

Figure 4. Sources of immune memory. Two major sources of circulating antibodies have been proposed: plasmablasts that emerge from active germinal centre reactions in secondary lymphoid organs and long-lived plasma cells that reside in the bone marrow. Mature naive B cells that encounter antigen may either proliferate extrafollicularly into short-lived plasmablasts, responsible for the initial IgM response, or enter germinal centre reactions (1). In the presence of antigen and cognate $CD4^+$ T helper cells, activated naïve B cells in germinal centres undergo somatic hypermutation to increase the affinity of their B cell receptors. After successful maturation, unswitched or switched memory B cells exit the germinal centre (2) and can give rise to circulating plasmablasts that secrete IgM, IgG or IgA (not shown) (3). These plasmablasts may differentiate into long-lived plasma cells which can migrate into the bone marrow niche (5). Supported by IL-6-secreting stromal cells and C–X–C motif chemokine ligand 12 (CXCL12)-abundant reticular (CAR) cells, they can survive for many years. CXCL13, C–X–C motif chemokine ligand 12; CXCR5, C–X–C motif chemokine receptor 5; FDC, follicular dendritic cell; MHCII, major histocompatibility complex class II. Image is replicated from (Sun et al, 2020[51], reproduced under CC BY 4.0).

1.4 Neuroglial surface antibody mediated diseases

An increasing number of autoimmune disorders of the central nervous system (CNS) are known to be associated with autoantibodies that target the extracellular domains of neuronal or glial proteins[68,69]. In these neuroglial surface autoantibody (NSAb)-mediated diseases, early immunotherapy can substantially reduce morbidity and mortality[70,71], therefore they are considered to be 'not-to-miss' conditions. Typically, these diseases are characterized by autoantibodies that target a single autoantigen in any individual patient. The most common autoantigens involved include aquaporin 4 (AQP4) in neuromyelitis optica spectrum disorders (NMOSD), and the NMDA receptor, leucine-rich glioma inactivated protein 1 (LGI1) and contactin-associated protein-like 2 (CASPR2) in clinically distinct syndrome (**table 2**). On the basis that these antigens are expressed on the surface of live cells, and increasingly robust evidence from *in vitro* and *in vivo* studies, the autoantibodies that target them are considered to be directly causative.

Table 2 | Clinical characteristics of central nervous system neuroglial surface antibody-mediated diseases.

CNS target	Median age (range)	Gender ratio (M:F)	Clinical presentation	CSF and CNS characteristics	Main IgG subclass[a]	Putative mechanisms
Neuronal targets[b]						
NMDA receptor[70,72–75]	~24 y (0-90 y)	1:4	Flu-like prodrome, psychiatric features which cross traditional categories, multimorphic movement disorder (dystonia, stereotypies and chorea, especially orofacial involvement); dysautonomia and coma are common; seizures typically a minor feature	CSF lymphocytic pleocytosis ± oligoclonal bands; normal in ~20%; MRI often normal (~80%) despite severe illness	IgG1	Internalisation via antigen crosslinking[73,76,77]
LGI1[71,78,79]	~60 y (30–80 y)	3:2	Very frequent focal seizures (including pathognomonic faciobrachial dystonic seizures), amnesia, behavioural change, insomnia	CSF normal in ~75%; MRI shows medial temporal lobe swelling in ~40%	IgG4	Functional block and internalisation[80–82]
CASPR2[83–86]	~60 y (30–80 y)	9:1	Neuropsychiatric changes, cognitive impairment, dysautonomia, sleep disturbance, neuromyotonia and neuropathic pain	CSF normal in ~70%; imaging normal in ~70%	IgG4	Functional modulation of antigen or neighbouring proteins[87–89]
$GABA_A$ receptor[90–92]	~40 y (0-90 y)	1:1	Seizures (including status epilepticus, epilepsia partialis continua), cognitive impairment, movement disorders	CSF pleocytosis in 25–50% ± oligoclonal bands and elevated protein; MRI abnormal in ~80%	IgG1	Selective decrease of receptor surface density[93,94]
$GABA_B$ receptor[95–97]	~60 y (16–80 y)	1.5:1	Seizures (including status epilepticus), amnesia and cognitive impairment, often with underlying small cell lung cancer	CSF pleocytosis in ~50%, MRI abnormal in ~70%	IgG1	Functional modulation of antigen[97]
Glial targets[b]						
AQP4[98–100]	~28 y (2–90 y)	1:10	Optic neuritis, longitudinally extensive myelitis, area-postrema syndrome, other rarer presentations	CSF pleocytosis in ~50%; swelling on MRI	IgG1	Complement activation; internalization[98,101]
MOG[102–105]	~31 y (0–80 y)	1:1	Myelitis and optic neuritis, plus forms of encephalitis, in particular acute disseminated encephalomyelitis (ADEM); recovery often better than with AQP4 autoantibodies	CSF pleocytosis in ~44-80% MRI abnormal in ~45%	IgG1	Complement activation[104,106,107]

ADEM, acute disseminated encephalomyelitis; AQP4, aquaporin 4; CASPR2, contactin-associated protein-like 2; CSF, cerebrospinal fluid; LGI1, leucine-rich glioma inactivated protein 1; MOG, myelin oligodendrocyte glycoprotein. [a]IgG1 subclasses can activate the complement system. [b]Some of the specified proteins are expressed in glia and neurons; categorization is based on the cell type that has received more study.

1.4.1 Putative sites of autoimmunisation

A consistent finding across all NSAb-mediated diseases is that median concentrations of the autoantibodies in the serum are 4-fold to 640-fold higher than those in the CSF[72,81,86,91,92,95,108–116]. Since less than 0.1% of peripherally administered IgG reaches the brain parenchyma[117], this observation supports the likely peripheral generation of autoantibody secreting PCs from antigen-activated precursor B cells. However, the exact sites of autoimmunisation remain unclear.

1.4.2 B cell tolerance in NSAb-mediated diseases

Supporting the peripheral origin of CNS autoantigen-specific B cells, circulating autoantigen-specific B cells can be readily detected in patients with NMOSD[118], LGI1 antibody encephalitis[81,119], NMDA receptor antibody encephalitis[119,120] and myelin oligodendrocyte glycoprotein antibody disease[121]. This consistent observation across autoantibody-mediated CNS diseases implicates a failure of B cell tolerance. Indeed, observations from *ex vivo* studies of B cells in NSAb-mediated diseases have shed light on the potential developmental checkpoints affected.

In NMOSD, an autoantibody-mediated disease of the CNS characterised by antibodies targeting the glial protein aquaporin-4 (AQP4), patient-derived naive and memory B cells secreted AQP4-reactive autoantibodies, whereas healthy donor-derived cells did not[122]. This observation confirmed the existence of AQP4-reactive B cells before and after germinal centre maturation. Using an alternative approach, a parallel study back-mutated plasma cell-derived AQP4-specific monoclonal antibodies to their unmutated common ancestors (UCAs) and found that UCAs lost their ability to bind AQP4[118]. However, some UCAs exhibited characteristics of polyreactivity and/or non-AQP4 autoreactivity. Taken together, these studies support a failure of both central and peripheral tolerance in NMOSD. These findings mirror those in non-neurological autoantibody-associated diseases, such as systemic lupus erythematosus (SLE)[123] and rheumatoid arthritis[124]. By contrast, in multiple sclerosis, another autoimmune disease of the CNS in which B cells are strongly implicated, only the peripheral checkpoints have been found to be dysfunctional in a subgroup of patients[125]. More recently, in vivo models of B cell tolerance to CNS antigens support the dura as the potential site of negative selection[126,127]. These early observations of impaired B cell tolerance mechanisms have yet to be translated across

other NSAb-mediated diseases, but may highlight shared or distinct aspects of their immunobiology for the educated future optimisation of therapeutic approaches.

1.5 CASPR2 autoantibody encephalitis

1.5.1 Prelude

In 1995, a distinct group of patients with acquired neuromyotonia and antibodies targeting voltage-gated potassium channels (VGKCs) were described[128]. Termed Isaac's syndrome, acquired neuromyotonia is characterised by cramps and impaired muscle relaxation, as a result of peripheral nerve hyperexcitability. Later, VGKC-antibodies were implicated in patients with limbic encephalitis[129] and Morvan's syndrome[130], characterised by a combination of neuromyotonia, cognitive symptoms, autonomic dysfunction and/or insomnia. Historically, VGKC antibodies were detected using radioimmunoassay (RIA); in this assay, mammalian brain derived ^{125}I-α-dendrotoxin labelled VGKC complexes are precipitated by patient sera. However, failed attempts to directly identify VGKC antibodies using VGKC-transfected cells, led to the discovery of autoantibodies to VGKC-associated proteins, LGI1 and CASPR2[78,79].

1.5.2 Clinical Features

Patients with autoantibodies targeting the extracellular domains of CASPR2 develop a wide variety of clinical syndromes[83–85,131]. For yet unclear reasons, men are predominantly affected (~90%) and disease onset typically occurs in late life (60-70 years of age). While it is increasingly recognised in the clinical setting, the disease remains rare with approximately 600 patients described across all reported studies to date[132]. The majority of patients with CASRP2-antibodies develop either limbic encephalitis or Morvan's syndrome. Core symptoms include, cognitive dysfunction (~40-70%), seizures (~40-50%), cerebellar symptoms (~14%), peripheral nerve hyperexcitability (~20-30%), autonomic dysfunction (~35-50%), insomnia (~40%) and neuropathic pain (~40%). Progression usually occurs over a few months and the subacute tempo is often the distinguishing feature for its differentiation from neurodegenerative disease mimics.

1.5.3 Clinical investigations

The presence of CASPR2 autoantibodies is the hallmark of CASPR2-antibody disease. CASPR2 antibodies are specifically confirmed with cell-based assays performed on either serum or cerebrospinal fluid (CSF)[78,79]. Adherent HEK293 cells

transfected with human CASPR2 protein provide the substrate, and binding of serum antibodies is detected using fluorescent immunohistochemistry (**figure 5B**). Typically, in CASPR2-antibody encephalitis, CASPR2 antibodies are predominantly IgG4 with some detectable IgG1 in a few individuals (*Varley and Irani unpublished*).

Ancillary tests are often non-specific but may aid synthesis of the diagnostic picture. Brain MRI is typically normal in patients, but hyperintensity of the medial temporal lobes may be present[83–85,131] (**figure 5A**). CSF analysis may reveal lymphocytosis and raised protein, but is often normal in up to 58% of cases. Electroencephalography (EEG) is typically non-specific. Thymomas have been reported in 21% of cases and are typically associated with Morvan's syndrome patients[83].

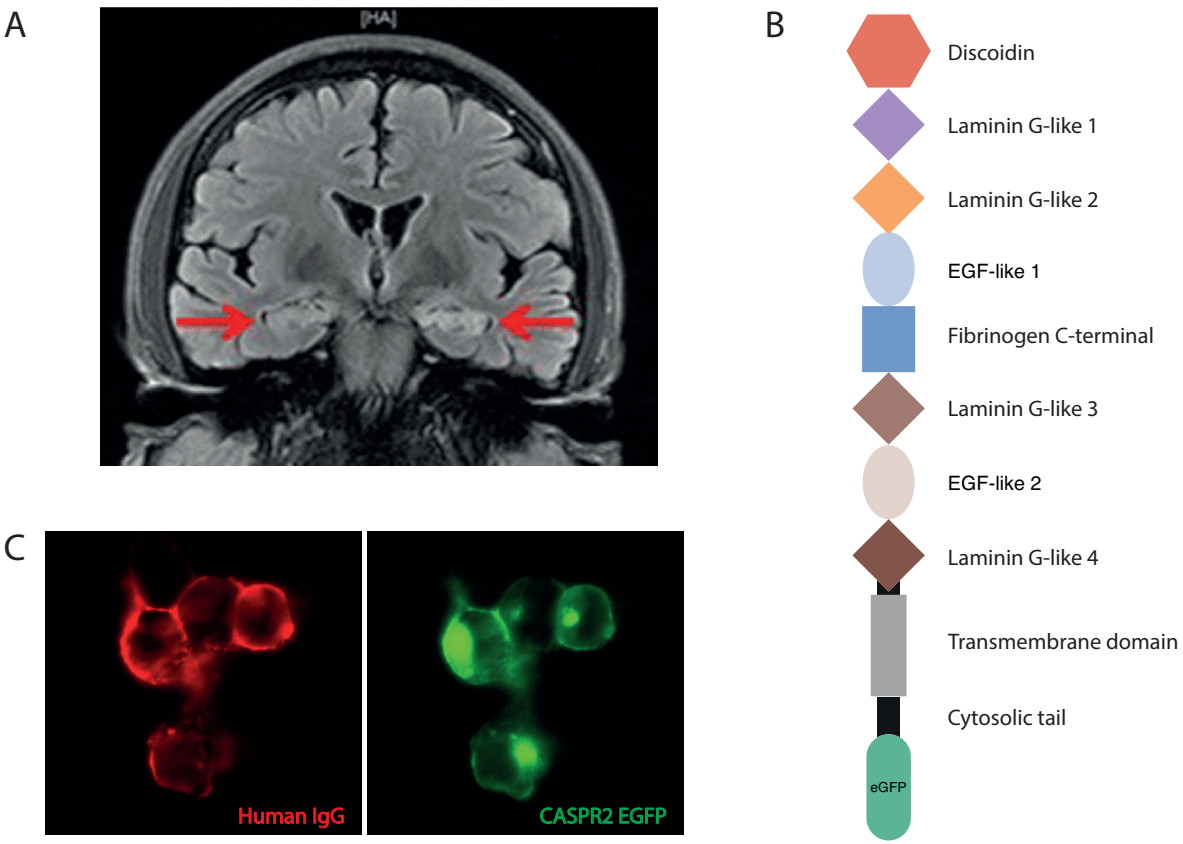

Figure 5. Investigations in CASPR2-antibody encephalitis. (A) Representative MRI scan showing bilateral hippocampus FLAIR sequence hyperintensities. (B) Cartoon representation of CASPR2 protein domain composition (C) Representative fluorescence immunohistochemistry images of a live-cell based assay. Red, indicates detection of human IgG binding with a goat anti-human secondary antibody. Green, indicates an antigen of interest (CASPR2), tagged intracellularly with EGFP.

1.5.4 Treatment and outcomes

The majority of patients have been reported to respond well to immunotherapy. Most frequently used therapies include corticosteroids, intravenous immunoglobulins (IVIg), plasma exchange (PLEX) and rarely, second line therapies such as rituximab or cyclophosphamide[83–86]. In our experience as a national referral centre, acute IVIg and corticosteroid therapy are often sufficient in the majority of cases with treatment

response in over 80% of patients. For patients with malignancy, successful treatment of the tumour appears paramount[83]. While outcomes appear favourable (modified rankin scale score ≤2) in ~70% of patients[83] with 2-year fatality rate of 10%, relapses can occur in a third of cases[83] (*Uy and Irani unpublished*).

1.5.5 Histopathology

Post-mortem or biopsy examination of brain tissue is rare, with only 1 published report. In that report, a 62-year-old male patient with subacute dyscognitive seizures, short term memory loss and acoustic hallucinations, is described. Resection of the right hippocampus revealed moderate parenchymal infiltration of CD8+ T cells along with mild activation of microglia[133]. CD20 B cells and CD138 plasma cells were visualised predominantly in the perivascular space of blood vessels. Immunoglobulin staining revealed strong leakage of Ig through the blood brain barrier and scattered deposition on neuronal membranes.

1.5.6 Evidence for antibody-mediated pathogenesis

1.5.6.1 *In vitro*

Some progress has been made to elucidate the effector mechanisms of CASPR2-antibodies, however, many aspects remain unclear. CASPR2-antibodies target the

extracellular domains of CASPR2 and show immunodominance for the N-terminal Discoidin and Laminin G-like1 domains[86,88,134]. It is proposed that patient sera are capable of binding denatured CASPR2 regardless of conformational integrity, and in solid-phase assays, block the interaction of CASPR2 and its proposed ligand CNTN2[87].

Autoantibodies often exact their mechanisms through direct or indirect modulation of antigen. In NSAb-mediated diseases, typical mechanisms of modulation are complement fixation and destruction of antigen, functional modulation of antigen and antibody-mediated internalisation (**table 2**).

Since CASPR2 antibodies are predominantly IgG4, dogma excludes complement fixation as a viable mechanism and implies that functionally monovalent (F(ab)-arm exchanged) IgG4 cannot cross-link and internalise antigens. Indeed, in two studies[87,88], patient sera did not result in significant CASPR2 internalisation in cell-based assays or primary neurons. However, in contrast, two other studies observed robust CASPR2 internalisation *in vitro*[89,135], albeit with variable effects of CASPR2 surface expression. To date, these contrasting data regarding CASPR2 internalisation have not been fully resolved.

1.5.6.2 *In vivo*

More recently, *in vivo* murine models of CASPR2 antibody pathogenicity have shed light on the effect of their passive-transfer. Intraperitoneal injection of purified plasma IgG of CASPR2-antibody patients, in presence of lipopolysaccharide (LPS) induced blood brain barrier breach, resulted in reduced working memory of exposed mice[135]. Furthermore, exposed mice also displayed longer latency to start interactions, associated freezing behaviour and reduced rearing and grooming. In an independent study, characterisation of CASPR2 plasma purified IgG revealed their ability to modulate synaptic α-amino-3-hydroxy-5-methyl-4-isoxazolepropionic acid receptors (AMPARs)[89] and perturb AMPAR-mediated synaptic transmission of murine V1-layer 2/3 pyramidal neurons *in vivo*. Lastly, intraperitoneal injection of serum-purified CASPR2 IgG into mice resulted in mechanical pain-related hypersensitivity, in the absence of neuronal injury. Taken together, these three mouse models independently recapitulate aspects of the clinical presentations seen in CASPR2-antibody disease.

1.5.7 CASPR2 protein

1.5.7.1 CASPR2 structure

CASPR2 is a large transmembrane glycoprotein member of the neurexin superfamily of proteins[136]. At the C-terminus, CASPR2 contains a 4.1B-binding motif (4.1Bb) and a type II PDZ-binding motif (PDZb) within its intracellular region. These facilitate its interaction with cytoskeleton-associated proteins containing a Four-point-one, Ezrin, Radixin, Moesin (FERM) domain[137], and PDZ domains, respectively[138,139]. Extracellularly, CASPR2 is a mosaic of domains comprised of an N-terminal Discoidin-like domain (F58C), four Laminin G-like domains (L1-L4), two Epidermal-like growth factor domains (EGF1-EGF2) and a Fibrinogen C-terminal domain (FibC) (**figure 5B**). In recent electron microscopy studies, it has been shown to have a compact structure that is organised into three lobes that are flexibly linked by the two EGF domains[140,141]. Notably, CASPR2 was shown to adopt two predominant orientations, vertical or horizontal[141]. The significance of these orientations has yet to be characterised, but could plausibly modulate its binding with cognate ligands or its localisation to subcellular structures[141].

1.5.7.2 CASPR2 expression

In adult murine brains, CASPR2 expression is most prominent in the cortex, cerebellum, basal ganglia, substantia nigra, amygdala and hippocampus[142]. Additionally, CASPR2 is also found in sensory pathways such as the visual, olfactory, auditory and somatosensory systems. In humans, CASPR2 expression localises to similar structures as those in rodents[136]. In murine pyramidal neurons of the CA3 region of the hippocampus and of the cortex, CASPR2 is visualised within both dendrites and cell bodies[136]. However, assessment of primary cultured neurons revealed its polarisation the axon initial segment (AIS) and within juxtaparanodal regions of the nodes of Ranvier in myelinated axons of the PNS and CNS[136,143–145] (**figure 6A**). In primary hippocampal neurons, CASPR2 is found at inhibitory and excitatory neurons at variable proportions[89,146–148] and as part of Kv1 voltage gated potassium channel complexes[149,150]. Further, it is also present in synaptosome fractions[151] and at excitatory and inhibitory synapses, as evidenced by its colocalisation with VGLUT1, VGAT[147] and the postsynaptic AMPA receptor GluA1 subunit[89,146]. Overall, the heterogenous distribution of CASPR2 protein confers further ambiguity of its exact functional role within the CNS and PNS.

1.5.7.3 Juxtaparanodes of myelinated neurons

Myelinated segments of neurons are separated by the nodes of Ranvier and are organised into distinct domains; the node, the paranode and the juxtaparanode (JXP) (**figure 6C**). The JXP region resides just under the compact myelin sheath and are characterised by the presence of a macromolecular complex comprising of CASPR2, Contactin-2 (CNTN2) – a GPI anchored protein, also known as TAG1 – and Kv1.1/1.2 VGKCs[152,153]. Kv1 VGKCs are proposed to regulate the repolarisation phase of action potentials[152,154] and their enrichment at JXP are dependent on CASPR2[152] and CNTN2[153]. Indeed, CASPR2 null mice exhibit decreased accumulation of Kv1.2 at the JXPs and perturbed post-synaptic responses[155]. Similarly, CNTN2 null mice also have decreased JXP accumulation of Kv1.2 complexes[153] and therefore, its direct interaction with CASPR2 was explored. While initial experiments confirmed their co-immunoprecipitation (co-IP) from tissue with antibodies against the respective proteins[152,153], experiments in transfected mammalian cell lines revealed that their co-IP was not possible from mixed lysates of the independently expressed proteins[88,152]. Similarly, a soluble CNTN2-Fc fusion protein was incapable of binding CASPR2 expressing cells[153]. A proposed explanation for these discrepant observations is that CASPR2 may require interaction in cis with CNTN2, however, studies examining their purified extracellular domains have led to

further conflicted findings[140,141]. It is perhaps not surprising then, that the CASPR2-CNTN2 complex has yet to be structurally characterised.

1.5.7.4 The axon initial segment and other localisations

CASPR2 has been reported to accumulate at the axonal initial segment (AIS)[143,146] (**figure 6B**). The AIS is positioned at the proximal axon and is the site of action potential initiation. As such, it is enriched for voltage-gated iron channels, membrane proteins and is molecularly defined by the presence of a master scaffolding protein, ankyrinG (ankG). While CASPR2 colocalises with Kv1 and CNTN2 at the AIS, its presence is not required for their AIS localisation[145,150]; therefore, on current evidence, CASPR2 is unlikely to play a direct role in the molecular assembly of the AIS.

The degree of CASPR2 expression in synapsis has been variably reported. Sub-fractional analysis of rat brain lysates found CASPR2 to be present in synaptosomes and synaptic membrane fractions[151,156]. When examined in cultured neurons, CASPR2 could be found at both glutamatergic and GABAergic synapses[89,146–148,157]. Additionally, knockout studies and models of induced CASPR2 loss, have implicated CASPR2 in the regulation of AMPAR turnover at synapses[89,146].

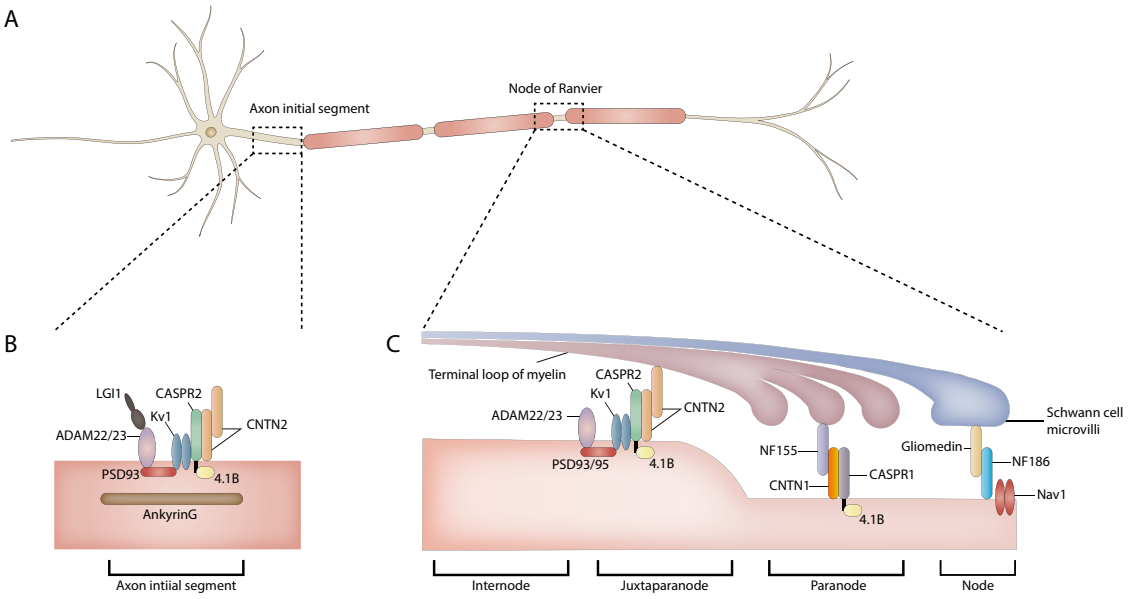

Figure 6. Schematic organisation of the axon initial segment (AIS) and node of Ranvier. (A) Representative cartoon of a myelinated neuron, highlighted in dashed boxes are the axon initial segment and node of Ranvier. (B) At the AIS, CASPR2 colocalizes with TAG-1 and Kv1 channels. Kv1 channel recruitment at the AIS is dependent on PSD-93. The AIS is molecularly defined by the presence of ankyrinG. (C) At the JXP, CASPR2 enrichment is dependent on its interaction with 4.1B protein and CNTN2. Here, Kv1 recruitment is dependent on the presence of CASPR2, CNTN2 and 4.1B.

1.5.7.5 CASPR2 and neurodevelopment

The role of CASPR2 in the developing nervous system has been well characterised in mice. Knockout studies have shown its importance in axonal growth, dendritic branching and correct cortical neuronal migration[158–160]. Further, CASPR2 null mice had deficiencies in subpopulations of inhibitory GABAergic interneurons in the striatum, hippocampus and the somatosensory cortex[148,160,161].

As a testament to its importance in neurodevelopment, mutations in CASPR2 have been associated with a wide spectrum of neurodevelopmental and psychiatric disorders[162]. Patients with mutations may present with autistic-spectrum disorders (ASD), intellectual disability, schizophrenia, attention deficit hyperactivity disorder and epilepsy secondary to cortical dysplasia. Similarly, in mice, knockout models often display behavioural traits similar to ASD, hyperactivity and seizures[155,159].

1.6 Aims and key questions

The pathogenesis of CASPR2-antibody encephalitis is poorly characterised. It remains unclear when and how CASPR2-antibody producing B cells escape innate B cell tolerance checkpoints, that would otherwise remove their existence. Further, the direct mechanisms of antibody pathogenicity have largely been examined using unrefined polyclonal sera, and remain inconsistent. Therefore, the aim of this thesis is to investigate the biological and molecular mechanisms of disease pathogenesis in CASPR2-antibody encephalitis, using the following broad framework of questions:

1.6.1 Is B cell tolerance impaired in CASPR2-antibody encephalitis?

1.6.2 Is autoantibody immunodominance of the N-terminal domains reproducible at a single-B cell level?

1.6.3 How do CASPR2-specific mAbs functionally modulate CASPR2 protein?

Chapter 2 The B cell receptor landscape in CASPR2-antibody encephalitis

2.1 Introduction

The breakdown of B cell tolerance in autoimmune diseases, is detectable by increased frequencies of autoantigen-reactive B cells downstream of known B cell developmental checkpoints[123–125,163]. In **chapter 1**, I summarised the three predominant B cell tolerance checkpoints that have been described in relation to B cell maturation. In this chapter, across CASPR2-antibody encephalitis patients and healthy donors, I aimed to investigate the CASPR2-reactive frequencies of pre-germinal and post-germinal B cell subsets, and characterise the properties of CASPR2-reactive monoclonal autoantibodies cloned from single-cell B cells.

Interrogation of B cell reactivities in antibody-associated autoimmunity, is crucial to understand the earliest point of autoantibody genesis and its potential for autoimmune B cell memory; of which little is known in NSAb-antibody diseases. Characterising the reactivities of CD19+IgD+CD27- naïve B cells and CD19+IgD-CD27+IgM- class-switched memory B cells can indirectly infer the integrity of pre-germinal centre and post-germinal centre immune tolerance checkpoints[42,44]. In the only study to address this in NSAb-antibody diseases, B cell cultures pre-enriched

for naïve and memory subsets in NMOSD, have shown both compartments to have capacity for producing Aquaporin-4 autoantibodies under direct stimulation[122]. This observation has significance, as persistent generation of autoreactive naïve B cells into the periphery may confer longitudinal risk of their activation and disease relapse. Therefore, translation of these findings to other NSAb-antibody diseases may help better characterise similarities and differences of disease pathogenesis, to provide insight towards more educated treatment strategies and identification of novel targets for intervention.

Early studies facilitated the characterisation of antigen-specific monoclonal antibodies (mAbs) from primary infection, vaccination and autoimmunity, using techniques such as antibody phage display (APD), hybridoma generation and amplification of paired IgH and IgL genes from single-cell sorted B cells[164–166]. These methods have been informative for our understanding of the functional properties of generated mAbs; however, each have their limitations. Whilst APD represents the highest throughput method, the random pairing of potentially non-cognate heavy and light chains is unlikely to recapitulate the *in vivo* BCR repertoire. Conversely, hybridomas retain natural heavy and light chain pairings, but remain labour intensive with low recovery of total individual clones. Lastly, direct cloning of IgH

and IgL genes from single-cell sorted B cells represents an unbiased, *in vivo*-representative, approach with reasonable throughput; however, this results in a large library of antibody sequences that require individual expression as mAbs and screening for target reactivity. To circumvent this, recombinant proteins of interest have been used to stain surface BCRs as a means to "bait" out antigen-specific B cells, allowing for their enrichment. Whilst this is effective, recombinant neuroglial membrane proteins are often complex integral transmembrane domains; therefore, concerns over conformational stability remain. In addition, promiscuous BCRs that bind antigen labelling reagents, such as fluorescent tags, may reduce the specificity of the bait. Further, naïve B cells expressing low affinity BCRs, or physiologically anergic B cells can be missed with a baited approach; these are important populations in the study of B cell-mediated autoimmunity. In more recent times, optimised *in vitro* differentiation of single B cells into antibody secreting cells, has facilitated the ability to screen single-cell BCR reactivities prior to downstream cloning of representative mAbs[167,168]. To date, this represents the best balance of throughput and resolution, allowing for inference of antigen-specific frequencies and characterisation of BCR-representative mAbs.

2.2 Hypothesis

2.2.1 CASPR2-reactive B cells are exclusive to patients, and break both pre and post germinal centre tolerance checkpoints.

2.2.2 Studying nucleotide sequences of CASPR2-reactive memory B cell-derived BCRs will reveal evidence of somatic hypermutation, as a proxy of germinal centre selection.

2.3 Methods

2.3.1 Study approval, subjects and specimens

Specimens from 6 patients referred to the Oxford autoimmune neurology clinic who were diagnosed with CASPR2 encephalitis and 3 healthy donors (supplementary table 1) were collected at the John Radcliffe Hospital, Department of Neurology after informed consent was obtained under research ethics approval committee (REC reference: 16/YH/0013, IRAS Project ID: 195152). De-identified blood specimens were processed for isolation of peripheral blood mononuclear cells by Ficoll-Paque (Sigma-Aldrich) and cryopreserved in liquid nitrogen until use. 3 healthy donor samples used for bulk B cell cultures were obtained from leukocyte cones under research ethics approval committee (REC reference: 16/ES/0048, IRAS Project ID: 186605).

2.3.2 Live cell-based assay

HEK293T cells were seeded on 96 well cell culture plates at 40,000 cells per well in complete medium; DMEM (Sigma #D6429) with 10% FCS and Antibiotic-Antimycotic (Thermofisher #15240062). The following day, 24ug of CASPR2-GFP expression plasmid[169] was complexed for 10 minutes with 72ug of branched PEI (Sigma #408727) in phosphate buffered saline (PBS) and added to the plate; final concentration of DNA was 250ng per well. After 24 hours of expression, media was exchanged for primary samples diluted to desired concentrations in complete medium buffered with 25mM of HEPES, and incubated for 1 hour at room temperature. Cells were then washed three times in complete medium and fixed with 4% formaldehyde for 10 minutes. After additional washes, goat anti-human AF594 detection antibody (Thermofisher #A48275) was incubated for 1 hour at 3ug/ml and binding visualised on an inverted fluorescence microscope.

2.3.3 Cell labelling and fluorescence activated cell sorting

Whole PBMCs were thawed at 37°C in a water bath and transferred to complete B cell media (RPMI supplemented with 5% IgG depleted foetal calf serum (FCS), penicillin-streptomycin, L-glutamine, IgG-depleted transferrin and 2-mercaptoethanol). Samples were washed x3 in PBS with 1% bovine serum albumin(BSA, Thermofisher) and subsequently labelled at 4°C for 30 minutes with

antibodies against CD3 (clone UCHT1, Pacific Blue, BioLegend), CD14 (clone HCD14, Pacific Blue, BioLegend), CD19 (clone SJ25C1, APC-Cy7, BD Biosciences), CD27 (clone O323, BV605, BioLegend), CD20 (clone 2H7, FITC, BD Biosciences), IgD (clone IA6-2, PE-CF594, BD Biosciences) and CD38 (clone HB7, PE-Cy7, BD Biosciences). Cells were then washed x3 and DAPI (Thermofisher) added prior to sorting with a FACS Aria III. Dead cells and unwanted populations were gated as CD3-CD14-DAPI- prior to cell sorting. B cells within gates corresponding to naïve B cells (CD19+IgD+IgM+CD27-) and class-switched memory B cells (CD19+IgD-IgM-CD27+)(**figure 7A**) were positively sorted into respective wells at either 10,000 cells per well for bulk B cell cultures, or a single cell per well for single cell cultures.

2.3.4 Cell culture

For bulk B cell culture experiments 10,000 B cells were sorted per well and plated in complete B cell media and incubated for 13 days in round bottom 96-well plates with a variety of cytokines and stimulants; namely, R848 (2.5ug/ml, Enzo Life Sciences), soluble CD40L (50ng/ml, R&D systems), interleukin-2 (50ng/ml Peprotech), interleukin-1β (1ng/ml), interleukin-21 (50ng/ml PeproTech), interleukin-6 (10ng/ml R&D Systems), tumour necrosis factor-a (1 ng/ml PeproTech) and B cell activating factor (200 ng/ml R&D Systems). For single cell cultures, single B cells were sorted from the naïve and memory B cell gates into RPMI (as above)

and MS40L^{lo} cells[167], kindly donated by the Kelsoe lab (Duke University) with cytokines IL-2, IL-21, IL-4 and BAFF.

2.3.5 Determination of total and CASPR2-reactive immunoglobulins

5ul of bulk culture or single cell culture supernatants were tested for total IgM and IgG by ELISA (Bethyl Laboratories kit) after 13 days and 26 days in vitro respectively. Also, 50ul was used to determine the presence of CASPR2-reactive IgM/IgGs using live cell-based assays. HEK293T cells were transiently transfected with 0.25ug of CASPR2 DNA per well in 96 well plates. After 24 hours, conditioned media was transferred for 50ul of culture supernatants and incubated at room temperature for 1 hour. Wells were subsequently washed with HEPES buffered Dulbecco's Modified Eagle's medium (DMEM) supplemented with 10% IgG depleted FCS (Thermofisher). Cells were then fixed for 10min in 4% formaldehyde (Sigma-Aldrich) and further washed twice with phosphate buffered saline (PBS) before staining with AF594 conjugated Goat anti-human IgM (Invitrogen) or IgG (Invitrogen). Positive wells on live cell-based assay were prepared in RNAsin plus (12.8ul/ml, Promega) in TE buffer pH8 (Bioultra), flash frozen on dry ice and stored at -80°C for downstream reverse transcriptase-polymerase chain reaction (RT-PCR).

2.3.6 cDNA synthesis and amplification of VH and VL sequences

post-culture RT-PCR was performed as previously described[32] with a volume of 15.5ul per sample containing 150ng of random primers $dT_{23}VN$ (New England Biolabs, NEB), 10ul of 5X Superscript IV buffer (Invitrogen), 2.5ul of 10mM dNTP mix (NEB), 0.5ul of 25% IGEPAL (Sigma-Aldrich), 1ul Superscript enzyme IV (Invitrogen) and 0.1M DTT (Invitrogen). For variable immunoglobulin (Ig) gene amplification of immunoglobulin heavy chain (IGH) and both possible light chains (IGK and IGL) from cDNA of each well, a nested PCR strategy in two steps was performed. PCRs were performed in 96-well plates containing 2ul of leader primer mix (supplementary table 1), 10ul of GoTaq G2 Green master mix (Promega), and 6ul of nuclease free water. cDNAs (2.0 ul) were used as templates for first PCRs, and 3.5ul of unpurified first PCR product for nested reactions. Each round of PCR was performed at initial 95°C for 3min, 45 cycles at 95°C for 30s, 55°C for 30 s and 72°C for 60s, before a final 72°C for 10min.

2.3.7 Immunoglobulin sequence annotation

The second PCR products were sequenced at the Weatherall Institute of Molecular Medicine Sanger sequencing facility. Sequences were aligned on IMGT High V-quest tool (http://www.imgt.org/HighV-QUEST/) to assign germline V(D)J gene segments with highest sequence homology. Somatic hypermutations in each

immunoglobulin chain sequence were counted in comparison to the annotated germline sequences to assess the possibility of culture induced mutations.

The COvid19 Multi-omics Blood Atlas consortium's (COMBAT)[170] BCR dataset was concatenated into fasta files of $1x10^6$ sequences and individually uploaded to International ImMunoGeneTics information system® (IMGT) High V-quest for annotation. The DeWitt [171]memory B cell dataset was obtained from VDJserver (https://vdjserver.org) and used with pre-existing annotations in tab delimited format.

2.3.8 Clonal assignment

Clonality was assigned using a custom algorithm based on established principles[172], but designed to be agnostic of pre-annotated IGHV and IGHJ genes. First, nucleotide sequences corresponding to the IGHV and IGHJ gene regions, as defined by the IMGT numbering system, were concatenated. The concatenated IGHV-J sequences were then clustered by similarity using the computationally efficient CD-HIT algorithm[173] with the identity threshold set to 60%. Once clustered, within-cluster pairwise normalised Levenhstein distances were generated using the following formula:

$$NLD(s,s') = \frac{2.LD(s,s')}{|s| + |s'| + LD(s,s')}$$

where LD(s,s′) denotes the Levenshtein distance and |s|,|s′| are the lengths of sequence s and s′ respectively.

The clonal threshold was then determined using a two-step process. First, the distance-to-nearest neighbour distribution is computed using kernel density estimation. Next, the threshold is determined by finding the first local minimum by calculating the first and second derivatives of the density estimate, using the optimize() function in R (http://www.R-project.org/). To avoid algorithm failure when the distribution is not bi-modal, which can occur when sequences are either entirely non-clonal or exclusively clonal, all clonal assignments are paired with a control dataset[170,171] containing canonical B cell subsets and diverse distribution of clonality.

2.3.9 Statistical analysis and visualisation

All post-alignment analysis was performed in R (http://www.R-project.org/) and visualised with ggplot2 (https://github.com/tidyverse/ggplot2).

2.3.10 Cloning

Immunoglobulin gene cloning was performed as previously described. Restriction sites were introduced into the heavy chain (AgeI and SalI) and light chains (AgeI and BsiWI for IGK, AgeI and XhoI for IGL) using individual immunoglobulin gene-specific primers (**supplementary table 2 and 3**). PCR conditions were as above for the second PCR for heavy chains. Restriction digest was performed at 37°C for 1h in 20ul with 10ng of purified specific PCR product and 1U of each enzyme AgeI, SalI, BsiWI and XhoI (NEB). Purified products were then ligated into expression vectors containing human IGHG1, IGHM, IGK and IGL constant regions with a cytomegalovirus (CMV) promotor and ampicillin resistance. 5ul of ligation product was transformed into 20ul of high efficiency 5-alpha competent Escherichia coli bacteria (NEB). Positive colonies were sequenced for inserts and products with 100% identity to the original PCR sequence were isolated and expanded in lysogeny broth (Sigma-Aldrich) for downstream purification (Maxiprep, Qiagen).

2.3.11 Recombinant expression of monoclonal antibodies

Antibody production was performed as previously described[32]. Human embryonic kidney cells (HEK293F) were cultured in 60mls of Freestyle expression medium (Thermofisher) in 250ml Erlenmeyer flasks at 120rpm at 37°C and 8% CO_2. Prior to transfection, cells were split during logarithmic growth at $1x10^6$/ml per flask. Following 24 hours of expansion, cells were transiently transfected with a

transfection solution of 4ml phenol-red free DMEM (Gibco), 30ug HC vector, 30ug LC vector and 90ul of polyethylenimine (PEI, 1mg/ml) solution (Sigma-Aldrich. Supernatant was harvested after 5 days. For IgM expression, a stable J chain expressing HEK293T cell line was used in place of HEK293F cells.

2.3.12 Antibody purification

Automated protein-A affinity chromatography (5ml HiTrap™ MabSelect™ columns), desalting and size exclusion was performed on a single ÄKTA™ pure 25M. The instrument was operated at 4°C. After loading, the HiTrap columns were washed with 15 column volumes (CV) of dPBS followed by a one-step elution at 5 mL/min with 100mM citric acid pH3. When the $A_{280\,nm}$ exceeded a threshold value of 400 mAU, the in-line pH neutralization of the eluted protein fraction was triggered by applying a gradient of 320 mM Tris base (Sigma–Aldrich). The samples were then applied to the SEC column HiLoad™ 26/600 Superdex™ 200 prep grade (320 ml column) and equilibrated with dPBS. IgG concentrations measured on nanodrop using a molar extinction coefficient of 210,000 M-1cm-1.

2.4 Results

2.4.1 Bulk culture of naïve and memory B cells in CASPR2 patients and healthy donors

To investigate the indirect abundance of circulating CASPR2-reactive B cells from peripheral blood of CASPR2 patients and healthy donors, *ex vivo* IgD+CD27- mature naïve and IgD-CD27+IgM- memory B cells (figure 1A), were fluorescence-activated cell-sorted (FACS) from PBMCs of CASPR2 patients (n=6) and healthy donors (n=3) (**supplementary table 1**). 10,000 B cells per subset, per well, were cultured over 13 days and respective supernatants screened on live-cell based assays for CASPR2 reactivity (**figure 7B**). Confirmatory to cell sort purity, culture supernatants of naïve and class-switched memory B cells only produced IgM and IgG antibodies, respectively (**figure 7C**).

As hypothesised, IgG CASPR2-reactivity was exclusively detected within the class-switched memory compartment of 3/6 patients at an average frequency of 28.7% of total wells, but not in healthy donors (**figure 7D**). Unexpectedly, IgM CASPR2-reactivity was detected in both patients (3/6) and healthy donors (2/3) within the mature naïve B cell compartment at average frequencies of 12.3% and 7% of total wells, respectively (**figure 7D**). This indicates, that whilst naïve B cells from both patients and healthy donors have potential for CASPR2-reactivity, only patients have permissive immunoglobulin class-switch events that allow formation of CASPR2-reactive memory B cells. Of the 3/6 patients that did not have detectable

CASPR2-reactivity in either B cell subset compartment (JR024, JR061 and JR068), all were on active treatment with corticosteroids and had low recovery of total B cells (**supplementary table 1**); therefore, under sampling is likely to have been an influence.

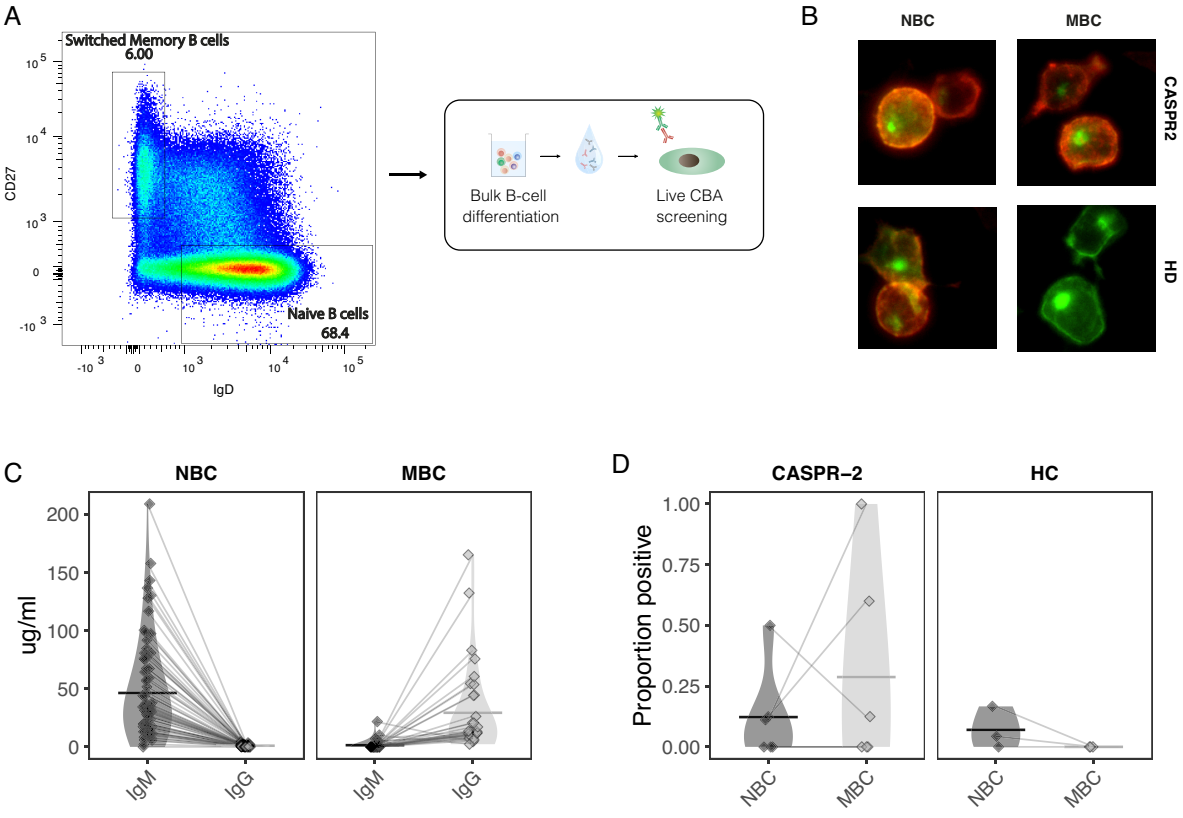

Figure 7. B cell bulk culture of CASPR2-antibody encephalitis patients and healthy donors. (A) Gating strategies for the isolation of naïve (DAPI-CD3-CD14-CD19+IgD+CD27-) and memory B cells (DAPI-CD3-CD14-CD19+IgD-CD27+) with schematic of workflow from sorted B cells to testing of culture supernatant reactivity on CASPR2-transfected HEK293T cells. (B) Representative live immunofluorescent cell-based assays are shown from tested culture supernatants demonstrating CASPR2-binding of IgMs in both patients and healthy donors, but exclusive IgG binding in patients. (C) Representative IgM and IgG ELISA data are shown from six CASPR2 patients and three healthy donors as a measure of cell sort purity, each point and connecting line is an individual well. Average IgM and IgG concentration (ng/ml) from each individual is plotted as a horizontal bar and plots are horizontally faceted for sorted B cell subsets. (D) Total proportion of positive wells are shown for all cultured B cell subsets. Lines represent each individual biological sample. HD= healthy donor; CASPR2 = CASPR2 patients; NBC = naïve B cell; MBC = memory B cell.

2.4.2 *Ex vivo* frequency of CASPR2-reactive B cells within naïve and memory compartments.

A weakness of bulk B cell cultures is the stochastic heterogeneity of antigen-specificities within each culture well; therefore, to remove the variability of cellular composition that confounds bulk B cell cultures, a single-cell B cell differentiation culture is required to identify CASPR2-reactive B cells and infer their *ex vivo* frequency. By adapting previously described single-cell B cell culture techniques[167,168,174], single sorted naïve and memory B cells were cultured on the 3T3-msCD40L feeder-line in the presence of selected cytokines (IL-2, IL-21, IL-4, BAFF, R848), inducing proliferation and differentiation into antibody-secreting cells with time-dependent expression of immunoglobulins (**figure 8A and B**). Two CASPR2-encephalitis patients with the highest proportion of positive wells, JR002 and JR060, were selected for single-cell cultures along with two healthy donors (**supplementary table 1**); notably, one patient (JR002) was untreated at the time of blood collection, allowing for an immunotherapy-free perspective of BCR reactivities in CASPR2-encephalitis. Additionally, two healthy donors were selected for parallel single-cell cultures. Due to difficulties in obtaining age and sex matched controls, the two donors were not well matched.

From all donors, a total of 6432 mature naïve B cells and 5726 class-switched memory B cells were cultured (**supplementary table 1**), of which 44 candidate naïve B cells and 13 memory B cells that bound CASPR2 live cell-based assays were chosen for cloning and recombinant expression of variable domains grafted into an IgM or IgG1 backbone, respectively. Whilst IgG4 is the predominant IgG subclass in patients with CASPR2- antibody encephalitis, it was not chosen as the representative constant region for binding characterisation, due to the possibility of IgG4-F(ab)-arm swapping in mildly reducing conditions[175]. Following reverse transcription and two step PCR with nested primers, 3 wells did not produce PCR products and 2 wells contained out of frame variable domain sequences resulting in a total of 52 B cell candidates that produced functional paired heavy and light variable domains. The absence of variable domain mutations in the naïve B cells suggests that activation of AID *in vitro* is unlikely to occur (**figure 8C**) and thus, post-culture memory B cell mutation frequencies are likely representative of parent wildtype variable domains. Of the productive candidate wells, 13/41 naïve and 1/11 memory B cell-derived mAbs did not bind when re-screened at 5ug/ml on live-cell based assay; when examined, contamination of non-binding wells from neighbouring binding wells was likely. Further, 3/41 naïve B cell-derived mAbs reacted to un-transfected HEK cells, leaving 25 naïve and 10 memory-derived CASPR2-reactive

BCRs for downstream analysis (**figure 8D**). Similar to the bulk culture observations, CASPR2-reactive naïve B cells were observed in both patients and healthy donors at a frequency, within the naïve B cell pool, of 0.3-0.4% and 0.4% respectively. Reassuringly, observations from bulk cultures remained consistent; CASPR2-reactive memory BCRs were only seen in CASPR2-encephalitis patients at a frequency of 0.2-0.3%, confirming the observation to be reproducible at the single cell resolution.

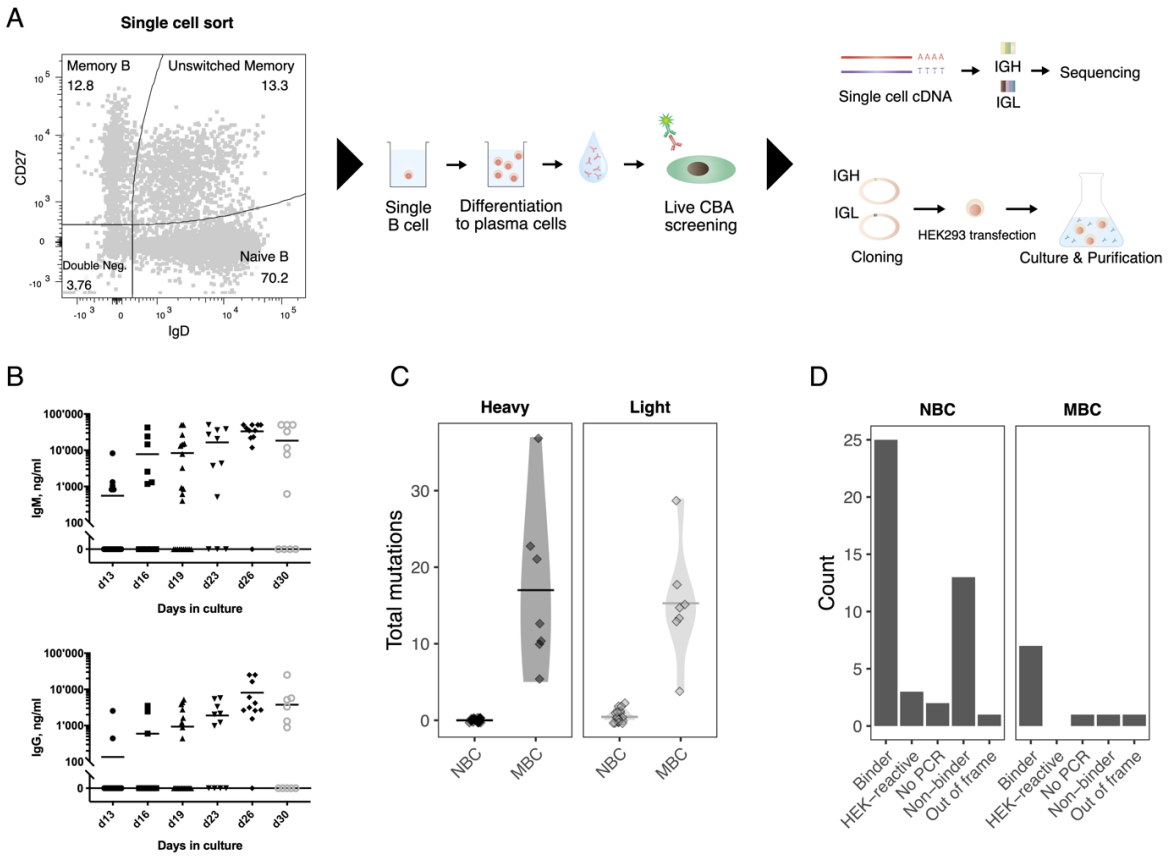

Figure 8. Single B cell culture, identification of CASPR2-reactive B cells and recombinant antibody generation. (**A**) Gating strategies for the isolation of naïve (DAPI-CD3-CD14-CD19+IgD+CD27-) and memory B cells (DAPI-CD3-CD14-CD19+IgD-CD27+) with schematic of workflow of single-cell culture of B cells. (**B**) IgM and IgG ELISA data are shown from optimisation cultures, demonstrating Ig production over days in culture. (**C**) Violin plots of somatic hypermutation counts from cultured B cells. Horizontal bars denote the mean mutations. (**D**) Bar plots of recombinant mAb screens of candidate wells. NBC = naïve B cell; MBC = memory B cell; IGH = immunoglobulin heavy chain; IGL = immunoglobulin light chain.

2.4.3 An optimised clonal assignment

In order to assess the clonality of the CASPR2-specific B cell repertoire, I generated a custom computational algorithm, modelled on principles established in the literature. Traditionally, clonal assignment is performed by grouping heavy chain

VDJ sequences by their closest-aligned IGHV and IGHJ gene pairing, followed by clustering of the HCDR3 region[172]. The HCDR3 region is the most variable portion of the variable domain, as this is where 3 gene segments (V_H-D_H-J_H) are joined. Further, due to non-template additions and recombination events of higher complexity such as inversion or fusion of D_H, the potential number of unique combinations is predicted to be 10^{14}; therefore, making this region an ideal co-discriminator of clonal identity. Whilst this traditional approach performs reasonably, there are limitations. Most importantly, it is reliant on post-hoc IGHV and J genes annotations by sequence alignment tools; whilst this may be robust in germline genes found in the naïve B cell populations, in memory B cells, the accuracy of gene annotations in variable domains that have high frequencies of somatic hypermutations is unpredictable. Therefore, the best approach should be agnostic of alignment-dependent gene annotations.

To circumvent the dependence on pre-annotated gene assignments, I concatenated full-length nucleotide sequences corresponding to the IGHV and IGHJ gene regions, as defined by the International ImMunoGeneTics information system® (IMGT) numbering system. Then, the concatenated IGHV-J sequences were clustered by similarity using the computationally efficient CD-HIT algorithm[173]. Once clustered,

within-cluster normalised Levenshtein's distance matrixes were generated for all CDR3 regions and clonal thresholding performed on the resulting pairwise distances. To validate my approach, a control SARs-CoV-2 BCR dataset, that I analysed for the COMBAT consortium[170], was clonally assigned together with the CASPR2-specific sequences (**figure 9A**). Indeed, when inspecting silent and non-silent mutations according to IMGT numbering, the clonal assignments are robust with preserved stem mutations in clonal members (**figure 9B and C**). Confirmatory, multiple sequence alignments of the HCDR3 region confirm within-clone homology (**figure 9D and E**).

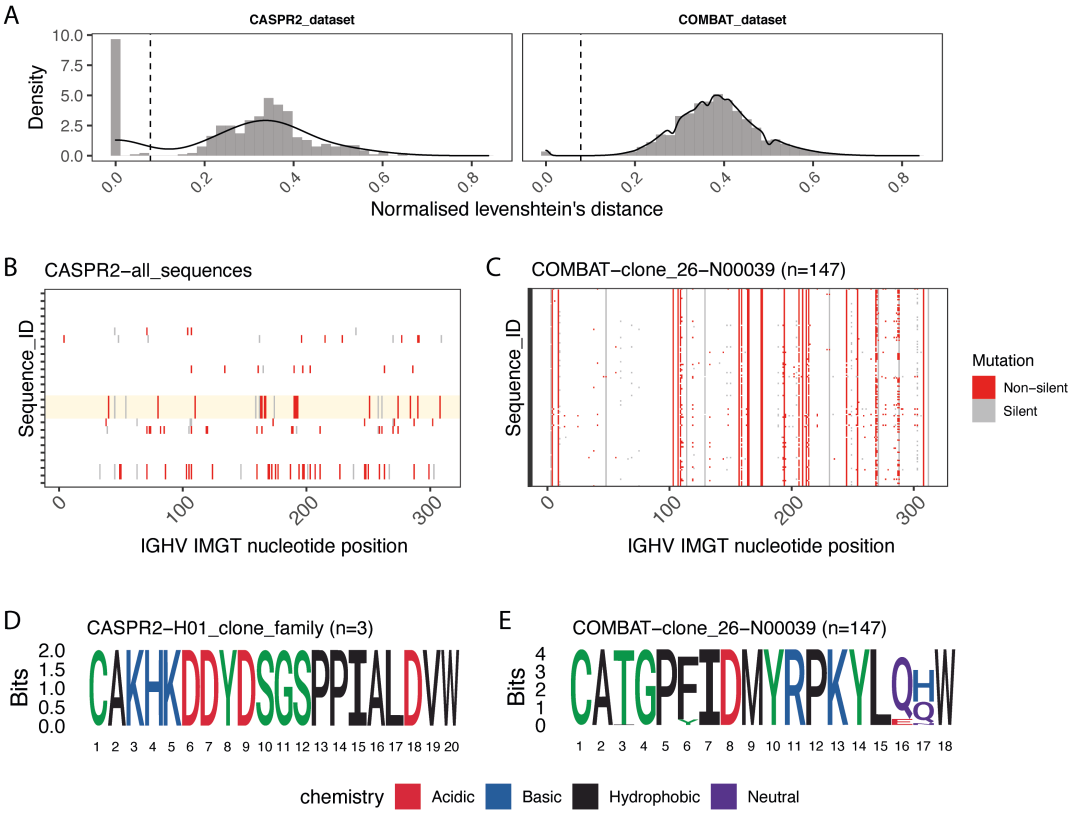

Figure 9. Clonal assignment of BCRs. (A) Density histograms of normalised Levenshtein's distances across CASPR2 BCR heavy chain sequences and SARs-CoV-2 BCR heavy chain sequences (COMBAT dataset). Solid black line is the density estimate as defined by ggplot2 function <geom_density()>. (B, C) Mutation position plots for all CASPR2 BCR heavy chain sequences (B) and an enlarged clone (clone26-N00039) of n=147 from the COMBAT dataset (C). In (B), the yellow band highlights the H01 clonal family. Red tiles indicate non-silent mutations at the relative IMGT defined nucleotide positions, as denoted by the x axis. Gray tiles indicate silent mutations. (D) Sequence logo of the junction region of the H01 clonal family. Sequence logo is coloured by biochemical properties as defined in the legend. (E) Sequence logo of clone26-N00039 family junction regions.

2.4.4 Clonality and variable domain features of CASPR2-reactive BCRs

To assess the clonality of the CASPR2-reactive BCR landscape, I applied the clonal assignment algorithm to the single-cell culture derived CASPR2-reactive sequences. As expected naïve B cell-derived sequences in all biological samples were highly

polyclonal (**figure 10A and B**), an observation consistent with the stochastic nature of VDJ recombination prior to selection bias by antigen-driven exposure. Conversely, within the memory B cell compartment of patient JR060, there was observable clonal expansion (**figure 10A**); from 5 CASPR2-specific memory B cell sequences, 3 and 2 sequences were identical respectively. To test if the detection of 2 independently expanded clones, from a total of 1598 memory B cells, occurred more than by chance, I subsampled randomly 2000 memory B cell heavy chain sequences without replacement over 1000 bootstraps from three published healthy individual memory B cell repertoires[171]. The total repertoire sizes of these healthy individual memory B cell compartments are; HD1 n=5.5x10^6, HD2 n=6.7x10^6 and HD3 n=5.2x10^6. In order to count number of expanded clones, clonal expansion was binned into two groups, clones of size >1 and clones of size >2, to account for the clone sizes of the expanded clonal families, H02 and H01 respectively. Over 1000 bootstraps, I observed averaged ranges of 8.7-22.6 (SE; 0.093-0.14 and SD; 2.9-4.5) clonally expanded B cells of >1 member, per 2000 subsampled contigs (**figure 10C**). For clonally expanded B cells of >2 members, the average range reduced to 1.1-1.5 (SE; 0.023-0.029 and SD; 0.3-0.72). Overall, the observation of 2 clonally expanded B cells in patient JR060, is within the expected *ex vivo* frequency. Additionally, whilst JR060 was clonal in their CASPR2-specific memory compartment, JR002 was highly polyclonal

(**figure 10A**); all 5 memory B cells detected from 2208 B cells were non-clonally related.

Next, I examined the frequency of IGHV and J gene usage across the CASPR2-specific BCRs (**Figure 10D**). Within the naïve compartment, there was an observational predominance of IGHJ6*02 gene usage (7/16) in CASPR2-encephalitis patients and IGHJ4*02 (4/8) in healthy donors. IGHV gene pairing within the naïve compartment did not show skewing towards one particular gene, however IGHV3 family genes were most represented, 9/16 and 6/8 in CASPR2 patients and healthy donors respectively. Within the memory compartment, 3/7 unique memory B cell BCRs used the IGHV3-23 gene paired with different IGHJ genes. While IGHV3-23 is the most prevalent IGHV gene in healthy donor repertoires[176], it is proposed to be less represented within the class-switched memory B cell population[177,178].

Finally, I assessed the mutational profile and HCDR3 biochemical properties to look for indirect evidence of affinity maturation and signatures of autoreactive/promiscuous binding (figure 9E-G). As stated prior, reassuringly, the recovered naïve B cell BCRs are predominantly mutation free (figure 9E). Where low number of mutations occurred within the light chains in 7 mAbs, 5 could be

mapped back to primer induced errors, with the remaining 2 deemed genuine mutations. The memory B cells had mutation counts ranging from 5-37 in both heavy and light chains, inferring that they have potentially undergone rounds of affinity maturation in germinal centre reactions. Inspecting the junction region, the CDR3 region with preservation of conserved flanking residues as defined by IMGT, there was no significant difference in mean amino acid length across patients and healthy donors, or across B cell subsets, p value = 0.78 and 0.89, respectively (figure 9F, two-way ANOVA). Similarly, the same comparisons yielded no significant difference in junction hydrophobicity, p value = 0.36 and 0.28, respectively (figure 9G).

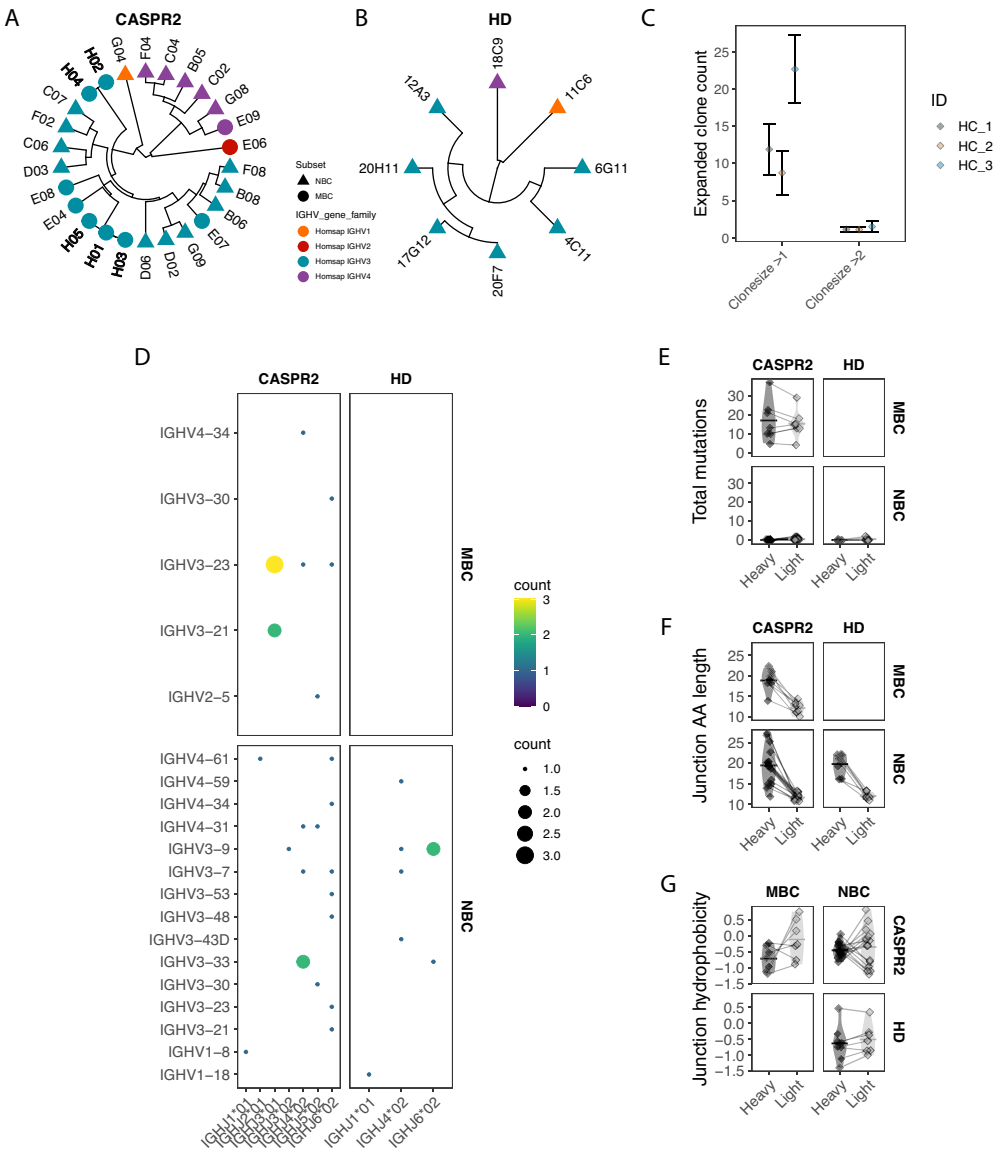

Figure 10. Sequence properties of CASPR2 patient and healthy donor derived BCRs. (A, B) Sequence phylogeny dendrograms of CASPR2 (A) and healthy donor (B) heavy chain sequences. Colours depict IGHV gene families and shapes depict B cell subsets from which sequences are derived. Clonal members are highlighted in bold. (C) Bootstrapped clonality testing. Memory B cell BCR repertoires from three healthy donors were subsampled randomly 2000 times without replacement over 1000 iterations. Assessment of clonality was binned into two groups, counting number of detected clones of n>1 and n>2. Mean clone counts over 1000 iterations are shown across three donors. Error bars depict standard deviation from the mean. (D) Paired IGHV and IGHJ gene usages are shown across each individual BCR sequence from CASPR2 patients and healthy donors. Point size and colour depict the total number of IGHV-IGHJ combinations. (E) Violin plots of total mutations, faceted horizontally across study groups and vertically across B cell subsets. (F) Violin plots of Junction amino acid lengths. (G) Violin plots of junction hydrophobicity. (E-F) All analysis was performed across heavy and light chains. Paired chains are denoted by the connecting horizontal lines.

2.5 Discussion

In this chapter, I have analysed bulk and single B cell culture data to investigate *ex vivo* frequencies and sequence characteristics of CASPR2-specific B cells in patients and healthy donors. I was able to demonstrate that both CASPR2-encephalitis patients and healthy donors have permissive early B cell tolerance checkpoints that allow the formation of a repertoire of CASPR2-reactive naïve B cells. From single cell cultures, healthy donors had comparable frequencies of CASPR2-specific naïve B cells (0.4%) to CASPR2-encephalitis patients (0.2-0.4%). Interestingly, I further identified that the presence of CASPR2-specific class-switched memory B cells, at a frequency of 0.2% and 0.3%, is exclusive to patients. This suggests that the formation of immune memory to CASPR2 protein may be a disease-specific defect in post-germinal centre B cell tolerance. These observations mirrored findings from prior bulk B cell cultures with higher magnitudes of biological replicates and total sampled B cells, thus supporting their reproducibility. Additionally, within the CASPR2-reactive BCR repertoire, across two patients, both clonal and polyclonal responses are detectable within the memory B cell compartment; suggesting that clonality of CASPR2-specific B cells can be heterogenous across individuals. IGHV3 family genes were highly represented but with no distinct biochemical features of the variable

domains. This is not surprising, as despite recovering 35 unique paired heavy and light chain sequences, there is insufficient power to detect shared features that overcome the heterogeneity of finer epitope targets. Indeed, this traditional approach to antibody feature analysis is likely to change as it has become clear that biochemical features are not shared across the discrete antibody paratope/epitope space[179].

Rationalising these findings, previous groups have shown that a degree of autoreactivity, defined as reactivity to Hep-2 cell lysate, is observed in ~20% of the healthy donor naïve B cell compartment[42,180], and are probabilistically derived from the semi-stochastic nature of VDJ-recombination. However, our observations of naïve B cell antigen specificity to a discrete neuronal target protein, has not been previously shown in NSAb-diseases. Intriguingly, distinct "autoantigen" reactivities within the naïve B cell population have been alluded to in studies of peripheral blood B cells in Anti-Neutrophilic Cytoplasmic Autoantibody (ANCA)-associated vasculitis[181], Pemphigus vulgaris[182] and Rheumatoid arthritis[183], at a frequency of ~2%, <0.2% and 0.14% of the naïve B cell (CD19+IgD-CD27-) populations, respectively. Additionally, consistent with my observations, differential enrichment of autoantigen tetramer-stained B cells within the class-switched compartment of

patients, has been reproducibly seen across diseases with a distinct autoantigen target[182–185]. However, only two of these studies have experimentally validated the specificity of autoantigen binding in the class-switched memory B cell population[183,185] and none in the naïve B cell population. Indeed, some studies recognise this limitation and postulate that naïve compartment reactivity may derive from innately polyreactive "natural" IgM antibody-producing B cell precursors[181,182]; however, this remains an unsubstantiated hypothesis.

Overall, my findings support a patient-exclusive post-germinal centre failure to negatively select autoantigen-reactive B cells in CASPR2-antibody encephalitis. This represents, to the best of my knowledge, is the first study to validate naïve B cell autoantigen-specific binding in patients and healthy donors. The latter validation is of particular importance, as the *bona fide* presence of circulating autoantigen-reactive naïve B cells, may plausibly be a persistent source of *de novo* antibody-secreting cells, if activated. Further, the presence of class-switched and highly mutated memory CASPR2-sepcific B cells, support the disease-specific breakdown of post-germinal centre tolerance checkpoints in patients but not healthy individuals and a likely role for T cell-dependent help. This is in harmony with the observed type 2 HLA-DRB1*11:01 association[131,186], as CD4+ T-cell mediated help is thought

to be MHCII-dependent, and strengthens the distinction of mono-autoantigen-associated antibody syndromes from systemic lupus erythematosus (SLE). In SLE, extrafollicular T-independent differentiation of naïve B cells to plasmablasts is the predominant feature[187–189] and is conversely associated with a multitude of autoantigen targets[190].

2.6 Conclusion

These findings demonstrate that post-germinal centre tolerance breakdown in CASPR2-encephalitis appears to be disease-specific, lending weight to the recently discovered HLA association and the likely important role of CD4+ T cells. Further, in health, pre-germinal centre tolerance checkpoints permit a natural degree of CASPR2 reactivity. Taken together, they support a model where the CASPR2-reactive naïve B cell repertoire may serve as a pool of resting autoreactive B cells that have potential to form aberrant B cell responses in disease. Indeed, such failures of peripheral B cell tolerance may be amenable to immune tolerance restorative therapies. This chapter highlights the importance of studying B cells at single cell resolution and across developmental checkpoints to gain better insights into the underlying B cell immunobiology of antibody-mediated autoimmunity.

2.7 Acknowledgements

Anne-Katrin Kienzler performed the bulk and single cell B cell cultures, and produced figure 2B. Mateusz Makuch, Deniz Akdeniz and Patrick Waters performed amplification of BCR variable domain sequences from single-cell lysates. Rachael Bashford-Rogers shared template B cell clone calling scripts as reference and provided invaluable advice on bioinformatic analysis approaches to BCR repertoire analysis.

Chapter 3, Binding properties of CASPR2-specific monoclonal antibodies

3.1 Introduction

Chapter 2 identified permissive B cell tolerance checkpoints that allow for presence of CASPR2-reactive naïve B cells in both patients and healthy donors, but only memory B cells in patients. These observations support the notion that formation of B cell memory, to CASPR2 protein, is an aberrant autoimmune response that appears to be suppressed in healthy individuals. However, in order to better understand the biological implications, it is crucial to characterise the binding properties of these CASPR2-targeting BCRs and their representative mAbs.

Studies to date have attempted to characterise the binding properties of CASPR2-reactive autoantibodies from patient sera. The diagnostic feature across all studied patients with CASPR2-antibody encephalitis, is the ability of sera to bind the extracellular domain of human CASPR2. Interestingly, across three studies, the epitope landscape appears to be consistently biased towards binding of the N-terminally located Discoidin and Laminin G-like 1 domains[86,134,147], implying domain-specific selection pressure. Further, sera are proposed to bind CASPR2 irrespective

of tertiary structure and glycosylation[134], thus supporting the potential existence of linear epitopes.

While these studies are informative, key limitations are evident. First, is the lack of single antibody resolution from unrefined polyclonal sera; this makes inference of epitopes susceptible to non-specific cross-reactivity from polyreactive antibodies. Second, an important, yet unaddressed factor within the wider NSAb-disease field is the interchangeable use of human vs. murine tissue in both diagnostic and research assays. Though CASPR2 is a conserved protein across humans and mice, with 94.1% amino acid homology, there are 21 total residue changes in the proposed immunodominant domains, Discoidin and Laminin G-like 1. In the context of antibody binding, any single residue change can potentially reduce or abrogate binding[191–193], thus making the validation of autoantibody binding across species an imperative experiment.

In this chapter, by using patient-derived mAbs, molecular techniques and cross-species immunoassays, I aimed to comprehensively characterise the binding strength, epitopes and cross-species reactivity of CASPR2 autoantibodies at monoclonal antibody resolution.

3.2 Hypothesis

3.2.1 Patient-derived CASPR2-reactive mAbs recapitulate epitope dominance observed in studies of patient sera.

3.2.2 CASPR2-reactive mAbs binding is dependent on tertiary structure and correct glycosylation.

3.2.3 Murine CASPR2 will not recapitulate CASPR2-reactive mAb binding to human CASPR2.

3.3 Methods

3.3.1 mAb cloning and expression

mAb cloning was performed as per **chapter 2 methods**. To generate an IgG4 expression vector, a gene fragment corresponding to the coding region of the human IGHG4 gene was synthesised by Integrated DNA Technologies (IDT) and subcloned into the AbVec vector[44] using restriction sites AgeI and SalI. The cloned sequence was validated with Sanger sequencing. Recombinant expression of mAbs was performed as per **chapter 2 methods**.

3.3.2 F(ab) fragment generation

F(ab)s were generated using the Pierce™ F(ab) preparation kit (Thermofisher # 44985). In brief, immobilised papain was first equilibrated with Pierce digestion

buffer. Purified mAbs were then incubated at 37^{0}C with agitation. Following digestion, Fc fragments and undigested IgG were removed by protein A adsorption. Purified F(ab)s were then concentrated and buffer exchanged into PBS using 3kDa Amicon® Ultra filters (Merck # UFC5003). Digestion efficiency was assessed via SDS page.

3.3.3 CASPR2-CASPR4 domain swaps

Full length CASPR2-EGFP[169] was used as template. Gene fragments corresponding to CASPR4 protein domains, Discoidin, Laminin G-like 1-4 and Fibrinogen C-terminal, were synthesised by IDT with complementary overhangs corresponding to the matched flanking 5' and 3' regions of CASPR2. Alignment of respective domains were defined by Uniprot (https://www.uniprot.org) numbering and MAFFT[194] multiple sequence alignment. Each individual domain was sequentially swapped by overlap extension PCR using an insert to donor vector ratio of 3:1 and Q5 high fidelity master mix. The insert and vector underwent denaturation (98^{0}C for 30s), annealing (60^{0}C for 30s) and polymerase-catalysed extension for 30s per kb, for a total of 34 cycles. To remove template plasmids, PCR products were then digested with DpnI at 37°C for 1 hour prior to transformation of competent E. coli cells. Colonies were subsequently screened and validated with Sanger sequencing by Source

Bioscience. All cell-based using CASPR2-CASPR4 domain swap constructs were performed as per **chapter 2** live-cell based assay (**section 2.3.2**).

3.3.4 Surface quantification of protein expression

All deletion and domain swap constructs were first individually transfected in triplicate. 3ug of expression plasmid was complexed with branched PEI at a DNA to PEI molar ratio of 1:3, for 10 minutes at room temperature (RT). DNA-PEI complexes were then added to 2mls of complete media and exchanged on a monolayer of HEK293T cells in 6 well culture plates; plated 24 hours before, at a cell density of 900,000 cells/well. After 24 hours of expression, wells were washed twice with PBS and stained for 1 hour at RT with a rabbit polyclonal anti-human CASPR2 antibody mix (Thermofisher, #PA5-28969) at a dilution of 1:400. Subsequently, cells were washed twice with PBS and stained for 1 hour at RT with a goat anti-rabbit secondary antibody, labelled with AF4594 (#A-11012). Following three further washes with PBS, AF594 and EGFP fluorescence was quantified on a BMG OMEGA FLUOstar using filters 485/520 and 560-10/650 respectively.

3.3.5 Protein expression and purification

The extracellular domain of CASPR2, fused to an AviTag and hexahistidine tag (gift from Jiandong Huo, Owens lab, Harwell, University of Oxford), was recombinantly

expressed in HEK293F cells for use in indirect ELISA. Expressed CASPR2-ECD was metabolically biotinylated with co-expression of BirA biotin ligase using a BirA expression plasmid[195] (gift from Benjamin Bishop, Strubi), in the presence of 5mM of D-biotin and purified by nickel-nitrilotriacetic (Ni-NTA) chromatography. Successful biotinylation was validated by streptavidin agarose precipitation and SDS page.

3.3.6 De-glycosylation and denaturation of CASPR2-ECD

De-glycosylated CASPR2-ECD was obtained by overnight incubation with PNGaseF (NEB# P0704S) in x1 Glycobuffer (NEB # B0701S), and band shift visualised on SDS-page (Figure XXXXXB). PNGaseF was then removed by 100kda size-exclusion ultrafiltration for downstream application in ELISA. Finally, to generate non-conformational protein, CASPR2-ECD was heat treated for 10 minutes at 95^0C and used immediately for indirect ELISA.

3.3.7 Indirect ELISA

Protein aggregates were first removed to ensure accurate coating concentrations. Untreated, de-glycosylated and heat treated CASPR2-ECD were centrifuged at 14,000xg and concentrations re-quantified by nanodrop at absorbance of 280nm. 96 well Nunc-Immuno plates (#446442) were then coated with 4ug/ml of each

CASPR2-ECD preparation at 4^0C, overnight. The next day, wells were washed with three times with pH7.4 Tris buffered Saline supplemented with 0.05% Tween-20 (TBS-T) and blocked for 1 hour with blocking buffer (TBS-T with 1% BSA). MAbs were applied at 5ug/ml and incubated at room temperature for 1 hour followed by three further washes. All mAbs were tested in triplicate to assess reproducibility. Next, goat anti-human HRP detection antibody (Thermofisher #A18805) or Streptavidin-HRP (Biolegend, #405210) were added at 50ng/ml and 200ng/ml respectively. After three further washes, plates were developed with TMB substrate (Bethyl laboratories #E102) for 20 minutes and reaction stopped with 0.16M sulfuric acid and absorbance measured on a BMG Omega FLUOstar at 450nm.

3.3.8 Immunohistochemistry staining

Adult female Wistar rat brains were harvested and fixed in 4% paraformaldehyde in PBS for 1 hour. Brains were then transferred to 40% sucrose for 48 hours and snap frozen in isopentane cooled with dry ice. 10µm section were cut and mounted on superfrost charged glass slides and stored at -20C until use.

Slide sections were first blocked using 4% goat serum and endogenous peroxidase quenched with 0.3% hydrogen peroxidase for 10 minutes. Primary mAbs were then applied at 50ug/ml in PBS and incubated overnight at 4^0C. Slides were then washed

in PBS and incubated with either AF488-conjugated or biotinylated goat anti-human secondary antibody at 1:500 dilution, for 1 hour at room temperature. For biotinylated goat anti-human secondary stains, the Vectastain® Elite® ABC HRP kit (PK8200, Vector Laboratories) was used and developed with diaminobenzidine. Slides were further counterstained with cresyl violet for 3 minutes and finally dehydrated with ethanol and mounted with VectaMount® (H-5000-60, Vector Laboratories).

3.3.9 Neuronal cultures

Brains from Wistar rat pups (postnatal Days 1–3) were placed into Hanks balanced salt solution (HBSS) with 10mM HEPES buffer (pH 7.3). Hippocampi were dissected and incubated with 2.5% trypsin at 37^0C for 15 min, washed three times in HBSS and taken up in 500ml neuron media. Hippocampi were dissociated with a narrowed glass pipette, cells counted and plated at 40 000 cells/well in neurobasal media on 12mm poly-L-lysine (PLL)-treated coverslips. After 4–5h, attached neurons were supplemented with astrocyte conditioned media and cultured for 7–21 days. Staining was performed as per live-cell based assay (**section 2.3.2**).

3.3.10 Surface plasmon resonance

200-250 RU of anti-CASPR2 mAbs were captured in flow cell 2 of a Series S Sensor Chip Protein A (Cytiva). 250RU of an anti-SARS-CoV-2 control mAb were captured into flow cell 1 of the same chip. Single cycle kinetics were performed using a 2-fold concentration series of CASPR2 using 6 concentrations per cycle and a blank. A contact time of 120s, dissociation time of 600s and a flow rate of 30ul/min were used. All experiments were performed at 37°C in HBS-P running buffer (Cytiva) using a Biacore 8k (Cytiva). For analysis sensograms were double reference subtracted (blank subtraction and reference flow cell subtraction) and analysis was performed using Biacore Insight Evalutation Software version 2.0.15.12933.

3.3.11 Epitope binning

HEK293T cells were seeded at a density of 40,000 cells per well. After 24 hours of incubation in complete media, cells were transfected with CASPR2-EGFP (**section 2.3.2**). CASPR2-expressing HEK cells were then saturated with an excess of each unlabelled mAb (100ug/ml). Once incubated for 60 minutes to allow full saturation of CASPR2 by the primary mAb, AF594 labelled mAbs (Thermofisher # A20185) were added at 10ug/ml. Following a further incubation of 30 minutes, wells were washed with PBS and finally, AF594 fluorescence detected on a BMG Omerga Fluostar fluorescence plate reader with excitation at 560nm and detection at 610nm. The level of each mAb's maximal binding fluorescence was assigned using the control

mAb A33 (supplied by UCB pharma), which is not expected to compete for CASPR2 protein; thus, percentage inhibition was calculated as the percentage reduction from maximal binding.

3.3.12 Mouse CASPR2 cloning

The full nucleotide sequence encoding mouse CASPR2 (Uniprot accession #Q9CPW0) was directly subcloned into a pre-linearised pcDNA3.1 vector through overlap extension PCR of two gene fragments with a 30bp homologous corresponding to nucleotide positions 1682-1712. The PCR reaction was further transformed in competent E. coli cells and correct colonies validated by Sanger sequencing.

3.4 Results

3.4.1 The influence of valency on CASPR2 binding

In **chapter 2**, I validated the specific reactivity of naïve B cells to CASPR2 protein in both patients and healthy donors. However, as initial reactivity screens were performed using IgM-containing culture supernatants and recombinant decavalent IgM mAbs, it remains unclear if these unmutated CASPR2-reactive BCRs are of sufficient avidity to bind as IgGs or monovalent F(ab) fragments. Such distinctions are important to make, as high affinity germline BCRs are anticipated to bind native

epitopes without further affinity maturation and therefore, may have disease-relevance if ever secreted as soluble IgG.

To investigate the influence of valency on CASPR2 binding across recovered BCRs, naive and memory B cell paired heavy and light chain VDJ sequences were screened as recombinant IgMs, IgGs and F(ab) fragments, at 5ug/ml (**figure 11A**). Dot-plots of cell-based assay (CBA) binding scores across immunoglobulin formats are shown in **figure 11B-C**. In patients, unmutated naïve B cell-derived mAbs reproducibly bound as native decavalent IgMs, but lost binding as bivalent IgG1s; thus, their binding is dependent on avidity (**figure 11B**). Similarly, in healthy donors all unmutated naïve B cell mAbs bound as IgM, but surprisingly, 3/8 mAbs also retained weak reactivity to CASPR2 as IgG1s (**figure 11C**). Exploring this further, the 3/8 mAbs did not bind as F(ab) fragments suggesting that their CASPR2 binding remains avidity dependent. In contrast to naïve B cell mAbs, mutated memory B cell-derived mAbs bound robustly as both IgM and IgG1s. As expected, all mAbs bound with higher CBA scores in IgM format (**Figure 11B**), validating the expected increase in binding strength with additional avidity. Further, all memory B cell F(ab)s displayed strong monovalent binding of CASPR2, confirming their superior affinity for CASPR2 when comparing to naïve B cell-derived mAbs.

I next explored whether degree of somatic hypermutation correlates with binding strength in memory B cell mAbs (**Figure 11 D-F**). Pseudo-quantitative CBA scores, scored identically by 3 independent readers, were correlated with non-silent and silent mutations as defined by IMGT alignments; whilst silent mutations do not contribute to variable domain structure, their accruement remains a footprint of affinity maturation, and thus, were included in this analysis. In these mAbs, higher numbers of mutations did not correlate with better binding strength (Pearson correlation coefficient); this is likely due to the distinct clonal identities of the mAbs, as non-related clones are not likely to have undergone linear trajectories of affinity maturation.

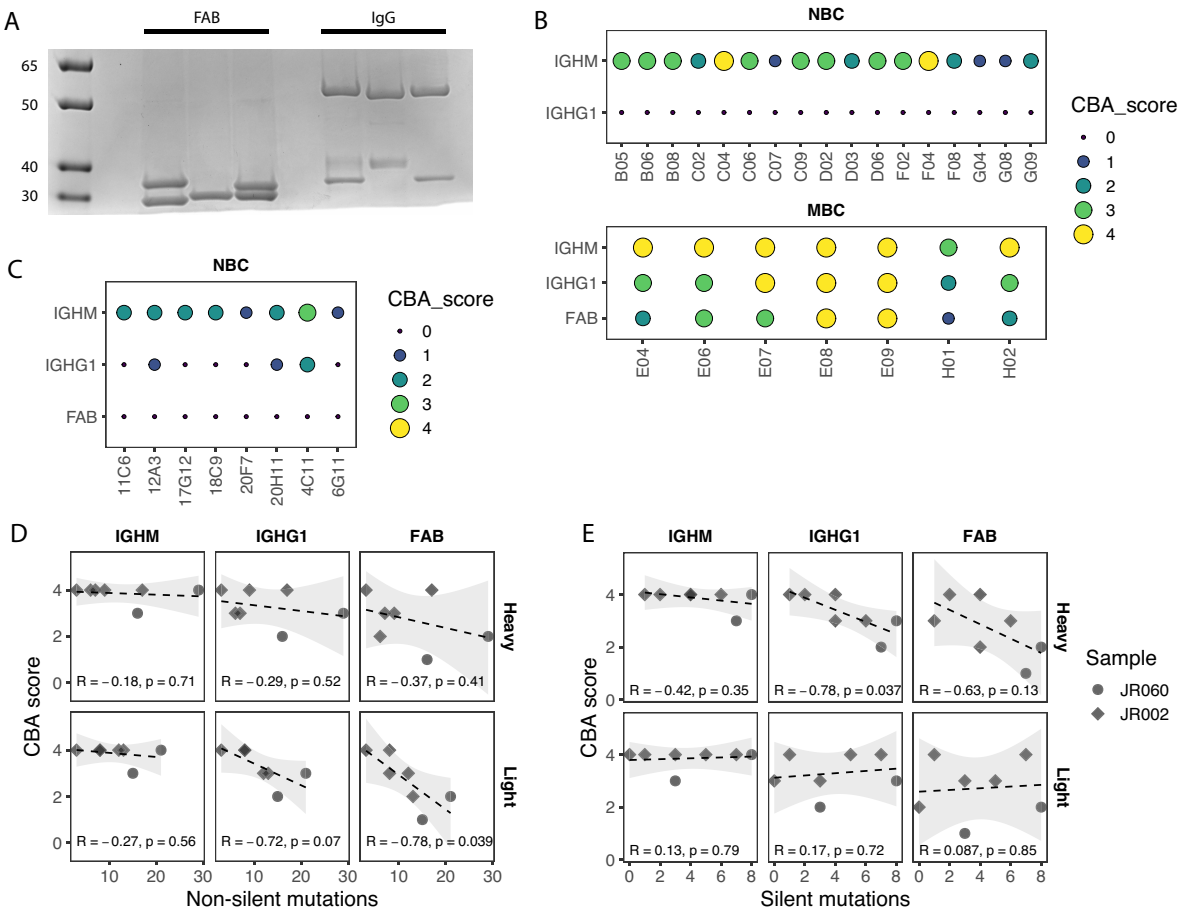

Figure 11. Assessment of isotype antibody binding avidity. (A) Reduced SDS page of F(ab) fragments and full IgG. Protein staining was performed with Coomassie blue. (B) Dot-plots of live-cell based assay scores of CASPR2 patient-derived naïve (NBC) and memory (MBC) mAbs in IgM, IgG1 and F(ab) fragment formats. (C) Dot-plots of live-cell based assay scores of healthy donor-derived naïve B cell mAbs in IgM, IgG1 and F(ab) fragment formats. (D) Correlation analysis of cell-based assay (CBA) scores and number of non-silent IGHV gene mutations across mAb formats and chains; Pearson correlation coefficient are indicated. (E) Correlation analysis of cell-based assay (CBA) scores and number of silent IGHV gene mutations across mAb formats and chains; Pearson correlation coefficient are indicated.

3.4.2 The epitope landscape of CASPR2-reactive B cells

One intriguing aspect from existing serological studies of CASPR2-encephalitis patients, is the prominent reactivity of patient sera to the Discoidin and Laminin G-like 1 domains[86,134,147]. Other domain reactivities have been alluded to, but their fine-

grained examination remains absent. Therefore, the patient-derived mAbs, offer an opportunity to probe domain specificities at the single-antibody resolution across independent clones.

Using deletion constructs (**figure 12A**, gifted from the neuropathic pain group, Prof. David Bennett, NDCN), reactivities of naïve and memory-derived mAbs were tested. First, surface expression of all constructs was validated using an anti-human CASPR2 polyclonal antibody cocktail raised against the extracellular domain of CASPR2 (**figure 12B**). Next, mAbs were incubated systematically and domain specificities inferred from the combinatorial binding to each construct (combinations depicted in **figure 12A**). In keeping with the literature, five out of seven memory-derived mAbs were predominantly reactive to the Discoidin domain whereas the remaining two were reactive to a region corresponding to the Laminin G-like 3, EGF2 and Laminin G-like 4 domains (**figure 12C**); due to the nature of the deletion constructs, it was not possible to distinguish between these domains. Unexpectedly, the reactivities of the naïve B cell-derived mAbs did not overlap with the memory compartment (**figure 12C-D**); nine mAbs bound only in the presence of the EGF1 and Fibrinogen-like C domains; eight bound the Laminin G-like 2 domain; three

bound the Laminin G-like 1 domain; and four were indeterminate, due to non-domain compatible staining patterns.

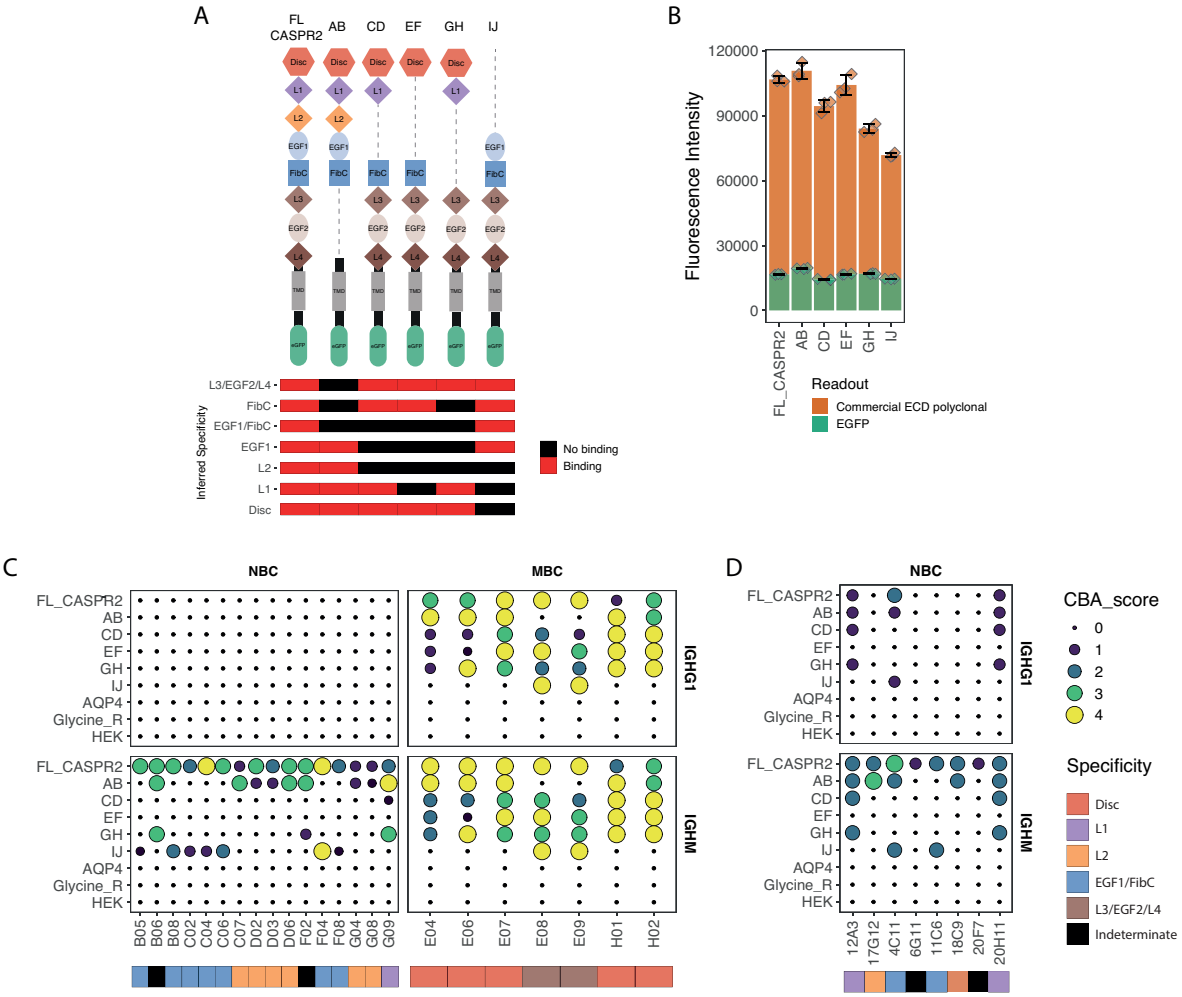

Figure 12. Assessing CASPR2 domain specificity using deletion constructs. (A) Cartoon linear representations of Bennett group (NDCN) deletion constructs and their combinatorial inference of domain specificity, located below. (B) Assessment of surface expression of individual deletion constructs compared to full length CASPR2 protein (FL_CASPR2). Orange denotes fluorescence intensity of detection secondary antibody and green denotes fluorescence intensity of EGFP. Bars are unstacked; therefore, points indicate absolute values of triplicate experiments. (C) Dot-plots of live-cell based assay scores across patient-derived naïve (NBC) and memory (MBC) mAbs across IgM and IgG1 formats. (D) Dot-plots of live-cell based assay scores across health donor-derived naïve (NBC) and memory (MBC) mAbs across IgM and IgG1 formats. (C, D) Specificities of binding combinations are indicated below each dot-plot. Colours indicate domains targeted as specified by the legend.

To dissect the specificities of the L3/EGF2/L4 targeting mAbs further, I generated CASPR2 domain swap constructs with the family-protein CASPR4 (**figure 13B**). Upon SIM (https://web.expasy.org/sim/) alignment with CASPR2, CASPR4 protein showed low amino acid homology of 48.4% and a gap frequency of 1.8%, however their predicted structures taken from the AlphaFold[196] protein structure database shows excellent similarity, template modelling (TM) score[197] of 0.89 (TM of 1 = perfect match) and a root mean squared deviation of atoms positions (RMSD)[198] of 3.49 (**figure 13A**). Here, predicted structures were used, as crystal structures of CASPR2 and CASPR4 are not yet resolved. AlphaFold is a state-of-the-art artificial intelligence system developed by DeepMind that placed first in the 13th Critical Assessment of protein Structure Prediction challenge, and regularly achieves accuracies competitive with experimental structures. As validation of its accuracy, the only existing experimental crystal structure of the CASPR2 Discoidin domain[199] was compared to the AlphaFold predicted structure. AlphaFold was able to achieve a TM-score of 0.99 and RMSD of 0.42, thus confirming its extremely accurate performance and lends support for the likely true structural homology between CASPR2 and CASPR4 proteins. Therefore, domain swap constructs between the two are likely to preserve a degree of global protein structure, while remaining sufficiently different at the amino acid level to disrupt mAb binding.

Sequential CASPR4 protein domains corresponding to the Discoidin, Laminin G-like 1, Laminin G-like 2, Fibrinogen C-terminal, Laminin G-like 3 and Laminin G-like 4 domains, identified by UniProt assigned residues, were swapped into corresponding domains in full length CASPR2 by overlap extension PCR. EGF-like 1 and EGF-like 2 domains were excluded from swaps on the rational basis that, structurally, they serve as molecular hinges and are relatively inaccessible when fully folded[141]. As before, all protein constructs were validated for surface expression (**figure 13C**) prior to testing with 5ug/ml of memory B cell-derived mAbs. Confirmatory with the previous deletion constructs, swapping of the native CASPR2 Discoidin domain abrogated binding of mAbs E04, E06, E07, H01 and H02, confirming their specificity for the CASPR2 Discoidin domain. Furthermore, only swapping of the Laminin G-like 3 domain abrogated binding of mAbs E08 and E09, therefore resolving their previously unclear specificity (**figure 13D**).

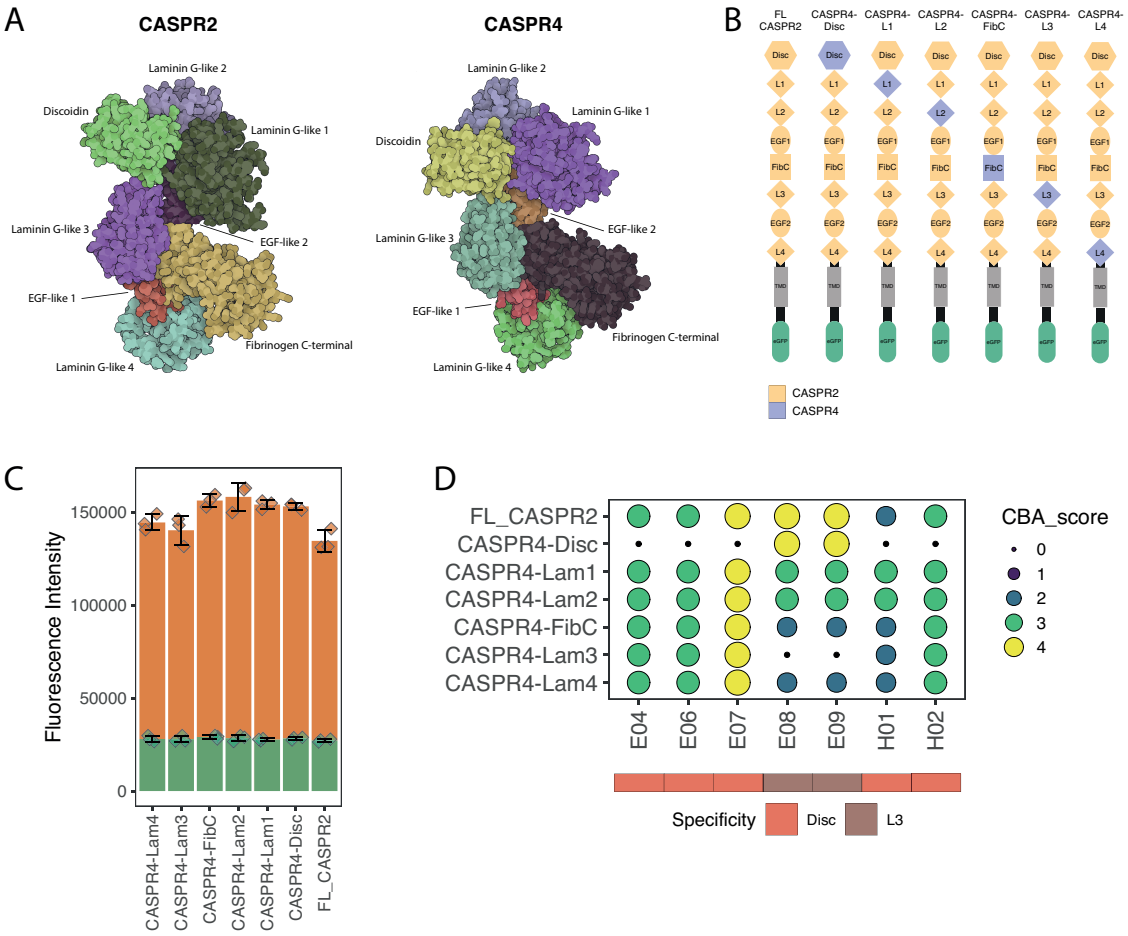

Figure 13. Assessing CASPR2 domain specificity using CASPR2-CASPR4 domain swap constructs. (A) AlphaFold predicted 3D structures of CASPR2 and CASPR4 proteins. Domains are labelled. (B) Cartoon linear representations of CASPR2-CASPR4 domain swap. (B) Assessment of surface expression of individual deletion constructs compared to full length CASPR2 protein (FL_CASPR2). Orange denotes fluorescence intensity of detection secondary antibody and green denotes fluorescence intensity of EGFP. Bars are unstacked; therefore, points indicate absolute values of triplicate experiments. (C) Dot-plots of live-cell based assay scores across patient-derived memory. Specificities of binding combinations are indicated below each dot-plot. Colours indicate domains targeted as specified by the legend.

To assess whether the memory B cell responses to CASPR2 converge towards shared or overlapping epitopes, I next performed an epitope-binning cross-competition assay. As expected, cross-competition of mAbs were restricted to their respective domain specificities (**figure 14A**); therefore, Discoidin and Laminin G-like 3 domains

are likely to be sufficiently distanced to avoid steric hinderance of respective mAb binding. However, interestingly, mAbs derived from different individuals competed for epitopes within a common domain, thus supporting public convergence towards overlapping epitopes. Using directed network analysis, I investigated the inferred pseudo-spatial relationships of the mAbs in regards to their epitopes (**figure 14B**). Here, I identify that within Discoidin-binding mAbs, E04 had the highest degree centrality; subsequently, two discrete trajectories branch away spatially from E04. The first, consisting of E07 and H01, can tridirectionally compete with E04, suggesting a shared epitope space. The second, consisting of H02 and E06, follow a linear trajectory away from E04. Forming their own cluster, E08 and E09, which both target the Laminin G-like 3 domain, were highly cross-competitive; therefore, likely share an overlapping epitope.

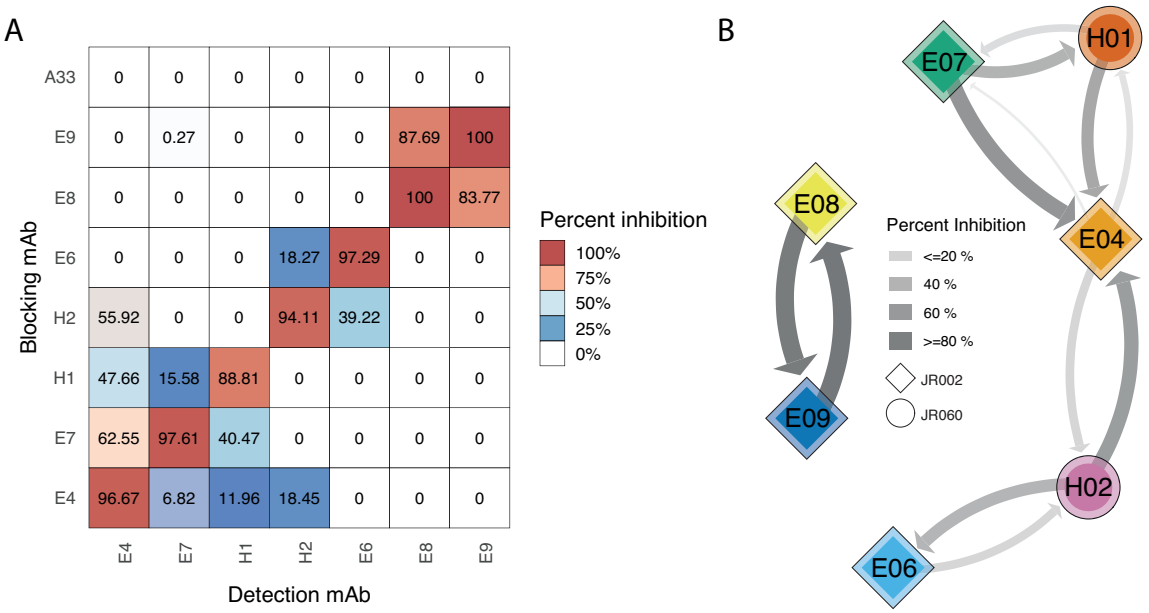

Figure 14. CASPR2 mAb cross-blocking and network representation. (A) Cross-blocking experiment presented as pairwise percent inhibition heatmap. Y axis denotes primary blocking mAb and x axis denotes fluorophore labelled detection mAbs. Fluorescence intensity of detection mAbs in the presence of non-competing mAb A33 were defined as maximal binding values. Therefore, percentage inhibition is presented as the percentage of fluorescence intensity reduction from maximal binding. (B) Network analysis of cross-blocking experiment. Percentage inhibition values were used to create a forced-direction network graph using the igraph package in R and visualised with the ggnetwork package. Thickness of lines indicates relative percentage inhibition and arrows represent directionality of inhibition. For interpretability, self-inhibition loops were not visualised.

3.4.3 The influence of CASPR2 conformation and glycosylation on mAb binding

B cells and their respective antibodies can bind conformational, linear and rarely, glycan epitopes. These binding modalities are important to characterise in diagnostic immunoassays, as the format of antigen presentation must be sensitive to the disease-consensus autoantibody binding dynamics. In CASPR2-encephalitis, patient sera have been proposed to bind non-conformational epitopes on western blot[134]; a somewhat surprising observation in the context of CASPR2's independently folded

extracellular domains. When scrutinised, the presence of extra non-specific bands in all published western blots and a lack of biological controls, shed doubt on this yet to be replicated observation. Therefore, I sought to investigate the dependence of patient-derived mAb binding on protein conformation and glycosylation.

The extracellular domain of CASPR2 has been characterised to have correctly folded tertiary structure when expressed as a monomeric protein from residues 32-1214[140,141], therefore its use in solid-phase assays can be assumed to be representative of a fully folded protein. Using preparations of untreated, heat-denatured and de-glycosylated CASPR2-ECD, memory B cell-derived mAbs and corresponding patient sera were tested for binding on indirect ELISA. Contradictory to the existing reports, I found that heat-denaturing of CASPR2 protein abrogated all mAb and sera binding (**figure 15B**). However, in agreement, all mAbs and sera retained appreciable binding to de-glycosylated CASPR2, albeit with a significant reduction in binding optical density values (OD) across all samples (33%-56%). This effect was independent of antigen coating efficiency (**figure 15B**).

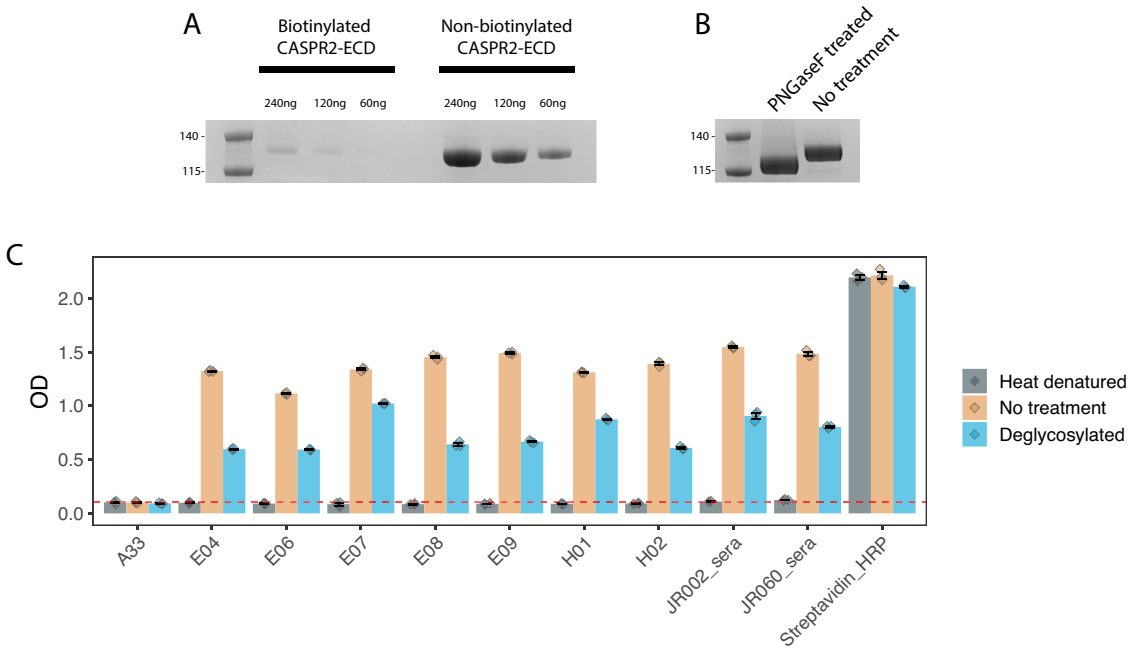

Figure 15. Assessment of mAb binding on de-glycosylated and heat denatured CASPR2 by indirect ELISA. (A) SDS page of streptavidin agarose adsorption experiment, showing efficient biotinylation of soluble CASPR2 extracellular domain (ECD). (B) SDS page validation of efficient PNGaseF de-glycosylation of CASPR2-ECD. (C) Indirect ELISA optical density values (OD) read at 450nm. Colour indicates the different treatments of CASPR2 as denoted by the legend. Streptavidin HRP was used to validate the efficient adsorption of CASPR2 protein to nunc 96 well plates. All experiments were performed in triplicates.

3.4.4 Tissue detection of CASPR2 protein

While the isolated expression of CASPR2 on the surface of HEK293T cells is a sensitive method to detect autoantibody binding, it cannot be considered 'representative' of native protein expression levels within the CNS. Indeed, the presence of native CASPR2 ligands may further hide distinct epitopes. As a proxy, murine tissue-based detection systems have been widely utilised for autoantibody screening[200,201]; with the caveat that cross-species reactivity is assumed to be

comparable. Therefore, I sought to characterise the binding of the mAbs when exposed to endogenous, neuronally expressed, CASPR2.

To achieve full representation of existing diagnostic assays, the mAbs were systematically tested across live primary hippocampal neurons (21 DIV) and *ex vivo* rat brain sections (**figure 16A**). Additionally, binding to IPSC-derived human sensory neurons was also assessed to exclude species-specific behaviours. Surprisingly, there was notable variability of binding between the mAbs. E08 and E09 consistently bound across neuronal and brain section-based assays and appear to be tissue and species agnostic, whereas E04, E06 and H02 showed no binding across the equivalent assays (**figure 16A**). E07 and H01 behaved unexpectedly, as neither bound rat hippocampal neurons, but had strong binding to rat brain sections with a pattern expected of CASPR2 protein distribution[142]. To examine whether antigen avidity was a factor, since neuron-dense brain sections are anticipated to present more CASPR2, staining of neurons were amplified with a tertiary detection antibody. Post-amplification, only mAb E07's specific pattern of staining became apparent on primary hippocampal and IPSC-derived human sensory neurons (**figure 16B-C**). Despite not resolving all mAb discrepancies, the detection of specific binding

upon signal enhancement supports an avidity gradient across neuronal and tissue-based assays.

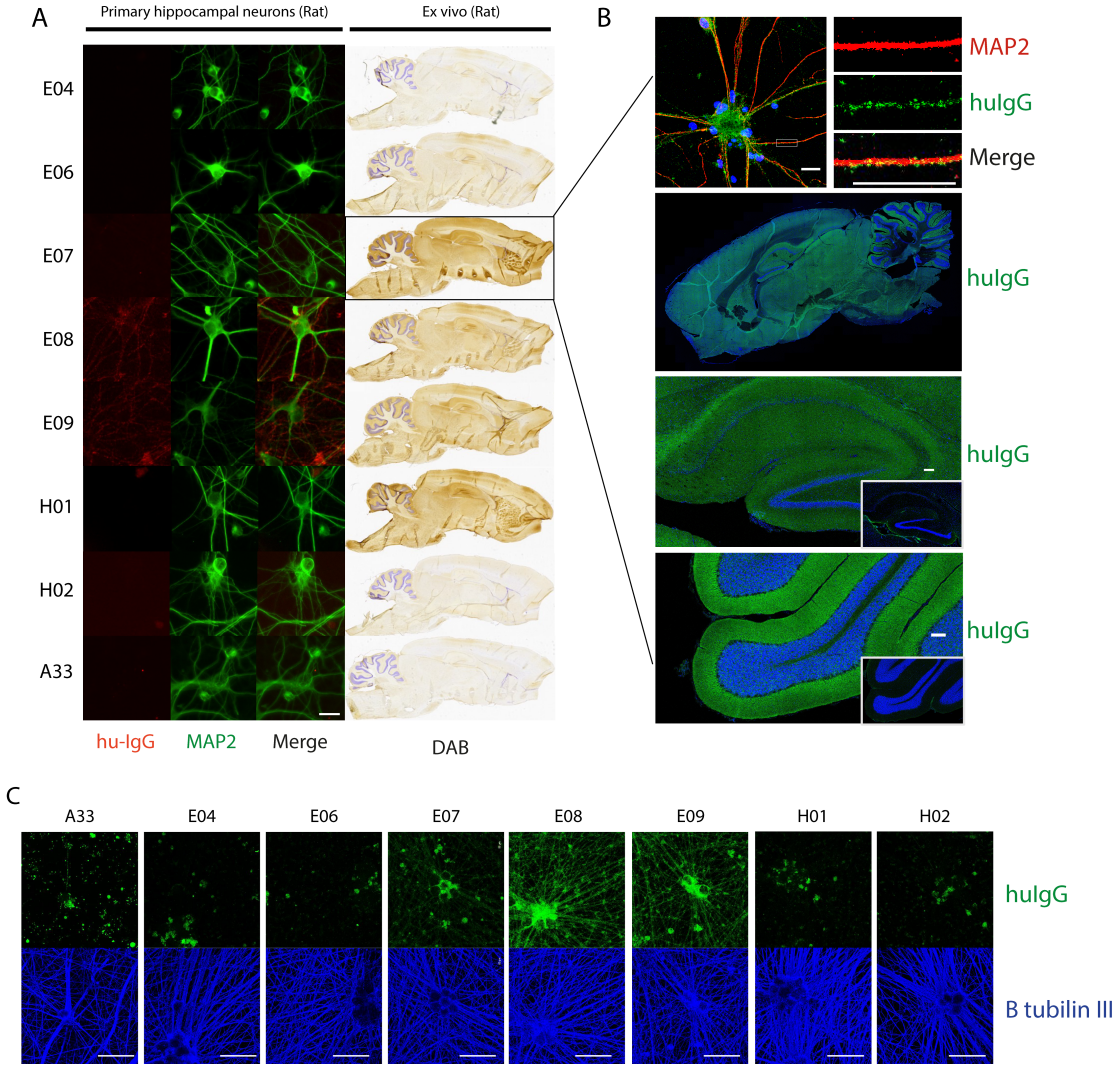

Figure 16. mAb binding to primary hippocampal neurons, rat brain sections and human IPSC-derived sensory neurons. (A) CASPR2 mAbs binding to primary hippocampal neurons and rat brain sections. At the bottom marker labels are indicated. (B) E07's binding to neuronal tissue. First row of panels visualises E07 binding of neurons when binding is enhanced with a tertiary detection antibody. Second panel visualises fluorescent immunohistochemistry of whole rat brain section stained with E07. Third and fourth panels indicate fluorescent immunostaining of unfixed rat hippocampus and cerebellum, respectively. Inlays in third and fourth panels indicate loss of staining in knockout

brain sections. (C) Fluorescent immunohistochemistry of CASPR2 mAbs and control mAb A33 on human IPSC-derived sensory neuronal cultures. huIgG = human IgG; MAP2 = microtubule associated protein (neuron specific cytoskeleton protein); DAB = 3, 3-diaminobenzidine; B tubulin III = beta tubulin III (neuron specific component of the microtube network).

3.4.5 Characterising affinities

One potential explanation for the heterogenous binding of mAbs on tissue, is their relative affinity for CASPR2. Antibodies can exist as IgM, IgA or IgG with ten, four and two binding sites, respectively. Additionally, within the IgG subclasses, IgG4 antibodies are proposed to exist as functionally monovalent species due to F(ab) arm exchange. Indeed, IgG4 is the predominant subclass detected in CASPR2 encephalitis[84–86,202] (*Varley and Irani unpublished*), therefore monovalent affinities of the mAbs are of physiological relevance. To obtain a controlled monovalent measure of affinity, each mAb was assessed for 1:1 binding kinetics against CASPR2-ECD using surface plasmon resonance (**figure 17**).

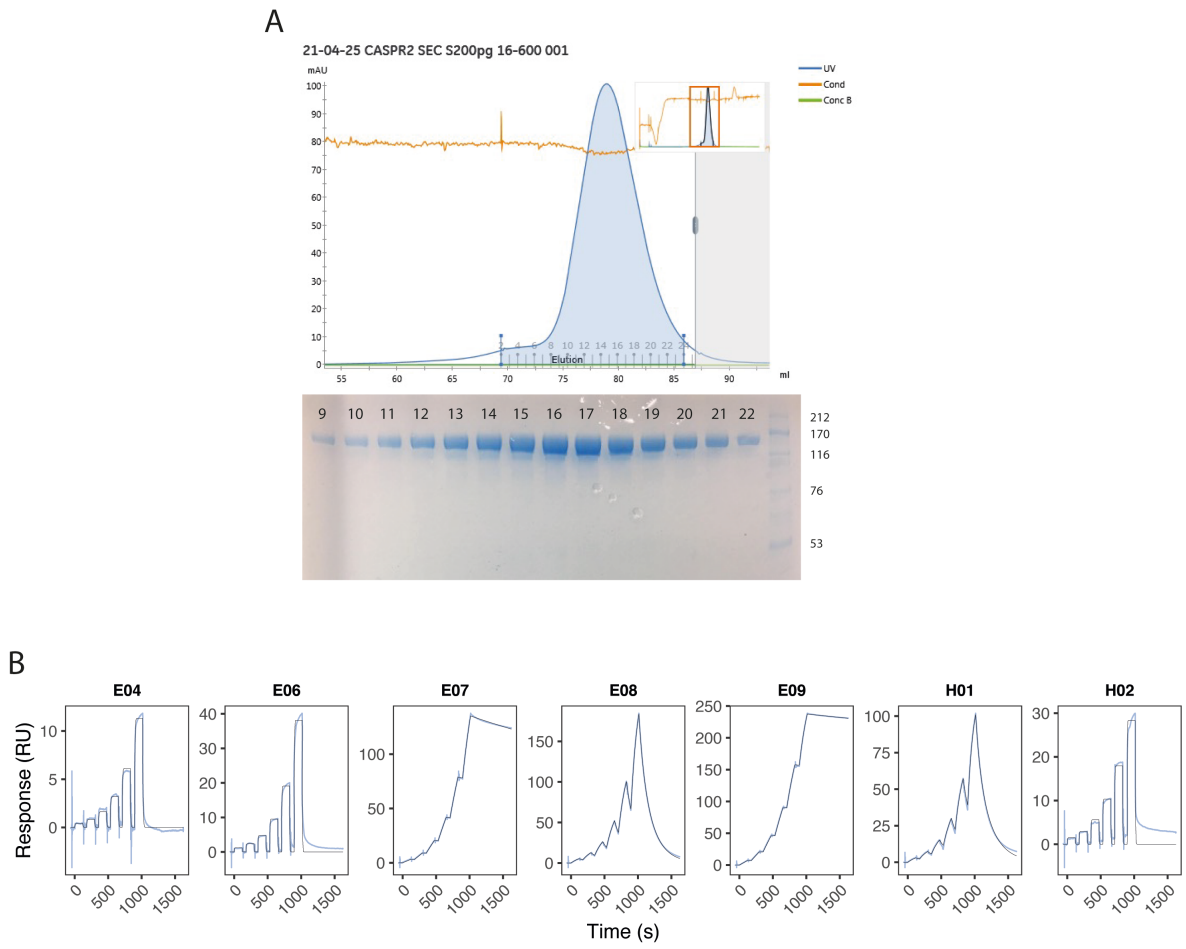

Figure 17. Surface plasmon resonance characterisation of CASPR2 mAb binding of CASPR2-ECD. (A) Size exclusion chromatography trace of purified CASPR2-ECD showing a single uniform peak consistent with monomeric fraction. Below is an SDS page of the wells pooled for downstream analysis. (B) Individual surface plasmon resonance traces of each mAb. Dissociation constant values are inlayed top left.

Having confirmed the monovalent dissociation constants (K_D) of each mAb, the ranked affinities were compared against their binding behaviours across cell and tissue-based assays (**table 3**). Concordantly, E08 and E09, the mAbs with the lowest K_D values and highest affinities, bound all assays convincingly. E07, the next strongest binder, bound brain sections, but required an amplification of detection

signal to visibly appreciate it's binding of neurons; this is consistent with the higher density of CASPR2 in mature rat brains vs. primary cultures[142]. Finally, mAbs H02, E04 and E06, with the highest K_Ds, only bound cell-based assays.

Table 3 Antibody binding kinetics and neuronal tissue binding.

Antibody	Ka ($M^{-1}s^{-1}$)	Kd (s^{-1})	K_D (M)	t 1/2 (s)	CBA	Neuron (rat)	Neuron (human)	IHC (rat)
E4	1.08E+03	2.89E-01	2.67E-04	2.40E+00	+	-	-	-
E6	3.21E+04	1.72E-01	5.37E-06	4.03E+00	+	-	-	-
H2	1.63E+07	1.37E+01	8.37E-07	5.07E-02	+	-	-	-
H1	4.79E+05	2.62E-01	5.47E-07	2.64E+00	+	-	-	+
E7	3.14E+03	1.54E-04	4.90E-08	4.51E+03	+	+/-	+/-	+
E8	3.70E+08	1.11E+01	3.00E-08	6.25E-02	+	+	+	+
E9	3.04E+05	4.64E-05	1.53E-10	1.49E+04	+	+	+	+

Ka = associate rate; Kd = dissociation rate; K_D = dissociation constant; t1/2 = dissociation half time; all values derived from the Cytiva biacore systems software.

3.4.6 mAb binding across species

Despite the seemingly good correlation, K_Ds are only one mAb-specific property that may influence binding across cell and tissue-based assays. An important factor that has yet to be investigated systematically in the field, is the effect of species-specific protein variation on autoantibody binding. This is pertinent for the accurate recapitulation of patient serostatus and disease pathophysiology, especially when

cross-species platforms are used for diagnostic and *in vivo* modelling in NSAb-mediated diseases. Here, I sought to characterise the binding capacity of human patient-derived mAbs on murine CASPR2.

First, a full-length mouse CASPR2-EGFP construct was directly subcloned by overlap extension PCR from 2 synthesised gene fragments of the mouse CNTNAP2 gene (IDT) corresponding to UniProt accession Q9CPW0. Following sequence validation with sanger sequencing, surface expression was validated as before, this time using a polyclonal anti-mouse CASPR2 commercial antibody cocktail (#PA5-28969). Next, the mAbs were each sequentially diluted and tested on human and mouse CASPR2 CBA, to identify end-point titres; defined as the last titre at which visible binding is detected (**figure 18B**). Interestingly, E04, E06 and H02 mAbs showed complete loss or near loss of binding, consistent with their dropout on murine-based assays, whereas mAbs E07 and H01 showed higher end-titres for murine CASPR2. This is compatible with the spatial epitope network generated from cross-blocking experiments, as E07 and H01 share no overlap of epitopes with E06 and H02. In this scenario, E04's degree centrality suggests there is likely a key residue change that abrogates its binding to mouse CASPR2, and confers divergent changes in binding properties of the two spatially branching mAb epitope groups. Taken

together, despite their sequence homology, human and mouse CASPR2 contain sufficient residue changes (**figure 18A**) to alter the binding strength of individual autoantibodies. This is an important observation and requires further study to explore how species-specific residue changes influences diagnostic assay sensitivity and specificity.

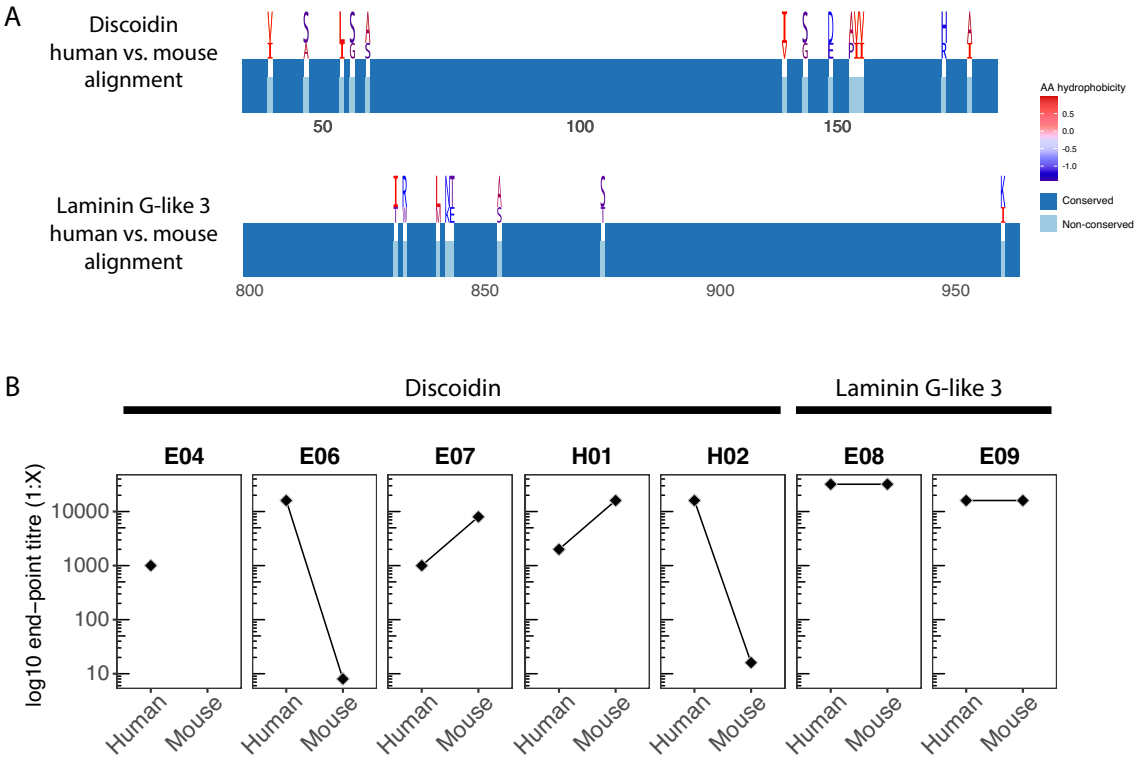

Figure 18. Comparison of binding between human and mouse full length CASPR. (A) residue alignments of human and mouse CASPR2. Top alignment represents residue positions of Discoidin domain and bottom alignment, the Laminin G-like 3 domain. Sequence logos of residue changes are visualised for non-conserved residues; top residues are human and bottom residues are mouse. (B) End-point titres of CASPR2 mAbs on human vs. mouse CASPR2 live cell-based assays. Titre is visualised as a log10 transformed dilution factor from a starting concentration of 20ug/ml.

3.5 Discussion

An autoantibody's binding strength, epitope and cross-species binding are key parameters for understanding disease pathogenesis and *in vivo* model development. To date, studies have utilised *ex vivo* patient sera to characterise the binding properties of CASPR2 autoantibodies. However, a key limitation is the lack of molecular resolution, making these observations difficult to generalise from unrefined polyclonal CASPR2 anti-sera. In this chapter, I have aimed to validate the binding properties of CASPR2 autoantibodies at the monoclonal antibody resolution, and in context of B cell development.

In NSAb-mediated diseases, direct sampling of naïve B cell reactivities has largely remained unexplored. Early evidence supports the existence of autoantigen-reactive B cells within the naïve B cell pool of patients[118,122], but their innate reactivity has not been explored at the single cell resolution. Here, I confirm that mAbs derived from CASPR2-specific naïve B cells, present in both patients and healthy donors, are avidity-dependent binders of CASPR2, and do not bind when expressed as F(ab) fragments. Together with the absence of circulating CASPR2-specific IgMs (**supplementary table 1**), this data does not support the direct contribution of CASPR2-reactive naïve B cells, without further affinity maturation. Conversely,

patient-exclusive memory B cell mAbs are capable of both IgG and F(ab) binding, validating their functionality if ever secreted as bivalent IgG subclasses or monovalent IgG4.

Consistent with the literature, Discoidin domain reactivity was prevalent in memory B cell-derived mAbs (5/7). However, for the first time, I show that mAbs derived from different individuals all bound within a narrow epitope space, raising the possibility of convergence to immunodominant epitopes within the Discoidin domain[199]. Interestingly, two memory B cell-derived mAbs, targeting the Laminin G-like 3 domain, displayed the highest monovalent affinities, as determined by SPR. Correspondingly, they also displayed the strongest binding to CASPR2 across all immune- and tissue-based assays. While the superior binding of Laminin G-like 3 domain mAbs are unexpected in the context of Discoidin domain immunodominance, it supports their functional relevance in CASPR2 encephalitis. Surprisingly, naïve B cell-derived mAbs did not bind overlapping domains with the memory B cell-derived mAbs. However, a critical experimental limitation was their weak binding to deletion constructs; therefore, dropout due to their low avidity for CASPR2 cannot be excluded.

It has previously been reported that patient sera are capable of binding CASPR2, independent of glycosylation and tertiary structure. In agreement, I show that all memory B cell-derived mAbs bound de-glycosylated CASPR2, albeit less efficiently. This is an intuitive finding, as the mAb targets, Discoidin and Laminin G-like 3 domains, are not predicted to be glycosylated. Indeed, Discoidin domain immunodominance in patient sera, may represent a harmonious cross-study explanation of glycan-independent binding. Alternatively, observed immunodominant responses may simply correspond to glycan free domains, as glycan shields have been shown to be capable of preventing antibody recognition[203,204]; however, this hypothesis requires further systematic validation. Rationalising the globally reduced binding to de-glycosylated CASPR2, glycosylation has been shown to be crucial to protein folding, stability and membrane localisation; therefore, loss of binding capacity may be due to conformational changes secondary to enzymatic removal of N-linked glycans.

In discordance with previous reports, the patient-derived mAbs and their matched sera were incapable of binding heat-denatured CASPR2. One possibility for this discrepancy is the use of live-cell CBAs and CASPR2-ECD in the screening of B cell cultures and ELISA, respectively. A desired feature of live-cell assays is their

selective presentation of conformational extracellular components of autoantigens; therefore, it is plausible that B cells targeting linear epitopes or the intracellular component of CASPR2 were missed in initial culture supernatant screens. Nonetheless, the relevance of linear and intracellular epitopes in NSAb-diseases remains of unclear significance, and lack experimental evidence to support their *in vitro/in vivo* pathogenicity. However, a limitation of the data at hand is the small number of biological replicates and sampling size of the repertoire; therefore, it cannot comprehensively exclude the presence of autoantibodies against non-conformational epitopes in CASPR2-encephalitis, regardless of their significance to disease.

Lastly, these human-derived CASPR2-reactive mAbs bound differentially to murine CASPR2. This is a crucial finding and supports the notion that human vs. murine comparability cannot be assumed on sequence homology alone. As murine models remain key to our understanding of *in vitro/in vivo* disease pathophysiology, this finding requires urgent systematic study and may necessitate the need for chimeric models to better represent autoantibody responses to human proteins.

3.6 Conclusion

These data reveal the heterogeneity of autoantibody binding and their potential biological and experimental relevance. Biologically, the discrepant bivalent binding across naïve and memory B cell-derived mAbs support the need for CASPR2-reactive naïve B cell BCRs to undergo further affinity maturation to become functionally active IgG. Cross-sectionally, this supports the presence and integrity of an immune checkpoint at the level of the germinal centre in healthy donors. Consistent with previous observations, Discoidin domain immunodominance was validated across the two study patients; however, Laminin G-like 3 reactive mAbs had observably higher affinities, a previously undescribed observation. Lastly, across all mAbs, conformation and full glycosylation of CASPR2 were required to achieve maximal binding. Taken with the species-specific binding bias, this chapter has elucidated key features that must be considered by the wider research community in future disease modelling and diagnostic immunoassays.

3.7 Acknowledgements

Deniz Akdeniz supervised my cloning of the variable domains into subclass specific vectors. Teodora Trendafilova generated and gifted the CASPR2 deletion constructs used for the initial characterisation of epitopes. Jiandong Huo, kindly gifted the

CASPR2-ECD-AviTag-His expression vector. Robert Donat performed SPR studies and provided raw data for analysis. Antonio Barretta supervised the culture of primary hippocampal neurons. Victor Mgbachi supervised the immunofluorescence and performed the immunohistochemical staining of rat brain sections. Alexander Davies generated **figure 16C**. Sofija Panjeva performed end-titres of CASPR2 mAbs on full length mouse CASPR2. Permission for use of data was obtained from all data contributors mentioned above.

Chapter 4 Assessing mechanisms of antibody-mediated disruption of CASPR2 protein

4.1 Introduction

The mechanisms of autoantibody-mediated pathogenicity are not fully understood in CASPR2 encephalitis. Indeed, much of this uncertainty derives from the enigmatic role of CASPR2 in neuronal homeostasis, summarised in **chapter 1, section 1.5.7**. Nonetheless, drawing from past studies of autoantibody pathogenicity, a few common modes of action are likely to be transferable. First, is the ability of antibodies to directly modulate the function of extracellular proteins; second, is the potential blocking of protein-ligand complex formation; and third, is antibody-mediated internalisation and downregulation of target proteins. All three mechanisms may result in the functional silencing of the target protein.

CASPR2, as its name suggests, is proposed to interact with contactin-2 protein (CNTN2)[136,153]. This proposed interaction is thought to occur both intracellularly and extracellularly based on live fluorescent microscopy[136,153], cell-based assays[136,153], ELISA[87,141], co-immunoprecipitation[88,136,151,153] and surface plasmon resonance[141]. Therefore, the proposed ability of patient-derived sera to block this interaction *in vitro*[87], is a potentially harmonious mechanism. However, contradictory findings in

the literature shed doubt on the reproducibility of their extracellular interaction. In particular, Poliak et al.,[136] and Traka et al.,[153] reported the interaction to only occur when the proteins are co-expressed, implying the need for the two proteins to associate in "cis" at the cell membrane. Further to this, in a series of experiments by Rubio Marrero et al.,[140] the interaction of CASPR2 and contactin-2 extracellular domains was refuted and they propose a novel interaction of CASPR2 with contactin-1 protein (CNTN1), a protein family member of CNTN2.

Whether CASPR2-autoantibody containing sera can internalise CASPR2 in an antigen-specific manner, also remains unclear. While Patterson et al.,[87] and Saint-Martin et al.,[88] report that CASPR2 sera did not reduce the total surface CASPR2 expression in cell-based assays or live primary neurons, Giannocaro et al.,[135] and Fernandes et al.,[89] independently showed patient-specific internalisation of surface bound IgG in the same respective assays. Further, Dawes et al.,[205] showed that CASPR2 and Kv1 expression was reduced at the juxtaparanodes of sciatic nerves in mice treated with CASPR2 patient-derived autoantibodies. Dawes et al., further validated this finding *in vitro*, showing that patient plasma treated mouse dorsal root ganglia neurons had reduced membrane expression of Kv1.2 channels; a protein known to complex with CASPR2.

In this chapter, I sought to characterise the potential mechanisms by which patient-derived CASPR2-reactive monoclonal antibodies can alter membrane surface CASPR2 protein. Studying these mechanisms at the monoclonal level across domain-specific epitopes may elucidate nuances that explain previously perplexing observations.

4.2 Hypothesis

4.2.1 Patient derived mAbs block CASPR2 CNTN2 ligand interaction

4.2.2 Patient derived mAbs internalise surface CASPR2

4.2.3 Patient derived mAbs disrupt neuronal homeostasis

4.3 Methods

4.3.1 Contactin-2 and Contactin-1 constructs

CNTN2 extracellular domain (L^{29}ESQ … VRNG^{1004}) was amplified from commercial mammalian expression plasmid HG10457-NH (Sinobiological), using the following primers (upper case represents annealing sites):

Forward:

atccttttctagtagcaactgcaaccggtCTGGGATCCCAAACCACCTT

Reverse:

cggccaagctttcagtgatggtgatggtggtgggaaccaccggaacctccggtaccTCCATTCCTCACGATGTGGAC

CNTN2 ECD was then subcloned into the pHL-avitag vector using restriction sites AgeI and KpnI.

CNTN1 extracellular domain (V^{32}SEE … KISGA^{995}) was directly subcloned into a pre-linearised pHL-avitag vector through overlap extension PCR of two gene fragments with a 30bp homologous corresponding to nucleotide positions 1629-1659. Both constructs were transformed in competent E. coli cells and colonies validated by Sanger sequencing.

4.3.2 Protein expression and purification

The extracellular domains of CNTN2 and CNTN1 were recombinantly expressed in HEK293F cells for use in cell-based assays and ELISA. 1ug/ml of DNA of each construct was first complexed at room temperature in a 1:3 ratio with linear PEI (1mg/ml). Complexes were then homogenously distributed with HEK293F cells in freestyle media (Gibco). After 5 days of expression, culture supernatants were purified by nickel-nitrilotriacetic (Ni-NTA) chromatography and buffer exchanged

into PBS using a 100kd Amicon centrifugal filter unit (UFC910024, Merck). Proteins were flash frozen on dry ice and stored at -80C until use.

4.3.3 F(ab) fragment generation

F(ab)s were generated using the Pierce™ F(ab) preparation kit (Thermofisher # 44985), as per **chapter 3** methods. To generate heavy chain F(ab) expression vectors, regions corresponding to the hinge region, CH2 and CH3, were substituted with a hexahistidine tag using NEB Q5 mutagenesis kit and validated with Sanger sequencing. The following primers were used (upper case represents annealing sites):

Forward:

ccaccaccatTGAAGCTTGGCCGCCATG

Reverse:

tgatgatgatgCTCAACTTTCTTGTCCACCTTGG

4.3.4 Direct pHrodo™ conjugation of mAbs

100ug of either mAb or F(ab) fragments were labelled at 4^0C overnight, protected from light, with 125uM of pHrodo™ dye in 100mM sodium bicarbonate buffer, pH8.3. Samples were then buffer exchanged into PBS using a 100kd Amicon centrifugal filter unit, stored at 4^0C protected from light and used within 2 weeks of labelling.

4.3.5 Indirect labelling of mAbs with Zenon™ pHrodo™

Labelling of mAbs with Zenon™ pHrodo™ was performed as per manufacturers protocol. In brief, 160nM of antibody were complexed with 480nM of Zenon™ pHrodo™ for 5 minutes at room temperature prior to use in assays. Complexed mAbs were used immediately.

4.3.6 pHrodo™ internalisation live cell-based assay

pHrodo™ internalisation assays were performed either across CASPR2 expressing HEK293T cells, or rat primary hippocampal neuronal cultures (as per **chapter 3** methods). For HEK293T cells, monolayers of HEK293T cells in 96 well plates were transfected with CASPR2-EGFP expression vectors as described in **chapter 2** methods. Following 24 hours of expression, pHrodo™ pre-labelled or pre-complexed mAbs were incubated overnight at 20ug/ml. Interval recordings were either image captured on a Leica DMi8 SP8 FALCON, or mean fluorescence quantified on a BMG OMEGA FLUOstar using a 560-10/650 filter. For dynasore inhibition assays, pre-treatment of CASPR2 expressing HEK293T cells for 1 hour with 50μM of dynasore was performed prior to incubation with mAbs.

4.3.7 pHrodo™ image quantification

pHrodo™ mean fluorescence was pre-processed in the FIJI distribution of ImageJ and analysed in R, using packages rstatix (https://github.com/kassambara/rstatix) and RKcolocal (https://github.com/lakerwsl/RKColocal). In FIJI, 12 regions of interested were selected across axonal and dendritic projections of neurons; cell bodies were excluded from analysis due to heterogeneity of focal planes. FIJI exported mean fluorescence intensities for each region of interest were then exported for analysis in R. Spatial colocalisation was calculated in R package RKcolocal using the function `colocalpixel()`, and visualised with ggplot (https://github.com/tidyverse/ggplot2). RKcolocal implements a novel framework for spatial adaptive colocalisation proposed by Wang et al.,[206]. For 2D spatial images, the Kendall tau correlation coefficient r between the green and red channels is calculated, and p values generated via permutation testing.

4.3.8 Bispecific mAb expression vectors

First to generate a single chain variable fragment (scFv), a gene block containing human Kappa CH1 region followed by a $(GGGGS)_3$ linker was synthesised, via IDT. This was inserted into an Abvec expression plasmid containing the IGHG4 S228P constant region using restriction sites, AgeI and SalI. Variable domains for both heavy and light chain sequences of either mAb E09 or the synthesised variable

domains of Daratumumab, an anti-CD38 therapeutic mAb, were inserted into the scFv mAb vector using cloning sites; AgeI and BsiWI, for the light chain; and NheI and SalI, for the heavy chain. Variable domain sequences of daratumumab were obtained from Thera-SAbDab[207]. Once sequences were validated by Sanger sequencing, Q5 mutagenesis was performed to insert either a hexahistidine tag or streptagII at the C-terminus of scFv mAb E09 and Daratumumab, respectively. The following primers were used:

Hexahistidine insertion primers

Forward:

caccaccacTGAGTGAGGAAAGCTTGG

Reverse:

atgatgatgTTTACCCAGAGACAGGGAG

StreptagII insertion primers

Forward:

cagtttgaaaaaTGAGTGAGGAAAGCTTGG

Reverse:

cggatggctccaTTTACCCAGAGACAGGGAG

4.3.9 Expression and purification of bispecific antibody

Protein expression was performed using transient transfection and culture of HEK293F cells as described above (**section 4.3.2**). Purification was performed from

clarified supernatant using a two-step process. First, supernatants were gravity flowed over Ni-NTA agarose beads (25214, Thermofisher), followed by three resin bed volume washes with wash buffer (PBS with 25mM imidazole). Subsequently, agarose beads were eluted with PBS containing 250mM of imidazole. Eluate was then gravity flowed over Strep-Tactin® conjugated agarose beads and washed with three resin bed volumes of PBS. Finally, beads were eluted with biotin containing Strep-Tactin®XT elution buffer and buffer exchanged into PBS using a 100kd Amicon ultra centrifugal filter unit. Bispecificity of the purified mAb was validated by adsorbing two aliquots using Ni-NTA and Strep-Tactin® agarose beads respectively. Flowthrough from both adsorptions were tested against HEK293T cells transfected with either CASPR2-EGFP or CD38-C-GFPSpark® (HG10818-ACG, Sinobiological).

4.3.10 Cortical neuron culture- Coimbra University

All cortical neuronal data from external collaborators were generated using methods described in Fernandes et al. Cortical neurons were cultured as previously described[89], mAbs were then tested on DIV15 cortical neurons and incubated at 20ug/ml for 2 hours prior to downstream assessment.

4.4 Results

4.4.1 Validating CASPR2 interactions with CNTN2 and CNTN1

The extracellular interaction of CASPR2 and CNTN2 remains contested. As antibodies have not been shown to passively transfer across an intact cell membrane, the proposed ability of patient-derived autoantibodies to block CASPR2-CNTN2[87] interactions is dependent on their genuine extracellular interaction. Therefore, I first sought to independently validate the interaction of the extracellular domain of CASPR2 with proposed ligands, CNTN2 and CNTN1; with a view for downstream use in antibody blocking assays.

First, the extracellular domains of CNTN2 and CNTN1 were subcloned into the PHL-avitag vector, followed directly by a C-terminal GTGGSGGSHHHHHH tag. Proteins were then expressed and purified as described in methods and purity determined by SDS page (**figure 19A**). The respective sizes of CNTN2 and CNTN1 on SDS pages were identical and visualised as a homogenous band at ~116kda. The predicted molecular weight of the two proteins are 106kda and 108kda respective, as determined by Protoparam (https://web.expasy.org/protparam/); however, both are predicted to have 11 and 8 glycosylation sites, respectively. Therefore, the size discrepancies are within expected shifts due to glycosylation.

To validate the interaction of CNTN2 and CNTN1-ECDs with CASPR2-ECD, assessments were performed across previously published assays. First, replicating live-cell based assays described by Poliak and Rubio-Marrero, soluble CNTN2 and CNTN1 ECDs were incubated at 3μM concentrations with CASPR2 expressing HEK293T cells, followed by detection with an anti-His AF594-conjugated secondary antibody. MAb E08, served as the positive control and endogenous expression of CNTN2/CNTN1 in HEK293T cells was excluded by staining with commercial antibodies #3.1C12 and #AF904 to the respective proteins (**figure 19B**). In these live-cell based assays, I did not observe any respective binding of CNTN proteins to membrane-tethered CASPR2 (**figure 19C-D**). Second, solid-phase assays described by Lu and Patterson, were implemented. Here, soluble CASPR2-ECD was first adsorbed to nunc 96 well plates and incubated, post-block, with either his-tagged E08-F(ab), CNTN2-ECD or CNTN1-ECD. All conditions were detected with an HRP-conjugated anti-His antibody. As before, no detectable binding of CNTN2 or CNTN1 was detected (**figure 19E**).

Whilst disappointing, the lack of interaction between CASPR2-ECD and CNTN2/CNTN1-ECDs, replicates discrepancies in the literature. With these data,

I have replicated both negative results of Lu et al.,[141] and Rubio-Marrero et al.,[140] where ECDs of CNTN1 and CNTN2 are shown not to bind CASPR2. However, conversely, I have also failed to replicate their respective positive binding to CASPR2-ECD, as differentially reported by the two groups. Taken together, I conclude that, in these assays, neither ECDs of CNTN2 nor CNTN1 bind CASPR2-ECD at concentrations below 3μM. Therefore, I was not able to validate receptor-ligand blocking experiments described by Patterson et al.,[87].

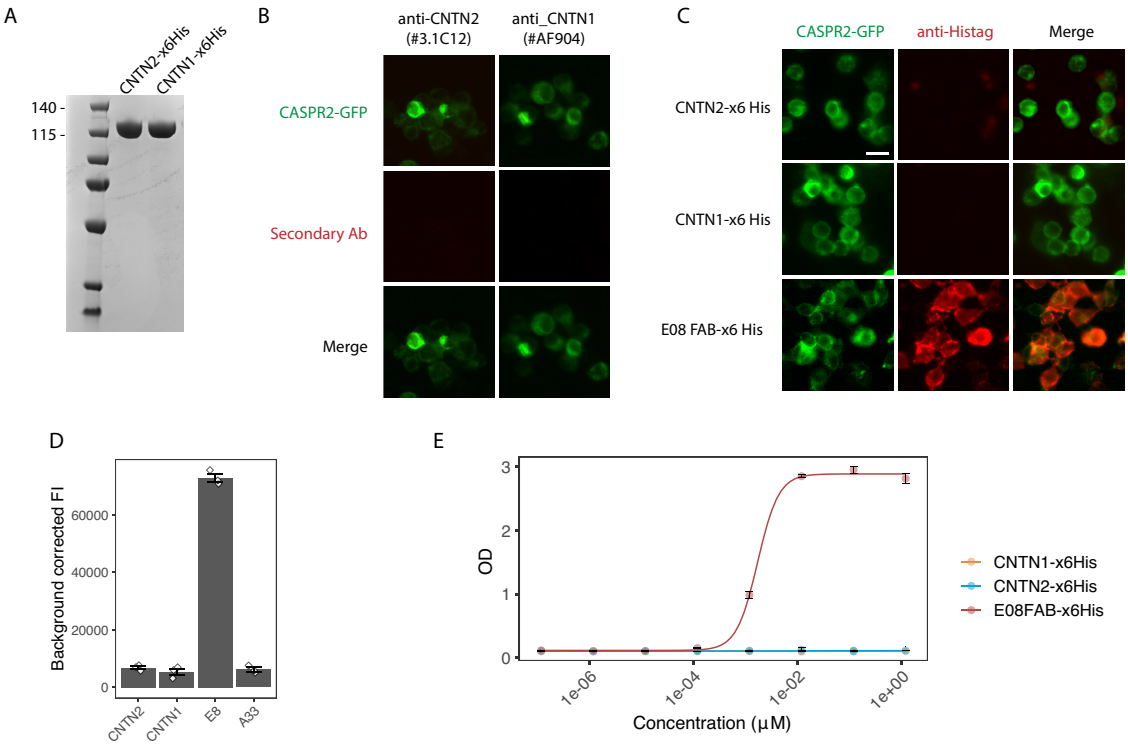

Figure 19. Assessing CASPR2 and CNTN2 interactions. (A) SDS page assessment of purity of CNTN2 and CNTN1 extracellular domain constructs. (B) Live cell-based assays showing absence of endogenous CNTN2 or CNTN1 expression in CASPR2-EGFP transfected HEK293T cells. Primary mAbs are indicated above their respective column of panels. (C) Live cell-based assays of CNTN2 and CNTN1 extracellular domain staining on CASPR2-EGFP expressing HEK293T cells. Detection

of CNTN2 and CNTN1 was performed using an AF594-labelled anti-histag antibody. His tagged E08 F(ab) was used as the positive control. (D) Fluorescence intensity readouts of an independent live cell-based CNTN2, CNTN1 and E08 F(ab) experiment. (E) Indirect ELISA assessment of CNTN2 and CNTN1 binding on immobilised CASPR2-ECD. X6His = hexahistag; CNTN2 = contactin-2; CNTN1 = contactin-1; FI = fluorescence intensity; OD = optical density, measured at 450nm. All experiments were performed in triplicate.

4.4.2 Autoantibody-induced internalisation of CASPR2

Internalisation of CASPR2 protein by patient CASPR2-specific autoantibodies, remains a contested mechanism. While the internalisation of surface bound human IgG on CASPR2 expressing HEK293T cells and neurons have been demonstrated[89,135,205], others report little change in surface CASPR2 protein levels[87,88]. Indeed, in some instances there appears to be a net increase in surface CASPR2 protein expression[88]. Therefore, to systematically investigate these findings, I sought to explore the capacity of the patient-derived mAbs to internalise CASPR2 protein.

To first characterise whether patient-derived mAbs could internalise upon CASPR2 binding and enter endosomal-lysosomal pathways, three of the highest affinity memory B cell-derived mAbs spanning two domain specificities, Discoidin and Laminin G-like 3 domain, were conjugated with pHrodo™; a pH-sensitive fluorescent probe. pHrodo™ exhibits little to no fluorescence at neutral pH, but dramatically increases fluorescence as pH decreases, making it an ideal probe to exclusively visualise proteins undergoing endocytic pathways[208–210]. After their addition to

CASPR2 expressing HEK293T cells, mAb pHrodo™ fluorescence was read hourly on a BMG Omega Fluostar plate reader and visualised at 10 hours with confocal microscopy (**figure 20**). pHrodo™ fluorescence could be reliably detected in CASPR2-binding mAbs regardless of domain-specificity, but was not detected in isotype control mAb, A33. Furthermore, this process was dynamic and increased with time.

To validate the colocalisation of internalised mAb and CASPR2 protein, I next quantified the level of spatial colocalisation between pHrodo™ signal and EGFP using the R package RKcolocal. Using the function `colocalpixel()`, the Kendall tau correlation coefficient *r* between the green and red channels is calculated, and p values generated via permutation testing[206]. For visualisation, a per-pixel matrix of z values filtered on pHrodo™ signal using Otsu's thresholding, is shown in figure 2B. Pixels reaching statistical significance for colocalisation are further visualised beneath (**figure 20B**). Indeed, this analysis confirms the colocalisation of internalised IgG with CASPR2-eGFP. Notably, some areas of non-significant colocalisation were identified (**figure 20B**). A possible explanation for this is the well-established observation that non-pH resistant green fluorescent proteins typically lose fluorescence intensity inversely proportional to environmental pH[211]. Therefore, non-

colocalising antibody aggregates may represent their presence in late endosomes, which reach a pH of 4.5-5.5[212]. Overall, these data validate previous reports of antigen-dependent CASPR2 autoantibody internalisation and confirm their colocalisation with CASPR2 protein.

For further experiments using pHrodo™ labelled mAbs presented in this thesis, a change of protocol was initiated. When purifying labelled mAbs, I noted that visual shades of pHrodo™ labelling differed between mAbs. As pHrodo™ succinimidyl ester labels primary amines, it is plausible that differences in variable domain residue composition can result in biased labelling. Additionally, binding of pHrodo™ to antigen binding domains may influence binding properties. Therefore, to circumvent these potentially confounding factors, all further internalisation experiments in this thesis utilised the Zenon™ pHrodo™ iFL IgG labelling system. In this assay, pHrodo™ is pre-conjugated to a monoclonal anti-human F(ab) fragment; therefore, allowing homogenous detection of antibody internalisation through direct labelling of the Fc region (**section 4.4.3**).

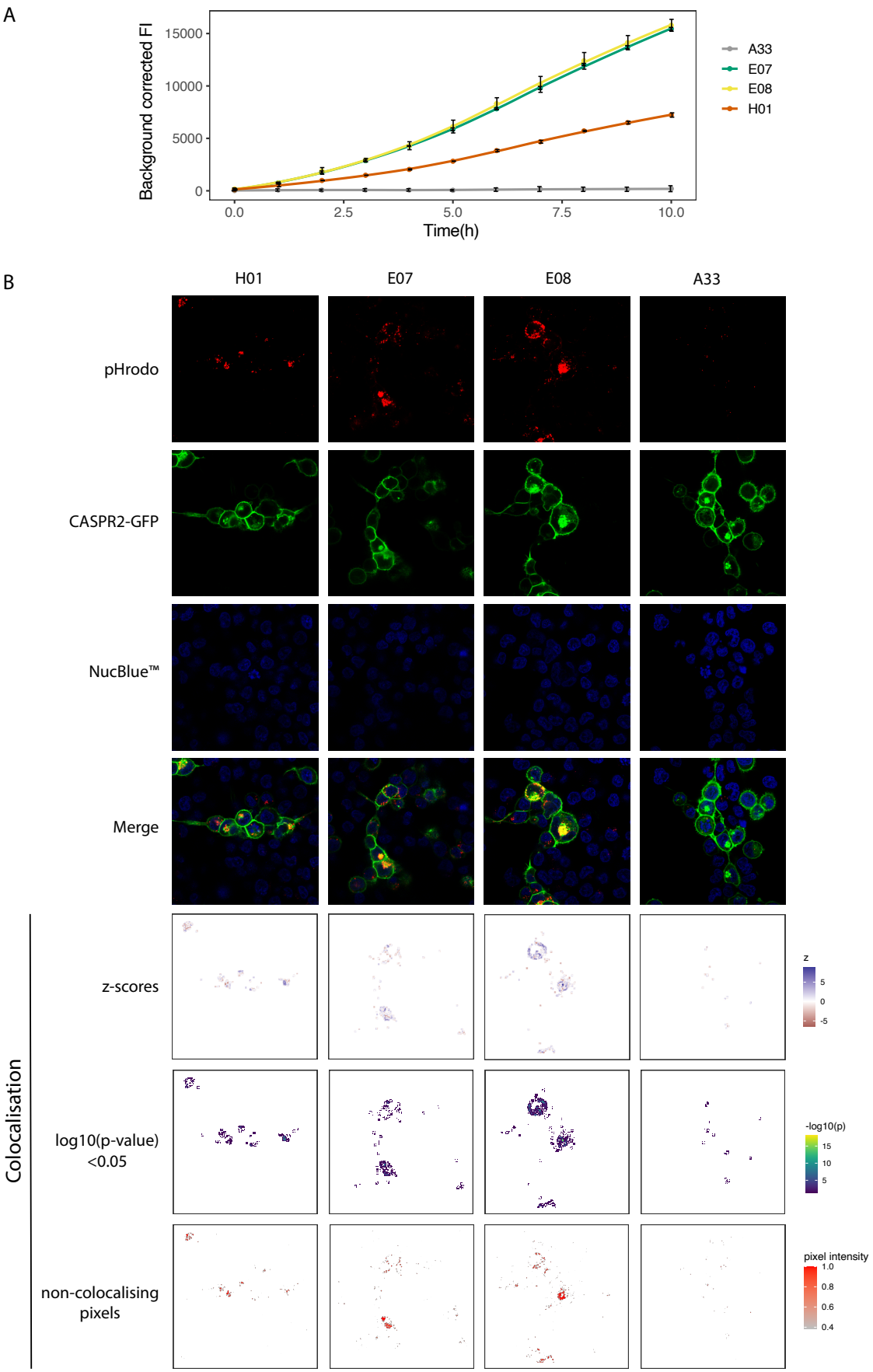
A
Background corrected FI
15000
10000
5000
0
0.0
2.5
5.0
7.5
10.0
Time(h)
A33
E07
E08
H01
B
H01
E07
E08
A33
pHrodo
CASPR2-GFP
NucBlue™
Merge
Colocalisation
z-scores
log10(p-value)
<0.05
non-colocalising
pixels
z
5
0
-5
-log10(p)
15
10
5
pixel intensity
1.0
0.8
0.6
0.4

Figure 20. Internalisation and co-localisation of CASPR2 mAbs. (A) Time dependent assessment of CASPR2 internalisation of a select panel of mAbs, measured by fluorescence intensity of pHrodo™. All mAbs were tested in triplicate and points indicate the mean fluorescence intensity and error bars depict standard deviation from the mean (B) Colocalisation assessment of pHrodo™ and CASPR2-EGFP. Z-scores generated from RKcolocal package are visualised as a heatmap; only pixel coordinates corresponding to pHrodo™ Otsu thresholds are shown. Pixels reaching significance of $p<0.05$ on permutation testing are visualised, as are non-colocalising pixels. Permutation test procedures are detailed in Wang et al., 2017.

4.4.3 Dynamin dependent CASPR2 autoantibody-mediated internalisation

While mechanisms of autoantibody internalisation in autoimmune encephalitis remain superficially studied, in LGI1-antibody encephalitis[81] autoantibody-mediated internalisation has been shown to be dynamin-dependent. However, in other autoantibody-mediated diseases, internalisation of autoantigens has been shown to be dynamin-independent[213–216]. Therefore, I next sought to understand whether autoantibody-mediated internalisation of CASPR2 was via dynamin dependent or independent pathways. To block dynamin, CASPR2 expressing HEK293T cells were pre-treated for 1 hour with dynasore, a cell permeable dynamin inhibitor, prior to the addition of Zenon™ pHrodo™ complexed mAbs. Across all mAbs, dynasore reproducibly reduced internalisation capacity (**figure 21A**, $p=0.018$, Wilcoxon sign-ranked test), confirming that CASPR2 autoantibody-mediated internalisation is dynamin dependent.

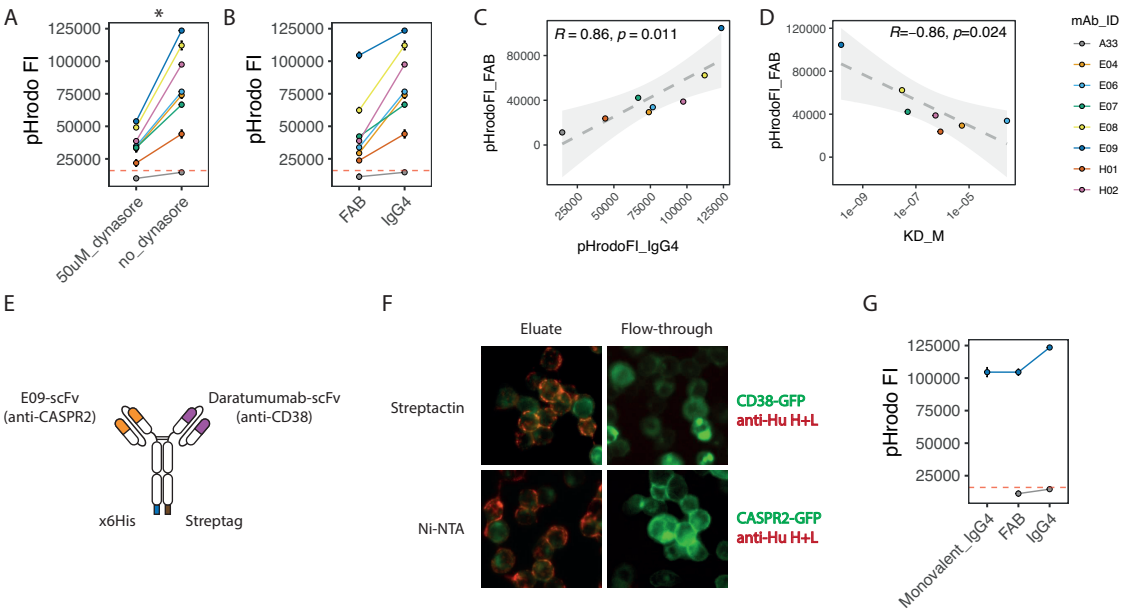

Figure 21. Functional properties of antibody-mediated CASPR2 internalisation. (A) Dynamin inhibition of mAb-mediated internalisation of CASPR2. Colours indicate the mAb IDs as per the far-right legend. Points indicate the mean fluorescence intensity and error bars depict standard deviation from the mean (B) Internalisation capacity of full IgG4 vs. corresponding F(ab) fragments. (C, D) Spearman correlation coefficient of F(ab) vs. IgG4 internalisation capacity (C) and Spearman correlation coefficient of F(ab) internalisation capacity with surface plasmon resonance-defined dissociation constants (KD). (E) Cartoon representation of bispecific scFv mAb. (F) Validation of bispecificity of the E09-Daratumumab scFv mAb using differential adsorption of respective heavy chain affinity tags. Flow-through and eluates of affinity adsorptions were tested on CASPR2 and CD38 expressing HEK cells. (G) Comparison of internalisation capacities of E09-Daratumumab scFv mAb (labelled as `Monovalent_IgG4`), E09 F(ab) fragment and E09 IgG4. Colour of lines and points are as per unified legend, above. All experiments shown were performed in triplicate. Wilcoxon sign-ranked test was performed; where significant: *= $p<0.05$.

4.4.4 Internalisation capacity of monovalent mAb species

An enduring dogma in the field of IgG4 predominant autoantibody-mediated diseases, is the proposed inability of functionally monovalent IgG4 antibodies to induce antigen internalisation. Whilst IgG4 antibodies are capable of undergoing F(ab)-arm exchange *in vivo*[22], the proportion of functionally monovalent IgG4 in circulation is unknown. Further, it is also unclear whether antibody-mediated

internalisation of antigen is truly dependent on cross-linking of antigen by either F(ab)-F(ab) ligation or Fc-Fc oligomerisation. Further, emerging evidence in muscle specific kinase (MUSK) myasthenia gravis, an IgG4 predominant autoantibody disease of the neuromuscular junction, suggests that monovalent IgG4 amplifies pathogenicity of patient-derived mAbs[217,218].

To explore whether our patient-derived mAbs were capable of inducing CASPR2 internalisation as a monovalent species, I tested their internalisation capacity as both monovalent F(ab)s and a monovalent IgG4 molecule. Interestingly, pHrodo™-labelled F(ab) fragments, were all capable of internalising CASPR2 protein, albeit globally less well than their bivalent IgG4 equivalents (**figure 21B**). Indeed, the spearman rank correlation coefficient, between F(ab)s and respective IgG4 mAbs, was high (**figure 21C**, R=0.86, p value=0.011). Additionally, F(ab) fragment internalisation capacity was correlated with surface plasmon resonance (SPR) defined K_Ds (**figure 21D**, R=-0.86, pvalue=0.024). These experiments confirm that CASPR2 autoantibodies can internalise CASPR2 protein independent of protein cross-linking.

The ability of the CASPR2-autoantibody F(ab) fragments to internalise CASPR2 protein may explain how functionally monovalent IgG4 modulates protein function; however, F(ab) fragments are not expected to be abundant *in vivo* and lack Fc-Fc interactions that may further enhance internalisation. To investigate whether a functionally monovalent IgG4 CASPR2-reactive mAb mediates higher internalisation than its F(ab) counterpart, I undertook steps to generate a bispecific IgG4 mAb. In order to prevent F(ab)-arm exchange, I introduced an S228P mutation into mAb E09; the S228P mutation robustly prevents F(ab)-arm exchange, both *in vitro* and *in vivo*[219]. Next, to ensure the correct pairing of heavy and light chain variable domains, the natively paired light chain variable and constant regions were inserted 5' of the heavy chain variable domain and separated by a flexible $(GGGGS)_3$ linker; creating a functional scFv antibody. The variable domains of Daratumumab, an anti-CD38 monoclonal antibody, were subcloned as an scFv antibody to serve as the complementary half of the bispecific antibody. In order to ensure robust downstream purification of a functionally bispecific mAb, each scFv plasmid was inserted with a unique purification tag; for E09, a hexahis tag was inserted and for Daratumumab, a Streptag. Each plasmid encoding the respective mAbs were then co-expressed in HEK293T cells and purified using staged Ni-NTA and Strep-Tactin® affinity chromatography. **figure 21E** depicts the final design. To validate the bi-

specificity of the final mAb, the final eluate and respective flow-throughs from each purification step were tested against either CD38-GFP or CASPR-GFP expressing HEK293T cells (**figure 21F**). Confirmatory of its bi-specificity, the final eluate bound both CD38 and CASPR2. Conversely, the flow through from Ni-NTA and Strep-Tactin® purifications did not bind CASPR2 and CD38 respectively, confirming the successful adsorption of E09 and Daratumumab respectively. Finally, when examining the internalisation capacity of the functionally monovalent E09 mAb, it had comparable internalisation capacity with the E09 F(ab) fragment. Therefore, this suggests little or no contribution of Fc-Fc mediated cross-linking, in the internalisation capacity of functionally monovalent E09 CASPR2-specific IgG4.

Unfortunately, due to the COVID19 pandemic, I was unable to investigate functionally monovalent IgG4s for the remaining mAbs. This remains a limitation, and further study is warranted to validate this paradigm across clonally distinct autoantibodies.

4.4.5 Autoantibody internalisation in primary neuronal cultures

It is possible that, despite robust mAb-mediated internalisation of CASPR2 in HEK293T cells, these patient-derived mAbs may behave differently when exposed to neuronally-native CASPR2. Endogenous CASPR2 on live primary neuronal

cultures, is likely to be more representative of the *in vivo* site of pathogenicity. Indeed, the presence of CASPR2-associated complexes may influence the availability of certain domains for mAb binding. To explore whether neuron-native CASPR2 influences mAb internalisation capacity, I proceeded to test Zenon™ pHrodo™ complexed mAbs in rat primary hippocampal neuronal cultures. For these series of experiments, I chose candidate mAbs identified in **chapter 3** that showed robust binding across different murine tissue-based assays; E07, E08, E09 and H01. In order to ensure reproducibility, each mAb was tested across three independent neuronal cultures. Live cell imaging was acquired over 4 hours on a Leica DMi8 SP8 FALCON, at intervals of 30 minutes. Surprisingly, post-acquisition analysis revealed robust internalisation of H01 and little relative internalisation of E07, E08 and E09. These findings are in contrast to HEK293T-based assays, where E07, E08 and E09 all internalised better than H01 (**figure 22A, B and D**). Furthermore, H01 had displayed no visible binding to primary hippocampal neurons in **chapter 3**. Nonetheless, these findings were reproducible across three independent cultures and supported by the absence of internalisation of isotype control mAb, A33.

A few theoretical explanations for these results exist. Hypothetically; native pairing of CASPR2 with unidentified ligands, may restrict availability of discrete mAb

epitopes; alternatively, natively complexed CASPR2 may respond to autoantibody binding in a conformationally distinct manner and fail to active endocytic pathways. While the exact mechanisms of these observations were not testable, parallel findings from international collaborators offered additional insight and are discussed below.

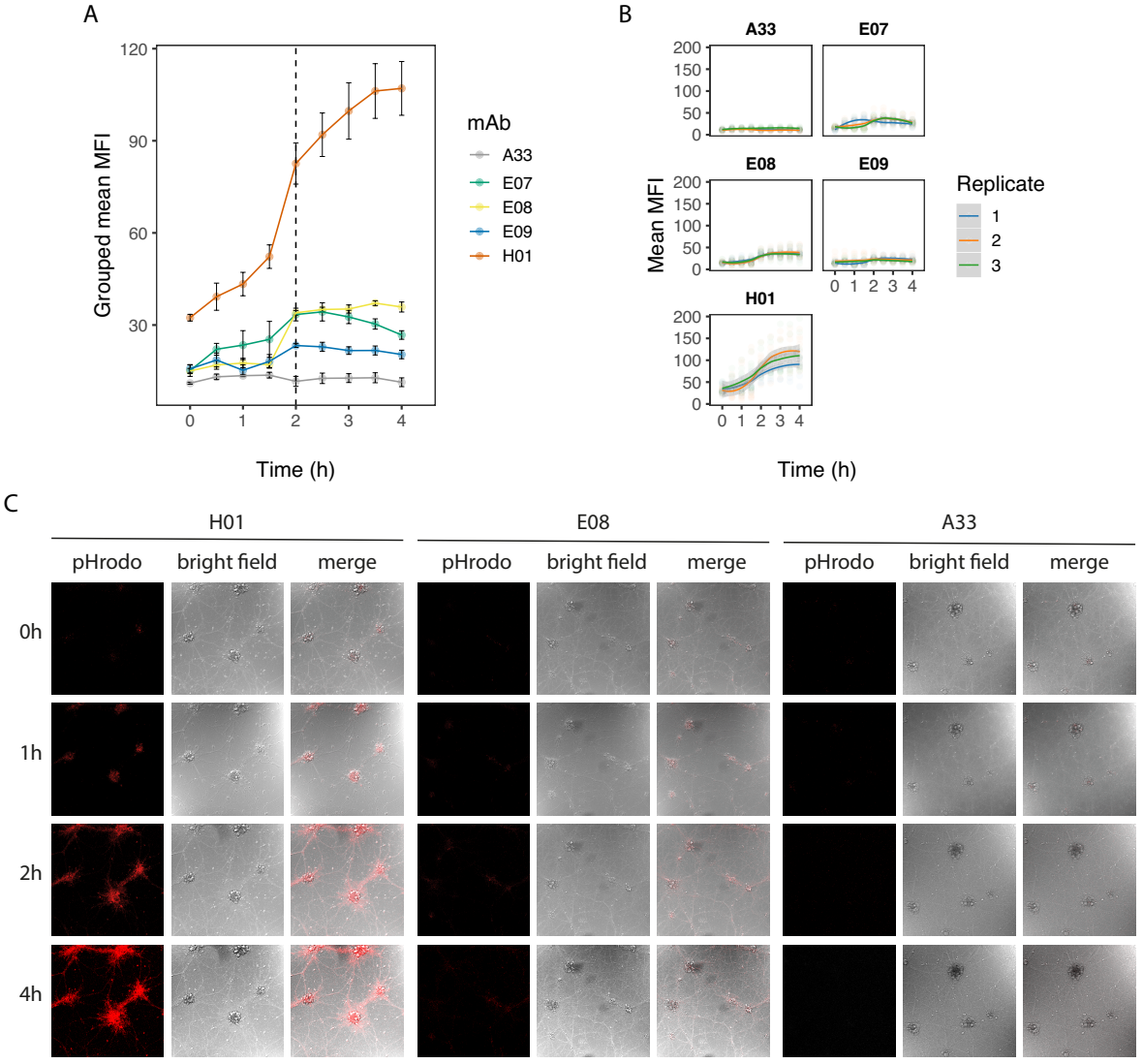

Figure 22. CASPR2 mAb internalisation in primary hippocampal neurons. (A) Interval internalisation analysis of selected mAbs, quantified by mean pHrodo™ fluorescence intensities of 12 regions of interest across three independent cultures. Error bars indicate standard deviations from the mean. The vertical line marks internalisation values at 2hours, the incubation times used for data presented in **section 4.4.6**. (B) Experimental variability assessment by generalised additive models fitted for each independent culture (labelled as `Replicate`) per mAb. Each translucent point represents a region of interest, coloured by replicate. (C) Confocal images of pHrodo™ and brightfield channels over time for two corresponding mAbs and isotype control mAb, A33.

4.4.6 Data from Carvalho group, generated by Dr. Dominique Fernandes PhD

To offer insight into the discrete internalisation capacity of the patient-derived mAbs, I herein present data from external collaborators. The Carvalho group have previously, and independently, shown that CASPR2 modulates AMPA receptor expression at neuronal synapses[89]. Further, patient autoantibodies were shown to decrease both dendritic CASPR2 and AMPA receptor expression in primary cortical neurons; resulting in reduced synaptic transmission as quantified by AMPA receptor-mediated miniature excitatory postsynaptic currents (mEPSCs). To investigate the effects of patient-derived autoantibodies on neuronal synaptic transmission, CASPR2 mAbs H01 and E08 were incubated with primary cortical neurons after 15 days *in vitro*, for 2 hours. Post-treatment, CASPR2 and AMPA receptor cluster intensities were then visualised with fluorescence immunostaining and quantified as fluorescence intensities of regions of interest (ROI) normalised for dendritic length (**figure 23A-F**). Synaptic CASPR2 and AMPA receptors were identified by their

localisation with post-synaptic scaffolding protein PSD-95. All data displayed here, were generated by Dr Dominique Fernandes (Carvalho group, Coimbra University, Lisbon).

Following incubation with CASPR2 mAbs H01 and E08, targeting the Discoidin and Laminin G-like 3 domains respectively, two divergent effects were noted. First, the Discoidin domain-specific H01 mAb significantly reduced total CASPR2 levels ($p<0.01$, Kruskal Wallis (KW) test with *post-hoc* Dunn test), whereas Laminin G-like 3 domain-specific E08 mAb increased both total and synaptic CASPR2 ($p<0.001$, KW with *post-hoc* Dunn). Second, H01 reduced total and synaptic AMPA receptor levels ($p<0.01$, KW with *post-hoc* Dunn), whereas E08 increased their expression (**figure 23A-B**). These findings were not observed with isotype control A33. Interestingly, despite the divergent effects on AMPAR accumulation at synapses, both mAbs impaired AMPAR function; as defined by reduced mean amplitudes of AMPAR-mediated mEPSCs (**figure 23G-O**). These observations suggest that decreased synaptic AMPAR expression and accumulation of non-functional AMPARs, define the mechanisms of CASPR2-associated AMPAR disruption in mAbs H01 and E08 respectively. Additionally, their effects on CASPR2 surface expression independently mirror those of my neuronal pHrodo™

internalisation assays. H01 decreased total and synaptic CASPR2, plausibly due to internalisation and degradation of CASPR2; whereas E08 facilitated increased CASPR2 accumulation, harmonious with its minimal internalisation capacity.

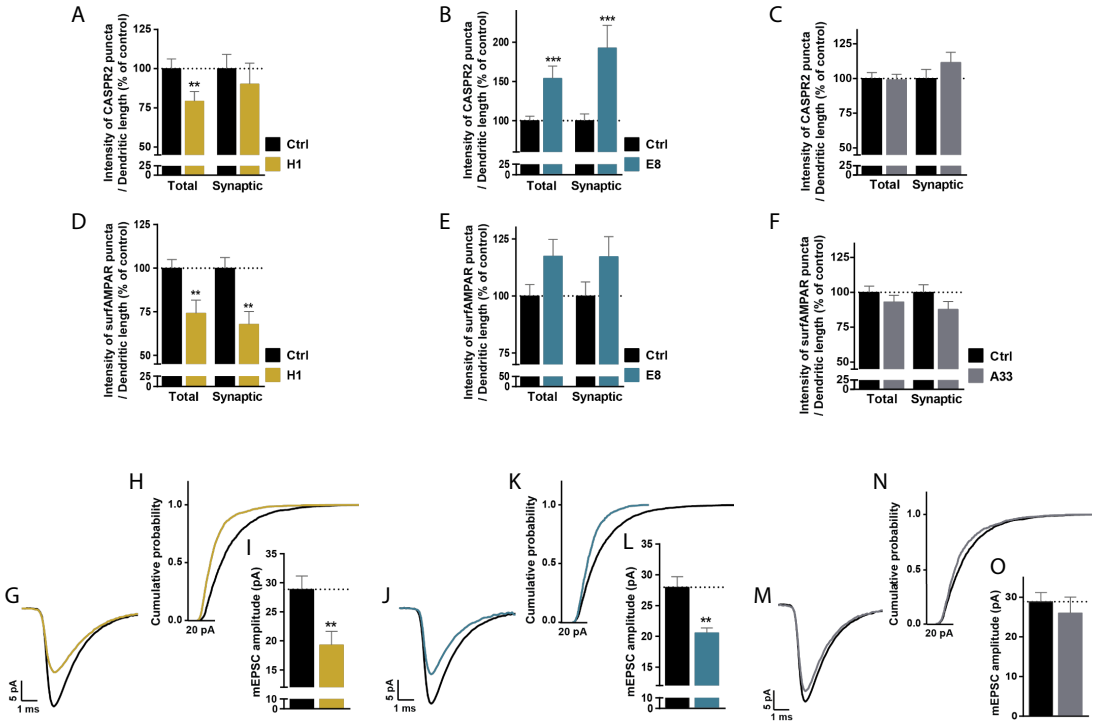

Figure 23. Characterisation of mAb effects on CASPR2 and AMPAR expression in cortical neurons. (A-F) DIV15 cortical neurons were incubated for 2h with 20ug/ml of either H01 (H1) or E08 (E8) mAbs. (A-C) Total and synaptic levels of CASPR2 were evaluated in cortical neurons incubated with H01, E08 and isotype control A33. Values are depicted as percentage of control (Ctrl); control values are derived from corresponding expression of CASPR2 in baseline untreated cultures. (D-E) Total and synaptic levels of AMPA receptors (AMPAR) were evaluated in cortical neurons. (G-O) AMPAR-mediated mEPSCs were recorded from DIV15 cortical neurons incubated with either H01 (G – I), E08 (J-L) or isotype control A33 (M-O). (G, J, M) Average mEPSC traces. (H, K, N) Cumulative histograms of mEPSCs. (I, L, O) Average amplitudes of mEPSCs. (A-F, I, L, O) Results are presented as means ± S.E.M., and statistical significance was determined either by the non-parametric Mann-Whitney test (control vs original mAb): ns – non-significant, *p< 0.05, **p<0.01, ***p<0.001 when compared to control.

4.5. Discussion

In this chapter, I have utilised molecular and fluorescence imaging techniques to investigate the functional effects of patient-derived CASPR2 mAbs *in vitro*. I was able demonstrate, using live cell-based assays, that CASPR2-specific mAbs can directly internalise CASPR2 protein in an antigen and dynamin-dependent manner. Logically, the internalisation capacity of the mAbs correlated strongly with their monovalent affinities, as characterised in **chapter 3**. In line with previous observations in LGI1 encephalitis[81], an IgG4-predominant disease with many similar traits, F(ab) fragments of patient-derived mAbs were capable of mediating antigen internalisation. Building on these observations, and to the best of my knowledge, I show for the first time that a stably monovalent CASPR2-specific IgG4 mAb did not internalise better than its representative F(ab). Together, these observations support the ability of patient-derived mAbs to directly internalise CASPR2 through F(ab) arm binding alone, independent of Fc-Fc interactions. The generalisability of these findings, to other autoantibody-associated IgG4-predominant diseases, remains to be explored; however, they offer novel insight into the long-debated internalisation capacity of functionally monovalent IgG4 antibodies.

Surprisingly, the ability of the mAbs to internalise CASPR2 were different in rat primary hippocampal neurons compared to HEK293T cells. Correspondingly, correlations of internalisation capacity with mAb affinities were lost in neurons. This change in functional property was supported independently by parallel observations from international collaborators. The precise reason for this discrepancy could not be elucidated by the data at hand, however there are a few hypothetical possibilities. Endogenous neuron-native CASPR2 is proposed to exist as part of potassium channel complexes or in complex with CNTN2 at the juxtaparanodes[138]. While the extracellular interaction of CASPR2 with potassium channel complexes remains uncharacterised, CASPR2-CNTN2 complexes are proposed to be dependent on Laminin G-like 1 and Laminin G-like 4 domains[88]. Therefore, it is possible that the mAb epitopes of E07, E08 and E09, are prevented from inducing internalisation due to their proximity to CASPR2-ligand domain interactions. Alternatively, differential mAb-induced disruption of intracellular interactions with PDZ proteins, via the CASPR2 cytosolic tail, may also contribute to their entry into endocytic pathways[139]. Despite their opposing ability to internalise CASPR2, mAbs H01 and E08 were both capable of disrupting AMPAR-mediated signalling in neurons, *in vitro*; suggesting that disruption of synaptic signalling is dependent on functionality of available CASPR2 and AMPARs, rather than observable expression levels.

Finally, I was unable to replicate the previously reported ability of CASPR2 autoantibodies to block CASPR2-CNTN2 interactions. In my hands, the extracellular domains of CASPR2 and CNTN2 had no observable interactions, as previously reported[87,141]. My findings are concordant with those observed by Poliak et al., Traka et al., Rubio-Marrero et al.,[136,140,153] and unpublished data from the thesis of Gabriele Vincelli[220] of the Cormoletti group[140]. The further molecular characterisations of discrepantly reported CASPR2 ligand interactions was not within the remit of this DPhil, but warrants further study. Indeed, the overarching role of CASPR2 protein in neuronal homeostasis and its direct molecular interactions, remains unclear; however, the data presented in this chapter indirectly support its modulation of AMPAR-mediated signalling.

4.6 Conclusion

Patient-derived CASPR2-specific mAbs were capable of disrupting homeostasis of neuronal excitability. In this chapter, I demonstrate that CASPR2 mAbs internalised CASPR2 protein via dynamin-dependent endocytic pathways. Contrary to dogma, internalisation capacity is not dependent on bivalent F(ab)-arm-mediated or Fc-mediated cross-linking of antigen, and differed across HEK and neuron-based assays.

Finally, mAb-mediated disruption of synaptic AMPAR signalling was reproducible across their divergent effects on CASPR2 and AMPAR expression levels, *in vitro*. Importantly, these observations highlight the insensitivity of immunofluorescent protein quantification, to downstream functionality of associated receptors and synaptic plasticity.

4.7 Acknowledgements

Dr Dominique Fernandes (Carvalho group, Coimbra University, Lisbon) performed all experiments and plots described in **section 4.4.6**, and gave permission, along with Associate Prof. Ana Carvalho, to represent this data in my thesis.

Chapter 5 Characterising unmutated common ancestors of CASPR2 memory B cells

5.1 Introduction

There are two proposed routes of acquired antigen specificity in the adaptive B cell response. First, reactivity to antigen can be conferred from paired heavy and light chain germline variable domain gene rearrangements[221,222]. Second, reactivity to antigen may be acquired from an otherwise non-reactive BCR through bystander activation and affinity maturation in germinal centres[62]. Innate reactivity to foreign antigens is typically "positively selected" for high affinity participation in both extrafollicular and germinal centre pathways of B cell maturation. Self-reactive clones in this context, are anticipated to be negatively selected at pre-germinal centre tolerance checkpoints, as described in **chapter 1**. Interestingly, previous observations have identified an increase in self-reactivity of post-germinal centre class-switched memory B cells, in health[44]. This observation is proposed to be an effect of germinal centre-mediated diversification, a desirable feature in the development of polyclonal antibodies to foreign antigens. However, the generation of self-reactive clones, from otherwise non-reactive BCRs, may be a plausible source of autoantibodies. Therefore,

the retrospective study of autoreactive memory B cell clones may offer insight into their origins.

In **chapter 2**, we observe that tolerance to CASPR2 protein, in both disease and health, is permissive for the development of CASPR2-reactive naïve B cells. Therefore, risk of developing CASPR2-antibody encephalitis is unlikely to be dependent on the existence of CASPR2-reactive naïve B cells alone. Indeed, these naïve B cell-derived mAbs failed to bind bivalently to CASPR2 protein, suggesting that their BCRs may not achieve sufficient avidity to actively participate in extrafollicular or germinal centre responses. Since our per repertoire sampling size is small, the question of whether CASPR2-reactive memory B cells are derived from high-affinity naïve B cells or non-reactive naïve B cells, remains.

Studying affinity maturation of individual B cell clones is challenging due to dynamic time and tissue dependent factors. There are currently no methods to robustly track individual B cell clones *ex vivo* in humans. Serial sampling may cross-sectionally capture clonal lineages over a window of time[223]; however, the likelihood of capturing the progenitor naïve B cell clone is confounded by both sampling size and the assumption that experimental capture of a single clone does not then exclude its

presence in the remaining repertoire[224]. Phylogenetic reconstruction of clonal lineages offers an attractive medium to study clonal diversification and infer ancestral clones[225,226]; however, modelling somatic hypermutation (SMH) remains challenging due to inability to accurately account for insertions and deletions. Further, the preferential targeting of mutational "hotspots" and their *de novo* generation by activation induced deaminase (AID), break the usual phylogenetic assumption of independent and identical processes between mutation sites[227]. Nonetheless, despite its limitations, inferring unmutated common ancestors by best alignment and reversion to germline variable domain genes, represents a powerful tool to study ancestral properties of *ex vivo* mutated BCRs, by proxy.

In this chapter, I use IMGT germline gene alignments to reverse somatic hypermutations (SMH) and infer representative "antigen naïve" variable domain sequences of the memory B cell-derived CASPR2 mAbs. By studying these "unmutated common ancestors" (UCA), I aimed to understand whether representative "naïve" BCRs of CASPR2-reactive memory B cell-derived mAbs are capable of germline encoded binding and modulation CASPR2.

5.2 Hypothesis

5.2.1 CASPR2-reactive memory B cell-derived mAbs bivalently bind CASPR2 as germline UCAs, inferring that they derive from high affinity naïve B cell precursors.

5.2.2 UCAs of CASPR2-reactive memory B cells have pathogenic potential *in vitro*.

5.3 Methods

5.3.1 UCA reversion method

To obtain representative unmutated VDJ sequences from mutated variable domains derived from memory B cells, the following procedure was followed. Somatically hypermutated anti-CASPR2 variable domain sequences were first aligned with IMGT-VQUEST for annotation. Selected sequences were then back mutated by replacing non-silent mutations with their corresponding germline template nucleotides, as defined by the best matched variable domain gene from IMGT's reference database. N region nucleotides, which are non-template random insertions at V-D, D-J and VL-JL junctions in the junction region of heavy and light chains, were not modified due to risk of inaccurate alignments. Finally, using the IMGT junctional analysis tool, CDR3 regions of the heavy and light chains were also back

mutated to the best aligned D-gene. All reverted sequences were then ordered as gene fragments from IDT with corresponding cloning sites flanking the 5' and 3' regions, and inserted into the Abvec expression vector as per **chapter 2** methods.

5.3.2 Domain specificity characterisation

Mammalian expression vectors either containing full length CASPR2-EGFP or the individual CASPR2-CASPR4 domain swap constructs, described in **chapter 3**, were individually transfected in 96 well plates of HEK293T cells with branched PEI at a DNA to PEI ratio of 1:3. After 24 hours of expression, media was exchanged for primary samples diluted to desired concentrations in complete medium buffered with 25mM of HEPES, and incubated for 1 hour at room temperature. Cells were then washed three times in complete medium and fixed with 4% formaldehyde for 10 minutes. After additional washes, goat anti-human AF594 detection antibody (Thermofisher #A48275) was incubated for 1 hour at 3ug/ml and binding visualised on an inverted fluorescence microscope.

5.3.3 Immunohistochemistry staining

Immunohistochemistry was performed as per **chapter 3**, detailed methods. In brief, pre-prepared sections of adult female Wistar rats, were first stained with primary mAbs at 50ug/ml overnight at 4^0C. Subsequently, staining with biotinylated goat

anti-human secondary antibody at a 1:500 took place for 1 hour at room temperature. Finally, HRP labelling was performed using the Vectastain® Elite® ABC HRP kit and developed with diaminobenzidine before ethanol dehydration and mounting.

5.3.4 Neuronal culture

Neuronal culture methods were as described in **chapter 3**. In brief, dissected hippocampi from Wistar rat pups (1-3 days postnatal) were dissociated with 2.5% trypsin at 37^0C and manual agitation using a narrowed grass pipette. 40,000 cells/well were seeded in neurobasal media on 12mm poly-L-lysine-treated coverslips. After attachment, cultures were supplemented with astrocyte conditioned media and cultured for up to 21 days in vitro (DIV). All experiments were performed at DIV15.

5.3.5 Surface plasmon resonance

Surface plasmon resonance was performed as per detailed methods in **chapter 3**. Memory-derived mAb and UCA data shown across **chapter 3** and in this chapter, are from the same experiment for comparability. Visualised sensograms represent the same batch and thaw of soluble CASPR2-ECD.

5.3.6 pHrodo™ internalisation live cell-based assay

pHrodo™ internalisation assays were performed either across CASPR2 expressing HEK293T cells, or rat primary hippocampal neuronal cultures (cultured as per **chapter 3** methods). For HEK293T cells, monolayers of HEK293T cells in 96 well plates were transfected with CASPR2-EGFP expression vectors as described in **chapter 2** methods. Following 24 hours of expression, pHrodo™ pre-labelled or pre-complexed mAbs were incubated overnight at 20ug/ml. All labelling procedures are detailed in **chapter 4** methods. Interval recordings were either image captured on a Leica DMi8 SP8 FALCON, or mean fluorescence quantified on a BMG OMEGA FLUOstar using a 560-10/650 filter. For dynasore inhibition assays, pre-treatment of CASPR2 expressing HEK293T cells for 1 hour with 50μM of dynasore was performed prior to incubation with mAbs.

5.3.7 Cortical neuron culture- Coimbra University

All cortical neuronal data from external collaborators were generated using methods described in Fernandes et al.,[89]. MAbs were tested on DIV15 cortical neurons and incubated at 20ug/ml for 2 hours prior to downstream assessment.

5.4 Results

5.4.1 Inferring unmutated common ancestors

To characterise their inferred naïve B cell ancestral BCRs, all memory B cell-derived mAbs were back-mutated to their inferred germline UCAs (schematic of reversion shown in **figure 24A**). Typically, reversion of heavy chain CDR3s (HCDR3) is not performed due to risk of inaccurate D-gene alignments. However, since HCDR3s are subject to somatic hypermutation, in these experiments, reversions were performed to comprehensively characterise the whole variable domain as a reconstructed germline rearrangement.

After cloning and expression of the UCAs, I obtained stable concentrations of 6/7 UCAs. The UCA of mAb E06 was not able to be expressed despite being in frame and productive. This was not overcome with bioinformatic re-optimisation of codons for mammalian expression. I hypothesise that artificial reversion, in this instance, is likely to have generated an unstable protein that was subject to intracellular degradation; therefore, the characterisation of E06 UCA was not possible. From the remaining UCAs, 4/6 bound when expressed as both IgG and IgM (**figure 24B**), of which 3/4 retained binding as F(ab) fragments, supporting their theoretical ability to bind as monovalent IgG4s. As expected, all UCAs targeted the corresponding

epitopes of their parent mAb (**figure 23C**). For the UCAs that did not bind, H01-UCA and H02-UCA, it plausible that their acquired binding as memory B cell-derived mAbs represents bystander convergence from non-reactive clones. While this is the difficult to prove definitively, their successful expression as soluble IgG supports their stability and theoretical existence as a functional IgG.

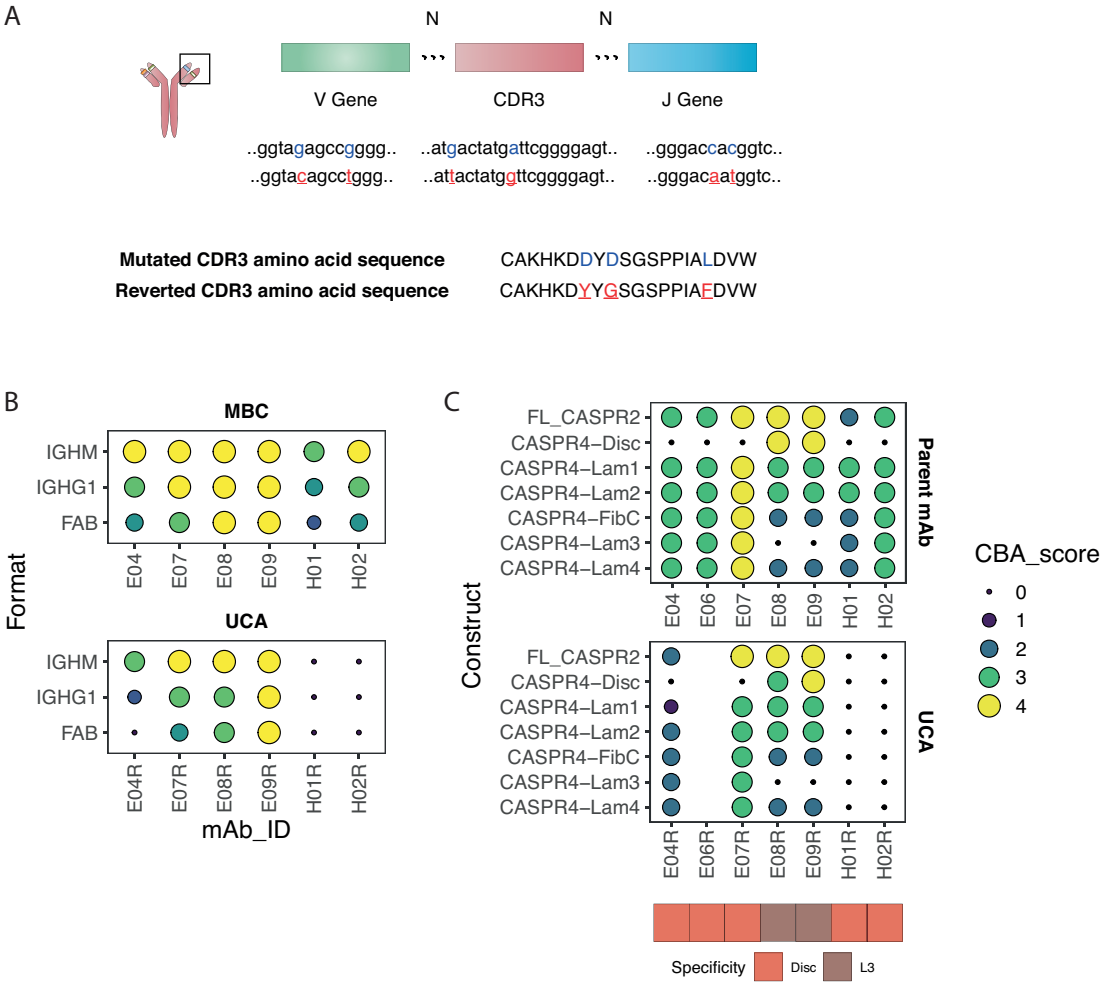

Figure 24. Generation of unmutated common ancestors (UCAs) and assessment of their CASPR2 binding. (A) Schematic of reversion technique to back mutate heavy and light chain sequences. (B) Dot-plots of CASPR2 cell-based assays scores across UCAs and their corresponding memory B cell (MBC)-derived mAbs. (C) Domain specificities characterised using CASPR2-CASPR4 deletion constructs (described in **chapter 3**). Dot-plots visualise cell-based assay scores and inferred specificities are visualised as coloured tiles below; domain assignments by colour are as per legend.

5.4.2 Affinities of UCAs

Somatic hypermutations are typically considered to be advantageous for antigen binding. Indeed, germinal centre dynamics, in acute viral infections, positively select for high affinity binding clones to contribute to plasmablast and memory B cell compartments[228]. However, murine models of auto-reactive B cell development suggest that some somatic hypermutations aid rescue of autoreactive clones by abrogating their self-reactivity[229].

To explore whether somatic hypermutations contribute positively or negatively to CASPR2-reactivity, UCAs of memory B cell-derived mAbs were investigated using two modalities; live cell-based assays (CBAs) and surface plasmon resonance (SPR). First, using live CBAs, which present CASPR2 in its full-length membrane-anchored form, I found that UCA binding were negatively impacted by the removal of SHM (**figure 25A**). However, two mAbs, E08 and E09, retained comparable end-titres to their mutated parents. To explore these dynamics using a one to one binding model, UCAs were characterised using SPR as per **chapter 3 methods**. Confirmatory to live cell-based assays, UCA binding to CASPR2 were globally worse than parent mAbs and all displayed undesirable changes in dissociate rates (**figure 25B**); resulting in faster off-rates and less optimal binding (Ka and t1/2 values in **table 4**). Notably,

although E09-UCA displayed a higher K_D to parent mAb E09, it remained superior in binding to other memory B cell-derived mAbs. Exploring this further, mutational counts revealed that mAb E09 contained only three non-silent mutations in the heavy and light chains respectively; supporting its true germline encoded high-affinity for CASPR2. Overall, SMH contributed positively to binding affinities of all CASPR2 mAbs.

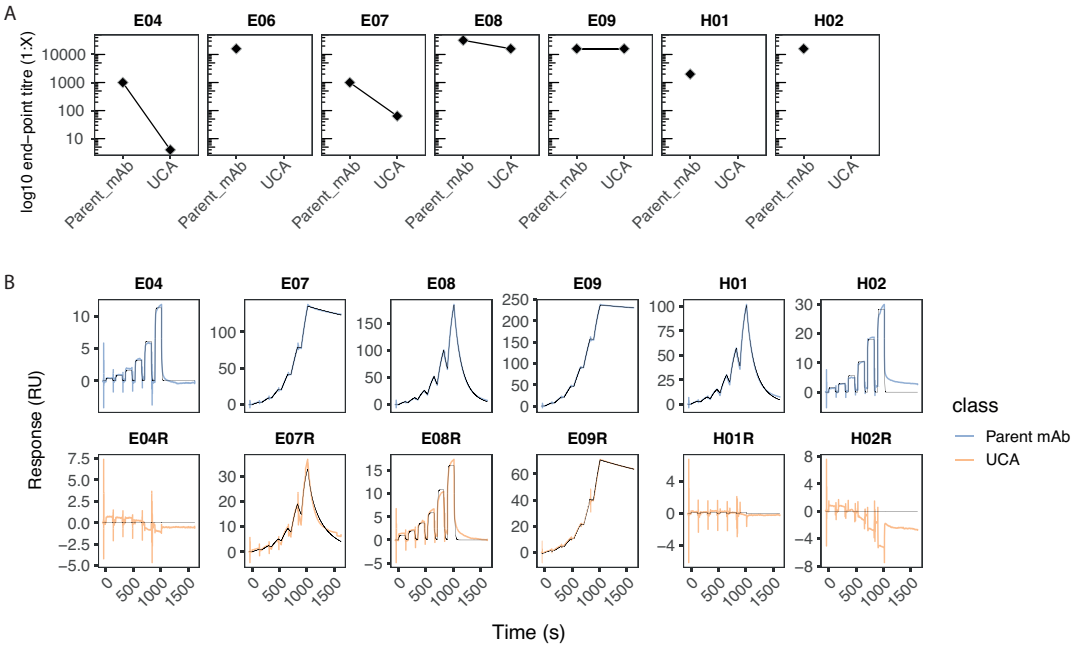

Figure 25. End-point titres and surface plasmon traces for CASPR2 mAbs and their respective UCAs. (A) Comparison of end-point titres of CASPR2 mAbs and their respective UCAs. End point titres visualised as log10 transformed dilution factors. (B) Surface plasmon resonance traces of mAbs (top) and their respective UCAs (below).

Table 4 UCA binding kinetics

Antibody	Ka ($M^{-1}s^{-1}$)	Kd (s^{-1})	K_D (M)	t 1/2 (s)
E09	3.04E+05	4.64E-05	1.53E-10	1.49E+04
E09-UCA	5.09E+04	1.70E-04	3.33E-09	4.08E+03
E08	3.70E+08	1.11E+01	3.00E-08	6.25E-02
E07	3.14E+03	1.54E-04	4.90E-08	4.51E+03
H02	4.79E+05	2.62E-01	5.47E-07	2.64E+00
H01	1.63E+07	1.37E+01	8.37E-07	5.07E-02
E08-UCA	6.38E+04	8.92E-02	1.40E-06	7.77E+00
E07-UCA	2.60E+03	3.99E-03	1.54E-06	1.74E+02
E04	3.21E+04	1.72E-01	5.37E-06	4.03E+00
E06	1.08E+03	2.89E-01	2.67E-04	2.40E+00
H01-UCA	NA	NA	NA	NA
E04-UCA	NA	NA	NA	NA
H02-UCA	NA	NA	NA	NA

Ka = associate rate; Kd = dissociation rate; K_D = dissociation constant; t1/2 = dissociation half time; all values derived from the Cytiva biacore systems software.

5.4.3 Tissue binding of UCAs

Next, UCA binding to target neuronal tissue was assessed across rat primary hippocampal neurons and rat brain sections (**figure 26**). Consistently, UCAs showed a reduction in binding to hippocampal neurons and did not acquire non-specific or polyreactive binding. While mAb E09-UCA did show some subtle staining of

neuronal dendrites, the binding was insufficiently consistent to be deemed reproducible. As seen before, the immunohistochemistry (IHC) staining of mature rat brain sections revealed robust binding to neuronal tissue when compared with primary rat hippocampal neurons; hypothesised to be due to CASPR2 avidity gradients across neuronal maturation[142]. Here, previously IHC-reactive mAbs E07, E08 and E09 retained binding as UCAs in a distribution consistent with CASPR2 expression, whereas H01-UCA lost binding.

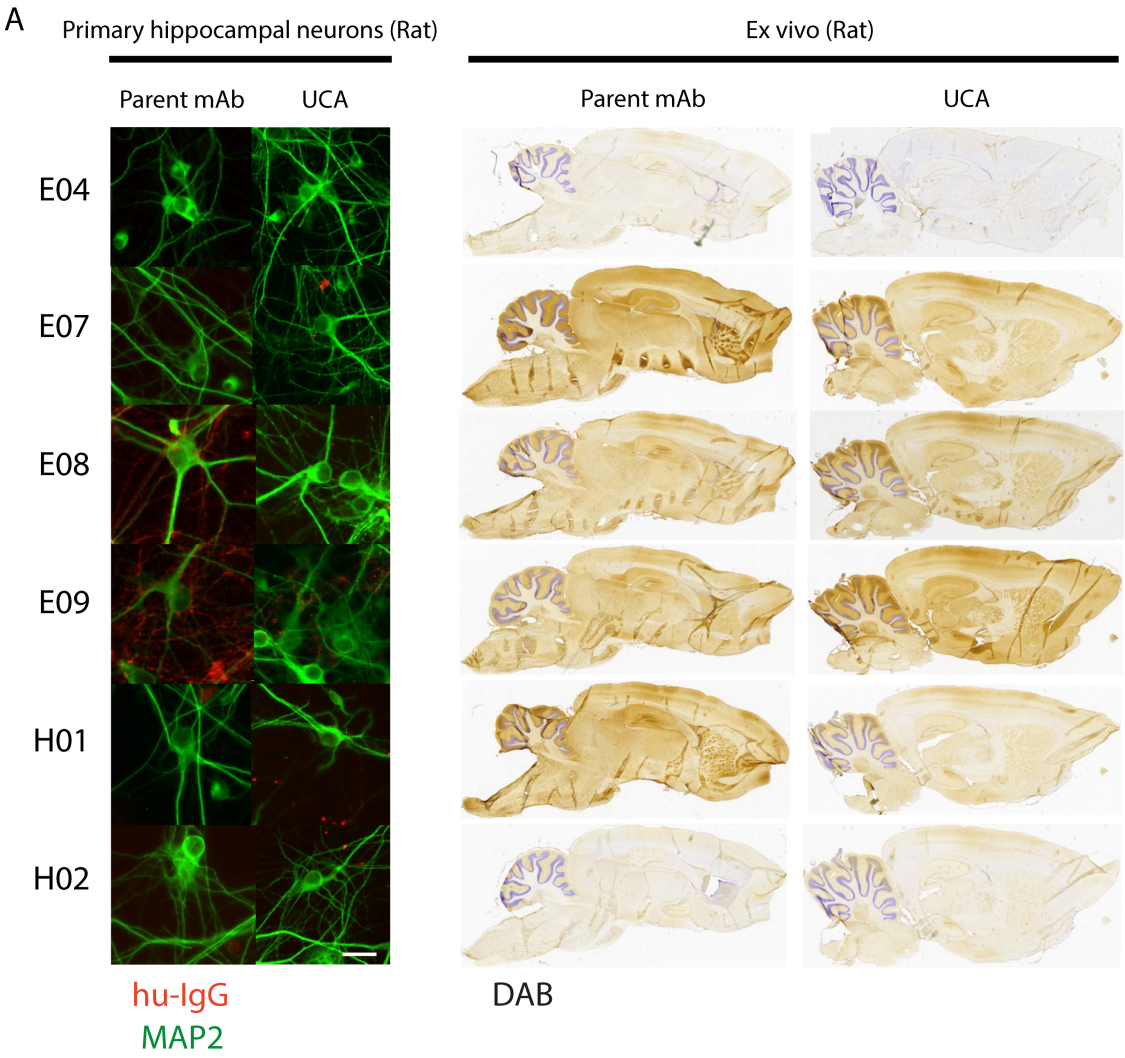

Figure 26. UCA and corresponding parent mAb binding to primary hippocampal neuron and rat brain sections. (A) Merged images of CASPR2 mAbs binding to primary hippocampal neurons and rat brain sections. Marker labels are indicated at the bottom. huIgG = human IgG; MAP2 = microtubule associated protein (neuron specific cytoskeleton protein); DAB = 3, 3-diaminobenzidine.

5.4.4 Internalisation capacity of UCAs

Having confirmed the ability of the UCAs to bind CBAs and neuronal tissue as bivalent IgG, their properties are already distinct from native naïve B cell-derived mAbs. Therefore, hypothetically, they may be capable of pathogenic potential as secreted IgG. To test this, their internalisation capacity was assessed against

corresponding parent IgG4 mAbs and parent F(ab) fragments (**figure 27A**). Utilising the previously described pHrodo™ HEK293T-based internalisation assay, I was able to demonstrate that mAbs E09-UCA, E08-UCA, E07-UCA and E04-UCA retained internalisation capacity, but with significantly less capacity than their parent mAbs (p=0.0328, post KW Dunn test, with BH correction). When compared to their parent F(ab) counterparts, UCAs had comparable internalisation capacity (p=0.6, post KW Dunn test, with BH correction). As before, the internalisation capacity in CASPR2 expressing HEK293T cells correlated with their SPR-defined K_D (**figure 27C**, spearman coefficient -0.94, p=0.017).

Consistent with findings in **chapter 4**, differential internalisation patterns were seen in primary neuronal cultures (**figure 27B**). In particular, mAbs E07, E08 and E09 did not internalise well when compared to H01. To examine whether their inferred UCAs were also capable of internalisation, neuronal pHrodo™ assays were performed and internalisation capacity quantified on a BMG-Omega FLUOstar plate reader. Consistent with the confocal imaging-based quantification, mAbs E07, E08 and E09 exhibited low internalisation capacity compared to mAb H01. E07-UCA and H01-UCA had notable loss of internalisation (p=0.04 and p=0.00002, respectively, post KW Dunn test, with BH correction) with the latter losing all internalisation capacity

as expected from its loss of CASPR2 reactivity. E08-UCA and E09-UCA retained a low-level internalisation capacity comparable to their parent mAbs, suggesting little change in their intrinsic properties; further confirmed by consistently absent correlation with SPR-defined affinities (**figure 27D**).

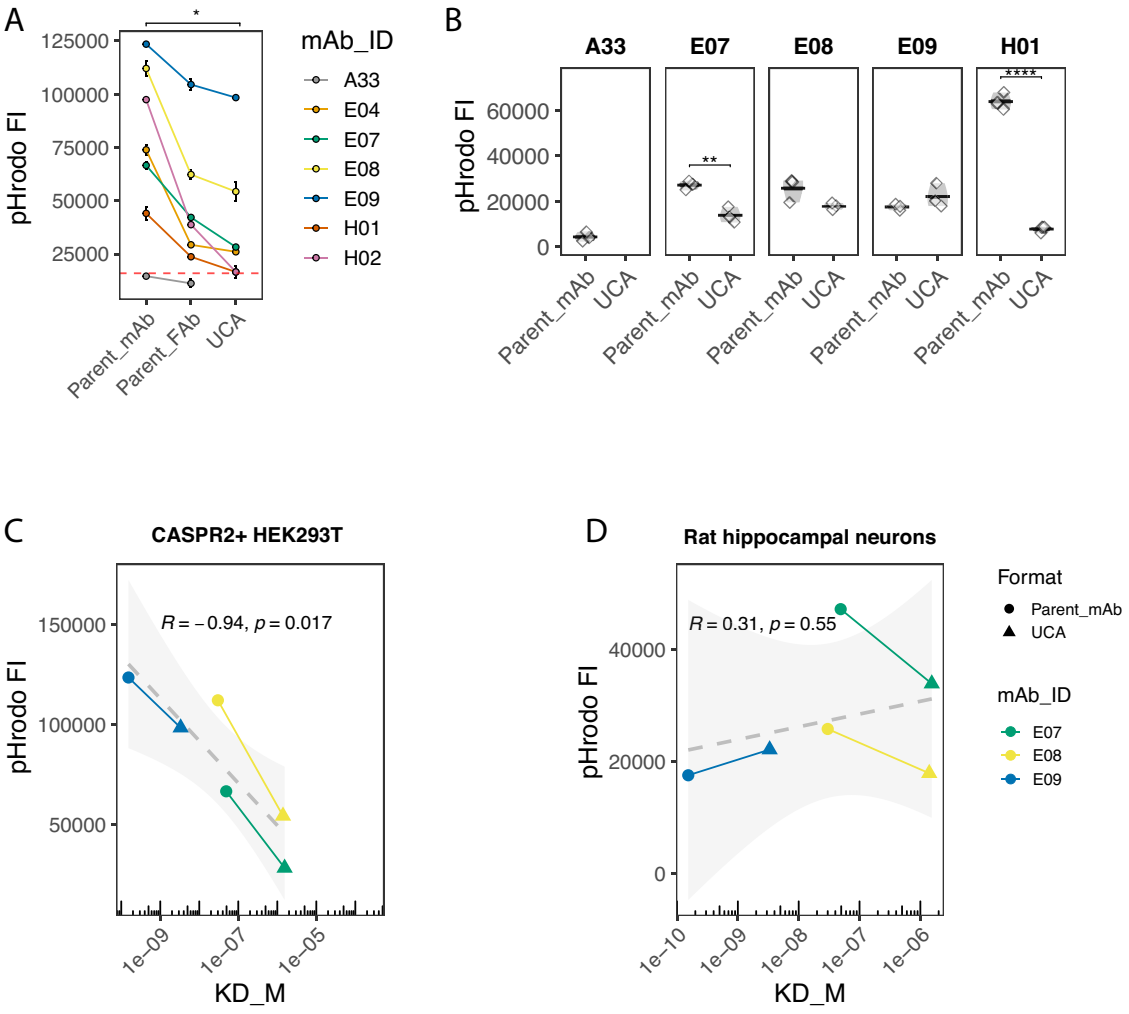

Figure 27. Comparing internalisation capacity of unmutated common ancestors (UCAs) vs. corresponding parent mAbs. (A) Comparison of internalisation capacity across UCAs, their corresponding parent mAb and parent mAb-derived F(ab) fragments. Internalisation is quantified by pHrodo™ fluorescence intensity. All experiments were performed in triplicate and points indicate the mean fluorescence intensity and error bars depict standard deviation from the mean. (B) Violin plots

comparing internalisation capacity of UCAs and corresponding parent mAbs in neurons. (C) Spearman correlation coefficient of CASPR2 mAb internalisation capacity vs. SPR defined dissociation constants (KD) on CASPR2 expressing HEK293T cells. UCAs and matched parent mAbs are coloured by parent mAbs and connected by solid lines. (D) Spearman correlation coefficient of CASPR2 mAb internalisation capacity vs. SPR defined dissociation constants (KD) on primary rat hippocampal neurons. UCAs and matched parent mAbs are coloured by parent mAbs and connected by solid lines. All statistical tests were performed as follows: Kruskal Wallis testing with post-hoc Dunn tests; multiple testing correction was performed using the Bejamini-Hochberg procedure (BH). If significant: * $p<0.05$, ** $p<0.005$, *** $p<0.0005$, **** $p<0.00005$

5.4.5 Data from Carvalho group, generated by Dr. Dominique Fernandes PhD

Finally, to examine whether UCAs abrogated effects on CASPR2 and AMPAR expression levels, data from external collaborators is presented. Data and plots displayed in this segment was generated by Dr Dominique Fernandes, Carvalho group, Coimbra University, Lisbon.

Following identical experimental procedures as to those described in **chapter 4**, the UCAs of H01 and E08, here depicted as H01R and E08R ("R" = revertant), displayed variable loss of influence on CASPR2 and AMPAR expression. H01R no longer significantly reduced CASPR2 and AMPAR expression levels compared to control (**figure 28 A, C**). E08R appeared to retain significant, albeit with less, upregulation of total and synaptic CASPR2 ($p<0.01$ and $p<0.001$, respectively), but was no longer able to upregulate AMPAR expression (**figure 28B, D**). The precise mechanism for this observation has yet to be characterised and is an active area of

study as part of the collaboration with the Carvalho group. Similarly, the ability of the UCAs to modulate AMPAR-mediated mEPSCs remains a work in progress. In summary, there appears to be early evidence that UCAs of memory B cell mAbs may lose pathogenic potential *in vitro*.

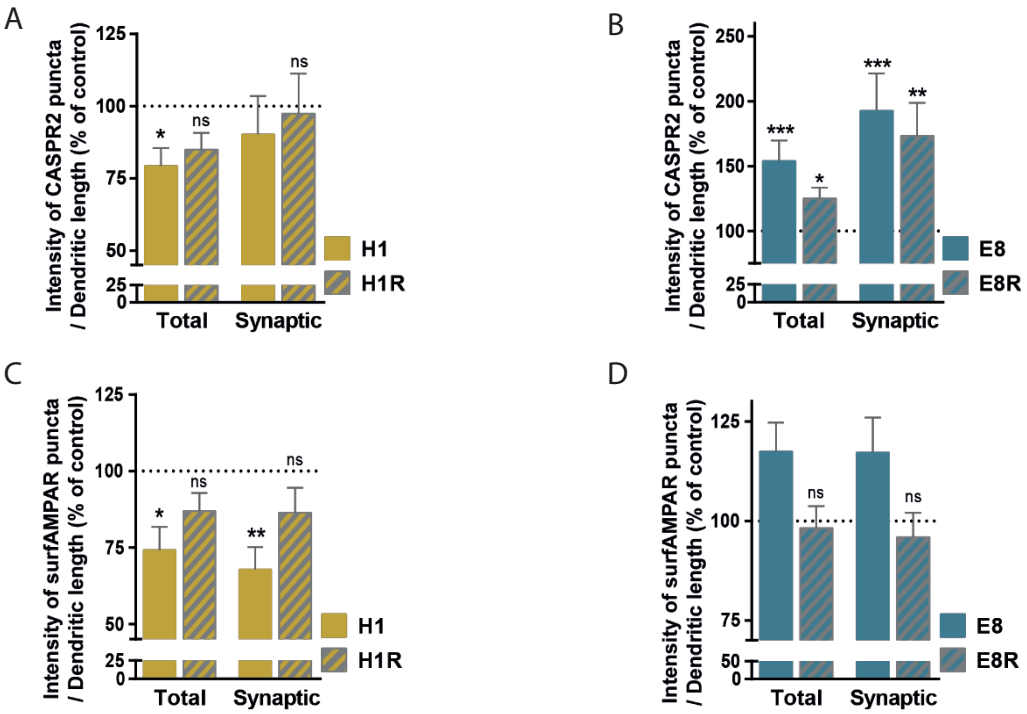

Figure 28. Comparison of UCA and parent mAb effects on CASPR2 and AMPAR expression in cortical neurons. (A-D) DIV15 cortical neurons were incubated for 2h with 20ug/ml of either H01 (H1) and H01-UCA (H1R) or E08 (E8) and E08-UCA (E8R) mAbs. (A-B) Total and synaptic levels of CASPR2 were evaluated in cortical neurons incubated with H01, H01-UCA, E08 and E08-UCA. Values are depicted as percentage of control (Ctrl). Control values are depicted as the horizontal dotted line and are derived from corresponding expression of CASPR2 in baseline untreated cultures. (C-D) Total and synaptic levels of AMPA receptors (AMPAR) were evaluated in cortical neurons. Results are presented as means ± S.E.M., and statistical significance was determined by non-parametric Kruskal-Wallis test, followed by Dunn's Multiple Comparison post-hoc test: ns – non-significant, *p< 0.05, **p<0.01, ***p<0.001 when compared to control.

5.5 Discussion

In autoantibody-mediated diseases, the characterisation of UCAs has offered insight into clonal development and the origin of autoreactive B cell clones. In pemphigus bullosa, an IgG4 predominant autoimmune disease of the skin, and systemic lupus erythematosus, a systemic inflammatory disease, UCAs of autoreactive memory B cell clones do not bind autoantigens[43,166,230]. Similarly, UCAs of anti-cytokine antibodies from autoimmune regulator (AIRE)-deficient patients follow the same pattern[231]. In diseases of the central nervous system, there are appear to be mixed observations. UCAs of AQP4-reactive plasma cells, derived from cerebrospinal fluid (CSF) of patients with neuromyelitis optica, did not bind AQP4[118]. Whereas in NMDA-receptor antibody encephalitis, unmutated germline B cells are readily detected and have pathogenic potential[232,233]. While these studies should be interpreted with caution, due to technical considerations and typically small sampling depth, they may imply dichotomous paradigms of autoreactive B cell generation. Where UCAs are not able to bind disease-associated autoantigens, central B cell counterselection is inferred to be intact and peripheral defects of immune tolerance may contribute to the generation of autoreactive clones. On the other hand, in diseases where UCAs do bind, such as muscle-specific kinase (MUSK)-

antibody myasthenia [218], defective central counterselection may be the main contributor to the ongoing supply of autoreactive naïve B cells.

My first observation, that CASPR2 memory B cell-derived UCAs can bind as monovalent F(ab)s, distinguishes them from the naïve B cell-derived mAbs described in **chapter 2**; which were only capable of binding as high avidity IgM. This supports a fundamental difference in germline-encoded CASPR2 affinity between B cells that go on to contribute to memory responses in patients, and those that reside within the naïve B cell pools. Additionally, the absence of binding of two memory B cell clones, H01 and H02, support a mixed model of autoantigen convergence in CASPR2 encephalitis. Unfortunately, these data alone, cannot distinguish between the potential activation thresholds of naïve and inferred UCA B cell receptors. This is an important consideration for their immunobiological relevance, as the potential participation of low-avidity naïve B cells cannot be excluded.

Intuitively, removal of somatic hypermutation negatively impacted the binding properties of memory B cell-derived mAbs. In particular, loss of desirable binding dynamics, such as a slow off-rate and low dissociation constants, were evident. Despite this, internalisation capacity of UCAs remained comparable to corresponding

parent F(ab)s. However, when tested in neurons, their ability to modulate CASPR2 and/or AMPAR expression was largely impaired; suggesting that affinity maturation remains a prominent contributor to their pathogenic potential.

There are a few key limitations of this data to consider. Despite the reproducibility of the observations across experimental variables, the number of memory B cell-derived mAbs that bind neuronal tissue remains low (n=4). Furthermore, only two were tested for their ability to modulate CASPR2 and AMPAR expression; based on their rat brain tissue and mouse CASPR2 reactivity. Therefore, the generalisation of these findings requires further validation. To address this in future, I have co-led the first experiment of a validation study where we have isolated ~500 CASPR-reactive mAbs from four patients and four healthy donors. Using this data, we hope to validate the findings described in this thesis.

5.6 Conclusions

CASPR2 reactive memory B cell-derived mAbs may derive from two distinct sources of precursor naïve B cells; those that are germline-encoded to bind CASPR2 protein, and those that are non-reactive. CASPR2-reactive UCAs of patient-derived memory B cells, have higher avidity for CASPR2 than the CASPR2-reactive naïve B cells

observed in both patients and healthy donors. However, UCAs reveal that memory B cell-derived mAbs require somatic hypermutation to enhance their potential pathogenicity. Further high-throughput experimental validation is required to extend these observations and establish their generalisability.

5.7 Acknowledgements

Dr Dominique Fernandes (Carvalho group, Coimbra University, Lisbon) performed all experiments and plots described in **section 5.4.5**, and gave permission, along with Associate Prof. Ana Carvalho, to represent this data in my thesis. Dr Victor MgBachi supervised immunohistochemical staining of rat brain sections. Robert Donat performed SPR studies and provided raw data for analysis; SPR data is presented with his permission.

Chapter 6 Summary and future work

6.1 Overall summary

In health, the sheer diversity of B cell receptors, generated through V(D)J recombination, is prone to formation of polyreactive or self-reactive species[42,180,229]. The majority of these poly/autoreactive B cells are negatively selected across proposed B cell developmental tolerance checkpoints[42,180,234], but their escape and pathogenic potential in neuroglial surface autoantibody-mediated diseases, remains poorly characterised. The aims of this thesis were to examine the integrity of B cell tolerance checkpoints and autoantibody properties in CASPR2-antibody encephalitis, to better understand disease pathogenesis. Here, I discuss the impact of my findings and suggest potential directions for further works to address remaining gaps in current scientific knowledge.

6.2 Is B cell tolerance impaired in CASPR2-antibody encephalitis?

In this thesis, CASPR2-reactivity across pre-germinal centre naïve B cells and post-germinal centre class-switched B cells, were investigated. Bulk *ex vivo* B cell cultures revealed that CASPR2-reactive class-switched memory B cells are exclusive to patients, whereas CASPR2-reactive naïve B cells exist in both disease and health.

However, mAbs generated from naïve B cells only bound CASPR2 as IgM and not as bivalent IgG. As CASPR2 IgM were not detected in patients or healthy donors, these naïve B cells are of unlikely relevance to the immediate circulating Ig pool. Since CASPR2-antibody encephalitis is characterised by the predominance of IgG4 autoantibodies[83,86,169], the monovalent binding of memory B cell-derived F(abs) supported their potential disease relevance as F(ab)-arm exchanged IgG4. Intriguingly, in contrast to naïve B cell-derived mAbs, some unmutated common ancestors (UCAs) of memory B cell mAbs retained monovalent binding. Furthermore, other UCAs had no detectable binding to CASPR2, supporting the possibility of their acquired autoreactivity secondary to somatic hypermutation. Taken together, these findings imply a disease paradigm of peripheral B cell tolerance failure. In health, despite the presence of naïve CASPR2-specific B cells, adaptive immune memory to CASPR2 protein appears to be effectively negated. However, in disease, the presence of CASPR2-specific memory B cells support their positive selection within germinal centres or *de novo* generation from acquired somatic hypermutation. These observations shed light on the pathogenesis of autoantibodies in CASPR2-antibody encephalitis and support the contribution of CD4+ T cells, especially in context of the recently reported HLA-DRB1*11:01 association[131,186].

A key limitation of these findings, is the small number of donors studied. Despite the rarity of this disease, further exploration of these established frameworks across larger numbers of patients and healthy donors will help validate and extend these observations. Additionally, the heuristic segregation of canonical naïve and class-switched memory B cells ignores their plasticity along key developmental trajectories and cell states. Future work should aim to sample B cells in an unbiased manner, to better determine the phenotypes of autoreactive B cells.

6.3 Is autoantibody immunodominance of N-terminal domains reproducible at the single-B cell level?

An intriguing observation from past studies, is the immunodominance of autoantibodies that target the Discoidin domain of CASPR2[86,134,147]. Whilst antibody immunodominance has been described in the context of foreign[235,236] and self-antigens[237–239], its characterisation across B cell developmental checkpoints has not been extensively explored. Using CASPR2 mAbs isolated from naïve and memory B cells, I was able to reveal a few distinct observations. First, naïve B cell-derived mAbs, from patients and healthy donors, did not bind the Discoidin domain, nor have overlapping domain specificities with memory B cells. This observation is difficult to rationalise, but it may imply that in health, negative selection of

immunodominant domain-specific B cells occurs at earlier B cell checkpoints within the bone marrow. The absence of Discoidin-specificity in patient naïve B cells may then reflect their positive selection into the memory compartment, thus depleting their presence in remaining naïve B cell pools. Second, while Discoidin domain immunodominance in memory B cells was observed, those targeting the Laminin G-like 3 domains displayed the highest affinity for CASPR2 protein. This is surprising because Laminin G-like 3 domain specificity has never been described in CASPR2-antibody encephalitis. The clinical relevance of this epitope remains to be determined, but their potential to modulate CASPR2 protein were later validated *in vitro*. Lastly, memory B cell mAbs displayed highly overlapping epitopes across the two patients studied. This supports the notion that CASPR2-specific B cells may publicly converge within a narrow epitope space across distinct domains. If reproducible across larger cohorts, this offers promise for the development of strategies to competitively inhibit CASPR2-specific B cells and their secreted autoantibodies.

A better understanding of the circulating epitope landscape will be essential in determining selection pressures of autoreactive B cells. Existing studies rely on serial CASPR2 domain deletion constructs to characterise autoantibody specificities from

sera; this method is fraught with experimental variability and relies on negative inference rather than positive detection of domain specificities. Negative inference of epitopes in the context of polyclonal sera is an unreliable proxy of specificity and is incapable of quantitative assessment of domain-specific titres. To address this, I co-conceived and am involved in a follow-on study that aims to utilise constructs displaying single CASPR2 domains, presented conformationally within CASPR4, to characterise the serological landscape of CASPR2 autoantibodies in a large cohort of CASPR2 patients. The use of these novel constructs will also facilitate the large-scale characterisation of future B cell derived CASPR2 mAbs.

6.4 How do CASPR2-specific mAbs functionally modulate CASPR2 protein?

The precise mechanisms by which CASPR2 autoantibodies cause neuronal dysfunction, remain unclear. In one study, patient sera inhibited CASPR2 interaction with CNTN2 but did not result in significant CASPR2 internalisation[87]. In contrast, two other studies observed robust CASPR2 internalisation *in vitro*[89,135], albeit with variable effects of CASPR2 surface expression. Additionally, a third study[88] shows an increase in CASPR2 cluster intensity following treatment with purified patient IgG. A key limitation in all these studies is the use of polyclonal

patient sera and the assumption of consensus effector mechanisms. Further, the influence of domain specificity on autoantibody modulation of CASPR2 has yet to be explored.

By leveraging the pH sensitive probe pHrodo™, I was able to directly visualise the internalisation of CASPR2 mAbs and their colocalisation with CASPR2 protein. In HEK293T cell-based assays, all mAbs were capable of dynamin-dependent internalisation and the degree of internalisation directly correlated with mAb affinities. Additionally, I was able to identify that CASPR2 mAbs were capable of monovalent internalisation of CASPR2 that is also independent of Fc-Fc interactions; therefore, their functional modulation of CASPR2 is irrespective of IgG4 F(ab)-arm exchange. Disappointingly, I could not replicate the proposed interaction between CASPR2 and CNTN2 extracellular domains and thus, cannot confirm whether CASPR2 mAbs were capable of blocking their association. In contrast to HEK293T cell-based assays, CASPR2 mAbs displayed heterogenous internalisation capacity in neurons; this was validated independently by collaborators. Data from said collaborators, reveal that a neuronal CASPR2 internalising mAb induced quantifiable reduction of CASPR2 and AMPAR puncta intensities, whereas a mAb that was incapable of internalising neuronal CASPR2

upregulated CASPR2 and AMPAR puncta intensities. Interestingly, both mAbs were capable of impairing synaptic AMPAR signalling. This was an unexpected end-point of mAb-mediated increases of CASPR2 and AMPAR, and suggests that mAb induced accumulation of synaptic AMPARs are non-functional.

To elucidate the paradoxical behaviours of CASPR2 mAbs in HEK293T and neuronal based assays, a better fundamental understanding of CASPR2 protein's role in neuronal homeostasis is required. Key to this, is the comprehensive investigation and validation of new and currently proposed CASPR2 ligands. Despite reports that the extracellular domains of CASPR2 and CNTN2 interact with nanomolar affinities[87,141], the structural characterisation of this proposed complex has yet to be presented. Indeed, contrasting bodies of work shed further doubt on the validity of their extracellular interaction[136,140,153]. Consistent with this, in my hands, recombinant extracellular domains of CASPR2 and CNTN2 did not interact. Frustratingly, the novel CASPR2 ligand proposed by a contrasting study[140], CNTN1, also did not interact. It is clear that the clarification of neuronally-native CASPR2 ligands is likely to be fundamental in understanding why certain mAbs induce contrasting effects on CASPR2 expression. Future studies should ideally aim to collaboratively examine data from contrasting groups and would benefit from a

systems approach. The use of bulk or single-cell RNA-seq approaches to characterise differentially expressed genes in CASPR2 knockout or knockdown models, would permit the analysis of gene regulatory pathways and potentially identify specific ligands[240,241].

6.7 Final thoughts

The escape of autoreactive B cells from immune tolerance checkpoints, in autoantibody-mediated diseases, represents a key developmental stage for potential therapeutic intervention. With further improvements of throughput in single B cell mAb characterisation methods, their expanded use in autoantibody-mediated diseases will likely provide valuable biological insights into B cell selection, across multiple diseases and health. Further, the emergence of single cell multi-omic approaches is likely to shift biologists away from hypothesis driven experiments to more exploratory analysis. If used correctly, this can be an incredibly powerful tool for immunobiological understanding and therapeutic target discovery that is not restricted or blinded by experimental priors. Future work in NSAb-mediated autoimmune encephalitis is likely to also focus on how peripheral autoreactive B cells cross the blood brain barrier, and aim to further refine our understanding of the molecular mechanisms by which autoantibodies disrupt neuronal homeostasis. The

importance of these strands of research cannot be understated, and their insights may offer immediate transferability to other aspects of neuroscience, such as delivery of therapeutics to the CNS, insight into immune mechanisms of psychiatric or neurodegenerative disorders and mechanisms of epileptogenesis.

Appendix

Supplementary table 1. Patient and healthy donor characteristics

HD=healthy donor; LE=limbic encephalitis; AF=atrial fibrillation; PLEX=plasma exchange; MMF = mycophenolate; T2DM=type 2 diabetes mellitus; IVIg=intravenous immunoglobulins.

ID	CASPR2 serostatus (IgG)	CASPR2 serostatus (IgM)	Sex	Age	HLADRB1*11:01	Disease duration (years)	Clinical syndrome	Immunotherapy	Treatment at time of collection	Comorbidities	Total wells NBC (bulk)	Total wells MBC (bulk)	Total wells NBC (single-cell)	Total wells MBC (single-cell)
JR002	Positive	Negative	M	63	Yes	2	LE, seizures	None	Nil	Nil	9	11	2112	2208
JR006	Positive	Negative	M	69	No	1	Cognitive, neuromyotonia	None	Nil	BPH, HTN, AF	10	6	N/A	N/A
JR024	Positive	Negative	M	75	Yes	1	LE, seizures	Corticosteroids	Corticosteroid	BPH, Gout, HTN	2	1	N/A	N/A
JR060	Positive	Negative	M	75	Yes	7	LE, seizures, pain	Corticosteroids, PLEX, MMF	Nil	BPH, T2DM	6	5	2400	1598
JR061	Positive	Negative	M	71	Yes	0.75	LE, seizures	Corticosteroids, IVIg	Corticosteroid	T2DM	3	2	N/A	N/A
JR068	Positive	Negative	M	81	No	7	LE, seizures, dysautonomia	Corticosteroids, methotrexate	Methotrexate	BPH, HTN, AF	4	1	N/A	N/A
HD1	Negative	Negative	N/A	N/A	N/A	N/A	N/A	N/A	N/A	N/A	23	4	N/A	N/A
HD2	Negative	Negative	N/A	N/A	N/A	N/A	N/A	N/A	N/A	N/A	46	3	N/A	N/A
HD3	Negative	Negative	N/A	N/A	N/A	N/A	N/A	N/A	N/A	N/A	30	3	N/A	N/A
HD4	Negative	Negative	M	46	N/A	N/A	N/A	N/A	N/A	Nil	N/A	N/A	960	960
HD5	Negative	Negative	F	33	N/A	N/A	N/A	N/A	N/A	Nil	N/A	N/A	960	960

Supplementary table 2 – PCR-1: Leader primers

Name	Chain	Primer Sequences (5' to 3')
CHG1	IgG H	GTTGTCCACCTTGGTGTTGCTGG
VHL1	IgG,M H	CCATGGACTGGACCTGGAG
VHL1 mod	IgG M H	CCATGGACTGSACCTGGAG
VHL2	IgG,M H	ATGGACATACTTTGCTCCAC
VHL2 mod	IgG M H	ATGGACATACTTTGYTCCAC
VHL3	IgG,M H	CCATGGAGTTKGGGCTGAGCTGG
VHL4	IgG,M H	ATGAAACACCTGTGGTTCTT
VHL4 mod	IgG M H	ATGAAACAYCTGTGGTTCTT
VHL5	IgG,M H	ATGGGGTCAACCGCCATCCT
CHm1	IgG M	GAAGCCAGCACCTGTGAGG
CK1	Kappa	ACACTCTCCCCTGTTGAAGCTCTT
VKL1	Kappa	CTCAGCTCCTGGGGCTCC
VKL1 mod	Kappa	CTCAGCTCCTGGGGCTYC
VKL2	Kappa	CTGCTCAGCTCCTGGGGC
VKL2 mod	Kappa	CTGCTCAGCTCYTGGGGC
VKL3	Kappa	GGAARCCCCAGCDCAGC
VKL4	Kappa	CTCTGTTGCTCTGGATCTCTG
VKL5	Kappa	GGGGTCCCAGGTTCACCTCCTC
CL1	Lambda	TGAACATTCTGTAGGGGCCAC
VLL1	Lambda	CCTCTCCTCCTCACCCTCCTC
VLL1 mod	Lambda	CCTCTCCTCCTSACCCTCCTC
VLL2	Lambda	CTCCTCACTCAGGGCACAG
VLL2 mod	Lambda	CTCCTCACTCAGGRCACAG
VLL3	Lambda	ATGGCCTGGAYCCCTCTCCTSCT
VLL3 mod	Lambda	ATGGCCTGGAYCCCTCTCCTBCT
VLL4a	Lambda	CTCCTCCTCTTCCCCCTCCCCCTC
VLL4a mod	Lambda	CTCCTCCTCCACTGCACAG
VLL4b	Lambda	TGGCCTGGGTCTCCTTCTACCTAC
VLL569	Lambda	ATGGCCTGGRCTCCTCTCCTYCTC
VLL710	Lambda	ATGGCCTGGRCTCCTCTCCTYCTG
VLL8	Lambda	ATGGCCTGGATGATGCTTCTCCTC

Supplementary table 3 – PCR2

Name	Chain	Primer Sequences (5' to 3')
CPEC VH1/5/7	Heavy	CTTTTTCTAGTAGCAACTGCAACCGGTGTACATTC CGAGGTGCAGCTGGTGCAG
CPEC VH2	Heavy	CTTTTTCTAGTAGCAACTGCAACCGGTGTACATTC CCAGGTCACCTTGAAGGAG
CPEC VH3	Heavy	CTTTTTCTAGTAGCAACTGCAACCGGTGTACATTC TGAGGTGCAGCTGGTGGAG
CPEC VH4	Heavy	CTTTTTCTAGTAGCAACTGCAACCGGTGTACATTC CCAGGTGCAGCTGCAGGAG
CPEC VH3-23	Heavy	CTTTTTCTAGTAGCAACTGCAACCGGTGTACATTC TGAGGTGCAGCTGTTGGAG
CPEC VH4-34	Heavy	CTTTTTCTAGTAGCAACTGCAACCGGTGTACATTC CCAGGTGCAGCTACAGCAGTG
CPEC VH1–18/69 (silent mut)	Heavy	CTTTTTCTAGTAGCAACTGCAACCGGTGTACATTC CCAGGTTCAGCTGGTGCAG
CPEC VH1-45/1-58	Heavy	CTTTTTCTAGTAGCAACTGCAACCGGTGTACATTC CCAGATGCAGCTGGTGCAG
CPEC VH1–24	Heavy	CTTTTTCTAGTAGCAACTGCAACCGGTGTACATTC CCAGGTCCAGCTGGTACAG
CPEC VH3–9/30/33	Heavy	CTTTTTCTAGTAGCAACTGCAACCGGTGTACATTC TGAAGTGCAGCTGGTGGAG
CPEC VH6–1	Heavy	CTTTTTCTAGTAGCAACTGCAACCGGTGTACATTC CCAGGTACAGCTGCAGCAG
CPEC VH4–39	Heavy	CTTTTTCTAGTAGCAACTGCAACCGGTGTACATTC CCAGCTGCAGCTGCAGGAG
CPEC VH3–33/11/30	Heavy	CTTTTTCTAGTAGCAACTGCAACCGGTGTACATTC TCAGGTGCAGCTGGTGGAG
CPEC JH1/2/4/5	Heavy	GATGGGCCCTTGGTCGACGCTGAGGAGACGGTGA CCAG
CPEC JH3	Heavy	GATGGGCCCTTGGTCGACGCTGAAGAGACGGTGAC CATTG
CPEC JH6	Heavy	GATGGGCCCTTGGTCGACGCTGAGGAGACGGTGA CCGTG
CPEC VK1	Kappa	CTTTTTCTAGTAGCAACTGCAACCGGTGTACATTC TGACATCCAGATGACCCAGTC
CPEC VK1-9/1-13	Kappa	CTTTTTCTAGTAGCAACTGCAACCGGTGTACATTC AGACATCCAGTTGACCCAGTCT
CPEC VK1D-43/1-8	Kappa	CTTTTTCTAGTAGCAACTGCAACCGGTGTACATTG TGCCATCCGGATGACCCAGTC
CPEC VK2	Kappa	CTTTTTCTAGTAGCAACTGCAACCGGTGTACATGG GGATATTGTGATGACCCAGAC
CPEC VK2-28/2-30	Kappa	CTTTTTCTAGTAGCAACTGCAACCGGTGTACATGG GGATATTGTGATGACTCAGTC
CPEC VK3-11/3D-11	Kappa	CTTTTTCTAGTAGCAACTGCAACCGGTGTACATTC AGAAATTGTGTTGACACAGTC

CPEC VK3-15/3D-15	Kappa	CTTTTTCTAGTAGCAACTGCAACCGGTGTACATTC AGAAATAGTGATGACGCAGTC
CPEC VK3-20/3D-20	Kappa	CTTTTTCTAGTAGCAACTGCAACCGGTGTACATTC AGAAATTGTGTTGACGCAGTCT
CPEC VK4-1	Kappa	CTTTTTCTAGTAGCAACTGCAACCGGTGTACATTC GGACATCGTGATGACCCAGTC
CPEC JK1/2/4	Kappa	ATGGTGCAGCCACCGTACGTTTGATYTCCACCTTG GTC
CPEC JK2	Kappa	ATGGTGCAGCCACCGTACGTTTGATCTCCAGCTTG GTC
CPEC JK3	Kappa	ATGGTGCAGCCACCGTACGTTTGATATCCACTTTG GTC
CPEC JK5	Kappa	ATGGTGCAGCCACCGTACGTTTAATCTCCAGTCGT GTC
CPEC JK150/3	Kappa	ATGGTGCAGCCACCGTACGTCTGATTTCCACCTTG GTC
CPEC VL1	Lambda	CTTTTTCTAGTAGCAACTGCAACCGGTTCCTGGGC CCAGTCTGTGCTGACKCAG
CPEC VL2	Lambda	CTTTTTCTAGTAGCAACTGCAACCGGTTCCTGGGC CCAGTCTGCCCTGACTCAG
CPEC VL3	Lambda	CTTTTTCTAGTAGCAACTGCAACCGGTTCTGTGAC CTCCTATGAGCTGACWCAG
CPEC VL4/5	Lambda	CTTTTTCTAGTAGCAACTGCAACCGGTTCTCTCTCS CAGCYTGTGCTGACTCA
CPEC VL6	Lambda	CTTTTTCTAGTAGCAACTGCAACCGGTTCTTGGGC CAATTTTATGCTGACTCAG
CPEC VL7/8	Lambda	CTTTTTCTAGTAGCAACTGCAACCGGTTCCAATTC YCAGRCTGTGGTGACYCAG
CPEC CL reverse	Lambda	GGCTTGAAGCTCCTCACTCGAGGGYGGGAACAGAG TG
3'CL Reverse	Lambda	CACCAGTGTGGCCTTGTTGGCTTG
panVK Forw.	Kappa	ATGACCCAGWCTCCABYCWCCCTG
3'CK494-516 R.	Kappa	GTGCTGTCCTTGCTGTCCTGCT
3' CgCH Reverse Tiller	Heavy	GGAAGGTGTGCACGCCGCTGGTC

References

1. Woof, J. M. & Burton, D. R. Human antibody-Fc receptor interactions illuminated by crystal structures. *Nat. Rev. Immunol.* **4**, 89–99 (2004).
2. Tonegawa, S. Somatic generation of antibody diversity. *Nature* **302**, 575–581 (1983).
3. Schatz, D. G. & Ji, Y. Recombination centres and the orchestration of V(D)J recombination. *Nat. Rev. Immunol.* **11**, 251–263 (2011).
4. Alt, F. W. *et al.* Synthesis of secreted and membrane-bound immunoglobulin mu heavy chains is directed by mRNAs that differ at their 3' ends. *Cell* **20**, 293–301 (1980).
5. Kwak, K., Akkaya, M. & Pierce, S. K. B cell signaling in context. *Nat. Immunol.* **20**, 963–969 (2019).
6. Vidarsson, G., Dekkers, G. & Rispens, T. IgG Subclasses and Allotypes: From Structure to Effector Functions. *Front. Immunol.* **5**, 520 (2014).
7. Mankarious, S. *et al.* The half-lives of IgG subclasses and specific antibodies in patients with primary immunodeficiency who are receiving intravenously administered immunoglobulin. *J. Lab. Clin. Med.* **112**, 634–640 (1988).
8. Lobo, E. D., Hansen, R. J. & Balthasar, J. P. Antibody pharmacokinetics and pharmacodynamics. *J. Pharm. Sci.* **93**, 2645–2668 (2004).
9. Schroeder, H. W. & Cavacini, L. Structure and function of immunoglobulins. *J. Allergy Clin. Immunol.* **125**, S41–S52 (2010).
10. Gong, S. & Ruprecht, R. M. Immunoglobulin M: An Ancient Antiviral Weapon – Rediscovered. *Front. Immunol.* **11**, 1–9 (2020).
11. Paus, D. *et al.* Antigen recognition strength regulates the choice between extrafollicular plasma cell and germinal center B cell differentiation. *J. Exp. Med.* **203**, 1081–1091 (2006).
12. Chan, T. D. *et al.* Antigen Affinity Controls Rapid T-Dependent Antibody Production by Driving the Expansion Rather than the Differentiation or Extrafollicular Migration of Early Plasmablasts. *J. Immunol.* **183**, 3139–3149 (2009).
13. Sacquin, A., Gador, M. & Fazilleau, N. The strength of BCR signaling shapes terminal development of follicular helper T cells in mice. *Eur. J. Immunol.* **47**, 1295–1304 (2017).
14. Geisberger, R., Lamers, M. & Achatz, G. The riddle of the dual expression of IgM and IgD. *Immunology* **118**, 429–437 (2006).
15. Sewell, H. F., Chambers, L., Maxwell, V., Matthews, J. B. & Jefferis, R. The natural antibody response to E. coli includes antibodies of the IgD class. *Clin. Exp. Immunol.* **31**, 104–110 (1978).
16. Forsgren, A. *et al.* Isolation and characterization of a novel IgD-binding protein from Moraxella catarrhalis. *J. Immunol.* **167**, 2112–2120 (2001).
17. Shan, M. *et al.* Secreted IgD Amplifies Humoral T Helper 2 Cell Responses by Binding Basophils via Galectin-9 and CD44. *Immunity* **49**, 709-724.e8 (2018).
18. Ferrante, A., Beard, L. J. & Feldman, R. G. IgG subclass distribution of antibodies to bacterial and viral antigens. *Pediatr. Infect. Dis. J.* **9**, S16-24 (1990).
19. Siber, G. R., Schur, P. H., Aisenberg, A. C., Weitzman, S. A. & Schiffman, G. Correlation between serum IgG-2 concentrations and the antibody response to bacterial polysaccharide antigens. *N. Engl. J. Med.* **303**, 178–182 (1980).
20. Aalberse, R. C., van der Gaag, R. & van Leeuwen, J. Serologic aspects of IgG4 antibodies. I. Prolonged immunization results in an IgG4-restricted response. *J. Immunol.* **130**, 722–726 (1983).

21. Vickery, B. P. *et al.* Peanut oral immunotherapy modifies IgE and IgG4 responses to major peanut allergens. *J. Allergy Clin. Immunol.* **131**, 123–128 (2013).
22. van der Neut Kolfschoten, M. *et al.* Anti-inflammatory activity of human IgG4 antibodies by dynamic Fab arm exchange. *Science* **317**, 1554–1557 (2007).
23. Margni, R. A. & Binaghi, R. A. Nonprecipitating asymmetric antibodies. *Annu. Rev. Immunol.* **6**, 535–554 (1988).
24. van der Zee, J. S., van Swieten, P. & Aalberse, R. C. Serologic aspects of IgG4 antibodies. II. IgG4 antibodies form small, nonprecipitating immune complexes due to functional monovalency. *J. Immunol.* **137**, 3566–71 (1986).
25. Lighaam, L. C. & Rispens, T. The Immunobiology of Immunoglobulin G4. *Semin. Liver Dis.* **36**, 200–215 (2016).
26. Perugino, C. A. & Stone, J. H. Treatment of IgG4-related disease : Current and future approaches. *Z. Rheumatol.* **75**, 681–686 (2016).
27. Binks, S. N. M., Klein, C. J., Waters, P., Pittock, S. J. & Irani, S. R. LGI1, CASPR2 and related antibodies: a molecular evolution of the phenotypes. *J. Neurol. Neurosurg. Psychiatry* **89**, 526–534 (2018).
28. AbdelRazek, M. A., Venna, N. & Stone, J. H. IgG4-related disease of the central and peripheral nervous systems. *Lancet. Neurol.* **17**, 183–192 (2018).
29. Pabst, O. New concepts in the generation and functions of IgA. *Nat. Rev. Immunol.* **12**, 821–832 (2012).
30. Aase, A. *et al.* Salivary IgA from the sublingual compartment as a novel noninvasive proxy for intestinal immune induction. *Mucosal Immunol.* **9**, 884–893 (2016).
31. Kumar Bharathkar, S. *et al.* The structures of secretory and dimeric immunoglobulin A. *Elife* **9**, e56098 (2020).
32. Steffen, U. *et al.* IgA subclasses have different effector functions associated with distinct glycosylation profiles. *Nat. Commun.* **11**, 120 (2020).
33. van Egmond, M. *et al.* IgA and the IgA Fc receptor. *Trends Immunol.* **22**, 205–211 (2001).
34. Hansen, I. S., Baeten, D. L. P. & den Dunnen, J. The inflammatory function of human IgA. *Cell. Mol. Life Sci.* **76**, 1041–1055 (2019).
35. Mantis, N. J., Rol, N. & Corthésy, B. Secretory IgA's complex roles in immunity and mucosal homeostasis in the gut. *Mucosal Immunol.* **4**, 603–611 (2011).
36. Wu, L. C. & Zarrin, A. A. The production and regulation of IgE by the immune system. *Nat. Rev. Immunol.* **14**, 247–259 (2014).
37. Kalinina, O. *et al.* Alternative mechanisms of receptor editing in autoreactive B cells. *Proc. Natl. Acad. Sci.* **108**, 7125–7130 (2011).
38. Vettermann, C. & Schlissel, M. S. Allelic exclusion of immunoglobulin genes: models and mechanisms. *Immunol. Rev.* **237**, 22–42 (2010).
39. ten Boekel, E., Melchers, F. & Rolink, A. G. Precursor B cells showing H chain allelic inclusion display allelic exclusion at the level of pre-B cell receptor surface expression. *Immunity* **8**, 199–207 (1998).
40. Fuentes-Pananá, E. M., Bannish, G., Shah, N. & Monroe, J. G. Basal Igalpha/Igbeta signals trigger the coordinated initiation of pre-B cell antigen receptor-dependent processes. *J. Immunol.* **173**, 1000–1011 (2004).
41. Jung, D. & Alt, F. W. Unraveling V(D)J Recombination: Insights into Gene Regulation. *Cell* **116**, 299–311 (2004).

42. Wardemann, H. *et al.* Predominant autoantibody production by early human B cell precursors. *Science* **301**, 1374–1377 (2003).
43. Mietzner, B. *et al.* Autoreactive IgG memory antibodies in patients with systemic lupus erythematosus arise from nonreactive and polyreactive precursors. *Proc. Natl. Acad. Sci. U. S. A.* **105**, 9727–9732 (2008).
44. Tiller, T. *et al.* Autoreactivity in human IgG+ memory B cells. *Immunity* **26**, 205–213 (2007).
45. Wardemann, H., Hammersen, J. & Nussenzweig, M. C. Human autoantibody silencing by immunoglobulin light chains. *J. Exp. Med.* **200**, 191–199 (2004).
46. Benschop, R. J., Brandl, E., Chan, A. C. & Cambier, J. C. Unique signaling properties of B cell antigen receptor in mature and immature B cells: implications for tolerance and activation. *J. Immunol.* **167**, 4172–4179 (2001).
47. Wing, J. B. & Sakaguchi, S. Foxp3(+) T(reg) cells in humoral immunity. *Int. Immunol.* **26**, 61–69 (2014).
48. Thien, M. *et al.* Excess BAFF rescues self-reactive B cells from peripheral deletion and allows them to enter forbidden follicular and marginal zone niches. *Immunity* **20**, 785–798 (2004).
49. Lesley, R. *et al.* Reduced competitiveness of autoantigen-engaged B cells due to increased dependence on BAFF. *Immunity* **20**, 441–453 (2004).
50. Chan, T. D. *et al.* Elimination of germinal-center-derived self-reactive B cells is governed by the location and concentration of self-antigen. *Immunity* **37**, 893–904 (2012).
51. Sun, B., Ramberger, M., O'Connor, K. C., Bashford-Rogers, R. J. M. & Irani, S. R. The B cell immunobiology that underlies CNS autoantibody-mediated diseases. *Nat. Rev. Neurol.* **16**, 481–492 (2020).
52. Maity, P. C., Datta, M., Nicolò, A. & Jumaa, H. Isotype Specific Assembly of B Cell Antigen Receptors and Synergism With Chemokine Receptor CXCR4. *Front. Immunol.* **9**, 2988 (2018).
53. Elgueta, R. *et al.* Molecular mechanism and function of CD40/CD40L engagement in the immune system. *Immunol. Rev.* **229**, 152–172 (2009).
54. Vos, Q., Lees, A., Wu, Z. Q., Snapper, C. M. & Mond, J. J. B-cell activation by T-cell-independent type 2 antigens as an integral part of the humoral immune response to pathogenic microorganisms. *Immunol. Rev.* **176**, 154–170 (2000).
55. Garside, P. *et al.* Visualization of specific B and T lymphocyte interactions in the lymph node. *Science* **281**, 96–99 (1998).
56. Hargreaves, D. C. *et al.* A coordinated change in chemokine responsiveness guides plasma cell movements. *J. Exp. Med.* **194**, 45–56 (2001).
57. Moyron-Quiroz, J. E., McCausland, M. M., Kageyama, R., Sette, A. & Crotty, S. The smallpox vaccine induces an early neutralizing IgM response. *Vaccine* **28**, 140–147 (2009).
58. Chua, C.-L., Sam, I.-C., Chiam, C.-W. & Chan, Y.-F. The neutralizing role of IgM during early Chikungunya virus infection. *PLoS One* **12**, 1–16 (2017).
59. Odegard, V. H. & Schatz, D. G. Targeting of somatic hypermutation. *Nat. Rev. Immunol.* **6**, 573–583 (2006).
60. Gojobori, T. & Nei, M. Relative contributions of germline gene variation and somatic mutation to immunoglobulin diversity in the mouse. *Mol. Biol. Evol.* **3**, 156–167 (1986).
61. Griffiths, G. M., Berek, C., Kaartinen, M. & Milstein, C. Somatic mutation and the

maturation of immune response to 2-phenyl oxazolone. *Nature* **312**, 271–275 (1984).
62. Victora, G. D. & Nussenzweig, M. C. Germinal centers. *Annu. Rev. Immunol.* **30**, 429–457 (2012).
63. Akkaya, M., Kwak, K. & Pierce, S. K. B cell memory: building two walls of protection against pathogens. *Nat. Rev. Immunol.* **20**, 229–238 (2020).
64. Toyama, H. *et al.* Memory B cells without somatic hypermutation are generated from Bcl6-deficient B cells. *Immunity* **17**, 329–339 (2002).
65. Taylor, J. J., Pape, K. A. & Jenkins, M. K. A germinal center-independent pathway generates unswitched memory B cells early in the primary response. *J. Exp. Med.* **209**, 597–606 (2012).
66. Purtha, W. E., Tedder, T. F., Johnson, S., Bhattacharya, D. & Diamond, M. S. Memory B cells, but not long-lived plasma cells, possess antigen specificities for viral escape mutants. *J. Exp. Med.* **208**, 2599–2606 (2011).
67. Radbruch, A. *et al.* Competence and competition: the challenge of becoming a long-lived plasma cell. *Nat. Rev. Immunol.* **6**, 741–750 (2006).
68. Varley, J., Vincent, A. & Irani, S. R. Clinical and experimental studies of potentially pathogenic brain-directed autoantibodies: current knowledge and future directions. *J. Neurol.* **262**, 1081–1095 (2015).
69. Ramanathan, S., Al-Diwani, A., Waters, P. & Irani, S. R. The autoantibody-mediated encephalitides: from clinical observations to molecular pathogenesis. *J. Neurol.* (2019). doi:10.1007/s00415-019-09590-9
70. Titulaer, M. J. *et al.* Treatment and prognostic factors for long-term outcome in patients with anti-NMDA receptor encephalitis: an observational cohort study. *Lancet. Neurol.* **12**, 157–165 (2013).
71. Thompson, J. *et al.* The importance of early immunotherapy in patients with faciobrachial dystonic seizures. *Brain* **141**, 348–356 (2018).
72. Armangue, T. *et al.* Frequency, symptoms, risk factors, and outcomes of autoimmune encephalitis after herpes simplex encephalitis: a prospective observational study and retrospective analysis. *Lancet. Neurol.* **17**, 760–772 (2018).
73. Hughes, E. G. *et al.* Cellular and synaptic mechanisms of anti-NMDA receptor encephalitis. *J. Neurosci.* **30**, 5866–5875 (2010).
74. Dalmau, J., Lancaster, E., Martinez-Hernandez, E., Rosenfeld, M. R. & Balice-Gordon, R. Clinical experience and laboratory investigations in patients with anti-NMDAR encephalitis. *Lancet Neurol.* **10**, 63–74 (2011).
75. Al-Diwani, A. *et al.* The psychopathology of NMDAR-antibody encephalitis in adults: a systematic review and phenotypic analysis of individual patient data. *The lancet. Psychiatry* **6**, 235–246 (2019).
76. Moscato, E. H. *et al.* Acute mechanisms underlying antibody effects in anti-N-methyl-D-aspartate receptor encephalitis. *Ann. Neurol.* **76**, 108–119 (2014).
77. Planaguma, J. *et al.* Human N-methyl D-aspartate receptor antibodies alter memory and behaviour in mice. *Brain* **138**, 94–109 (2015).
78. Irani, S. R. *et al.* Faciobrachial dystonic seizures precede Lgi1 antibody limbic encephalitis. *Ann. Neurol.* **69**, 892–900 (2011).
79. Lai, M. *et al.* Investigation of LGI1 as the antigen in limbic encephalitis previously attributed to potassium channels: a case series. *Lancet. Neurol.* **9**, 776–785 (2010).

80. Petit-Pedrol, M. *et al.* LGI1 antibodies alter Kv1.1 and AMPA receptors changing synaptic excitability, plasticity and memory. *Brain* **141**, 3144–3159 (2018).
81. Ramberger, M. *et al.* Distinctive binding properties of patient-derived monoclonal LGI1-autoantibodies determine pathogenicity. *Brain* (2020). doi:In Press
82. Ohkawa, T. *et al.* Autoantibodies to epilepsy-related LGI1 in limbic encephalitis neutralize LGI1-ADAM22 interaction and reduce synaptic AMPA receptors. *J. Neurosci.* **33**, 18161–18174 (2013).
83. van Sonderen, A. *et al.* The clinical spectrum of Caspr2 antibody-associated disease. *Neurology* **87**, 521–528 (2016).
84. Lancaster, E. *et al.* Investigations of caspr2, an autoantigen of encephalitis and neuromyotonia. *Ann. Neurol.* **69**, 303–311 (2011).
85. Sunwoo, J.-S. *et al.* Clinical manifestations of patients with CASPR2 antibodies. *J. Neuroimmunol.* **281**, 17–22 (2015).
86. Joubert, B. *et al.* Characterization of a Subtype of Autoimmune Encephalitis With Anti-Contactin-Associated Protein-like 2 Antibodies in the Cerebrospinal Fluid, Prominent Limbic Symptoms, and Seizures. *JAMA Neurol.* **73**, 1115–1124 (2016).
87. Patterson, K. R., Dalmau, J. & Lancaster, E. Mechanisms of Caspr2 antibodies in autoimmune encephalitis and neuromyotonia. *Ann. Neurol.* **83**, 40–51 (2018).
88. Saint-Martin, M. *et al.* Impact of anti-CASPR2 autoantibodies from patients with autoimmune encephalitis on CASPR2/TAG-1 interaction and Kv1 expression. *J. Autoimmun.* **103**, 102284 (2019).
89. Fernandes, D. *et al.* Disrupted AMPA Receptor Function upon Genetic- or Antibody-Mediated Loss of Autism-Associated CASPR2. *Cereb. Cortex* **29**, 4919–4931 (2019).
90. Pettingill, P. *et al.* Antibodies to GABAA receptor alpha1 and gamma2 subunits: clinical and serologic characterization. *Neurology* **84**, 1233–1241 (2015).
91. Spatola, M. *et al.* Investigations in GABAA receptor antibody-associated encephalitis. *Neurology* **88**, 1012–1020 (2017).
92. Petit-Pedrol, M. *et al.* Encephalitis with refractory seizures, status epilepticus, and antibodies to the GABAA receptor: a case series, characterisation of the antigen, and analysis of the effects of antibodies. *Lancet. Neurol.* **13**, 276–286 (2014).
93. Ohkawa, T. *et al.* Identification and characterization of GABA(A) receptor autoantibodies in autoimmune encephalitis. *J. Neurosci.* **34**, 8151–8163 (2014).
94. Kreye, J. *et al.* Encephalitis patient-derived monoclonal GABAA receptor antibodies cause epileptic seizures. *J. Exp. Med.* **218**, (2021).
95. van Coevorden-Hameete, M. H. *et al.* The expanded clinical spectrum of anti-GABABR encephalitis and added value of KCTD16 autoantibodies. *Brain* **142**, 1631–1643 (2019).
96. Dogan Onugoren, M. *et al.* Limbic encephalitis due to GABAB and AMPA receptor antibodies: a case series. *J. Neurol. Neurosurg. Psychiatry* **86**, 965–972 (2015).
97. Nibber, A. *et al.* Pathogenic potential of antibodies to the GABAB receptor. *Epilepsia open* **2**, 355–359 (2017).
98. Waters, P. *et al.* Aquaporin-4 antibodies in neuromyelitis optica and longitudinally extensive transverse myelitis. *Arch. Neurol.* **65**, 913–919 (2008).
99. Collongues, N. *et al.* Neuromyelitis optica in France: a multicenter study of 125 patients. *Neurology* **74**, 736–742 (2010).
100. Pandit, L. *et al.* Demographic and clinical features of neuromyelitis optica: A review. *Mult.*

Scler. **21**, 845–853 (2015).
101. Roemer, S. F. *et al.* Pattern-specific loss of aquaporin-4 immunoreactivity distinguishes neuromyelitis optica from multiple sclerosis. *Brain* **130**, 1194–1205 (2007).
102. Waters, P. *et al.* Serial Anti-Myelin Oligodendrocyte Glycoprotein Antibody Analyses and Outcomes in Children With Demyelinating Syndromes. *JAMA Neurol.* (2019). doi:10.1001/jamaneurol.2019.2940
103. Hoftberger, R. *et al.* Antibodies to MOG and AQP4 in adults with neuromyelitis optica and suspected limited forms of the disease. *Mult. Scler.* **21**, 866–874 (2015).
104. Jarius, S. *et al.* Screening for MOG-IgG and 27 other anti-glial and anti-neuronal autoantibodies in 'pattern II multiple sclerosis' and brain biopsy findings in a MOG-IgG-positive case. *Mult. Scler.* **22**, 1541–1549 (2016).
105. Jarius, S. *et al.* MOG-IgG in NMO and related disorders: a multicenter study of 50 patients. Part 1: Frequency, syndrome specificity, influence of disease activity, long-term course, association with AQP4-IgG, and origin. *J. Neuroinflammation* **13**, 279 (2016).
106. Mader, S. *et al.* Complement activating antibodies to myelin oligodendrocyte glycoprotein in neuromyelitis optica and related disorders. *J. Neuroinflammation* **8**, 184 (2011).
107. Hoftberger, R. *et al.* The pathology of central nervous system inflammatory demyelinating disease accompanying myelin oligodendrocyte glycoprotein autoantibody. *Acta Neuropathol.* **139**, 875–892 (2020).
108. Lehmann-Horn, K. *et al.* Intrathecal B-cell activation in LGI1 antibody encephalitis. *Neurol. Neuroimmunol. neuroinflammation* **7**, (2020).
109. Bien, C. G. *et al.* Immunopathology of autoantibody-associated encephalitides: clues for pathogenesis. *Brain* **135**, 1622–1638 (2012).
110. Irani, S. R. *et al.* N-methyl-D-aspartate antibody encephalitis: temporal progression of clinical and paraclinical observations in a predominantly non-paraneoplastic disorder of both sexes. *Brain* **133**, 1655–1667 (2010).
111. Gresa-Arribas, N. *et al.* Antibody titres at diagnosis and during follow-up of anti-NMDA receptor encephalitis: a retrospective study. *Lancet. Neurol.* **13**, 167–177 (2014).
112. Lancaster, E. *et al.* Antibodies to the GABA(B) receptor in limbic encephalitis with seizures: case series and characterisation of the antigen. *Lancet. Neurol.* **9**, 67–76 (2010).
113. Jarius, S. *et al.* Cerebrospinal fluid antibodies to aquaporin-4 in neuromyelitis optica and related disorders: frequency, origin, and diagnostic relevance. *J. Neuroinflammation* **7**, 52 (2010).
114. Dujmovic, I. *et al.* Temporal dynamics of cerebrospinal fluid anti-aquaporin-4 antibodies in patients with neuromyelitis optica spectrum disorders. *J. Neuroimmunol.* **234**, 124–130 (2011).
115. Sato, D. K. *et al.* Cerebrospinal fluid aquaporin-4 antibody levels in neuromyelitis optica attacks. *Ann. Neurol.* **76**, 305–309 (2014).
116. Majed, M., Fryer, J. P., McKeon, A., Lennon, V. A. & Pittock, S. J. Clinical utility of testing AQP4-IgG in CSF: Guidance for physicians. *Neurol. Neuroimmunol. neuroinflammation* **3**, e231 (2016).
117. St-Amour, I. *et al.* Brain bioavailability of human intravenous immunoglobulin and its transport through the murine blood-brain barrier. *J. Cereb. blood flow Metab. Off. J. Int. Soc. Cereb. Blood Flow Metab.* **33**, 1983–1992 (2013).
118. Cotzomi, E. *et al.* Early B cell tolerance defects in neuromyelitis optica favour anti-AQP4

autoantibody production. *Brain* **142**, 1598–1615 (2019).
119. Kornau, H.-C. *et al.* Human Cerebrospinal Fluid Monoclonal LGI1 Autoantibodies Increase Neuronal Excitability. *Ann. Neurol.* **87**, 405–418 (2020).
120. Sharma, R. *et al.* Monoclonal antibodies from a patient with anti-NMDA receptor encephalitis. *Ann. Clin. Transl. Neurol.* **5**, 935–951 (2018).
121. Winklmeier, S. *et al.* Identification of circulating MOG-specific B cells in patients with MOG antibodies. *Neurol. Neuroimmunol. neuroinflammation* **6**, 625 (2019).
122. Wilson, P. *et al.* Distinct B cell subsets give rise to antigen-specific antibody responses against SARS-CoV-2. *Res. Sq.* (2020). doi:10.21203/rs.3.rs-80476/v1
123. Yurasov, S. *et al.* Defective B cell tolerance checkpoints in systemic lupus erythematosus. *J. Exp. Med.* **201**, 703–711 (2005).
124. Samuels, J., Ng, Y.-S., Coupillaud, C., Paget, D. & Meffre, E. Impaired early B cell tolerance in patients with rheumatoid arthritis. *J. Exp. Med.* **201**, 1659–1667 (2005).
125. Kinnunen, T. *et al.* Specific peripheral B cell tolerance defects in patients with multiple sclerosis. *J. Clin. Invest.* **123**, 2737–2741 (2013).
126. Brioschi, S. *et al.* Heterogeneity of meningeal B cells reveals a lymphopoietic niche at the CNS borders. *Science* **373**, (2021).
127. Wang, Y. *et al.* Early developing B cells undergo negative selection by central nervous system-specific antigens in the meninges. *Immunity* 1–11 (2021). doi:10.1016/j.immuni.2021.09.016
128. Shillito, P. *et al.* Acquired neuromyotonia: Evidence for autoantibodies directed against K+ channels of peripheral nerves. *Ann. Neurol.* **38**, 714–722 (1995).
129. Buckley, C. *et al.* Potassium channel antibodies in two patients with reversible limbic encephalitis. *Ann. Neurol.* **50**, 73–78 (2001).
130. Barber, P. A., Anderson, N. E. & Vincent, A. Morvan's syndrome associated with voltage-gated K+ channel antibodies. *Neurology* **54**, 771–772 (2000).
131. Muñiz-Castrillo, S. *et al.* Anti-CASPR2 clinical phenotypes correlate with HLA and immunological features. *J. Neurol. Neurosurg. Psychiatry* **91**, 1076–1084 (2020).
132. Boyko, M., Au, K. L. K., Casault, C., de Robles, P. & Pfeffer, G. Systematic review of the clinical spectrum of CASPR2 antibody syndrome. *J. Neurol.* **267**, 1137–1146 (2020).
133. Körtvelyessy, P. *et al.* Complement-associated neuronal loss in a patient with CASPR2 antibody-associated encephalitis. *Neurol. Neuroimmunol. NeuroInflammation* **2**, e75 (2015).
134. Olsen, A. L., Lai, Y., Dalmau, J., Scherer, S. S. & Lancaster, E. Caspr2 autoantibodies target multiple epitopes. *Neurol. Neuroimmunol. neuroinflammation* **2**, e127 (2015).
135. Giannoccaro, M. P. *et al.* Behaviour and neuropathology in mice injected with human contactin-associated protein 2 antibodies. *Brain* **142**, 2000–2012 (2019).
136. Poliak, S. *et al.* Caspr2, a new member of the neurexin superfamily, is localized at the juxtaparanodes of myelinated axons and associates with K+ channels. *Neuron* **24**, 1037–1047 (1999).
137. Denisenko-Nehrbass, N. *et al.* Protein 4.1B associates with both Caspr/paranodin and Caspr2 at paranodes and juxtaparanodes of myelinated fibres. *Eur. J. Neurosci.* **17**, 411–416 (2003).
138. Horresh, I., Bar, V., Kissil, J. L. & Peles, E. Organization of myelinated axons by Caspr and Caspr2 requires the cytoskeletal adapter protein 4.1B. *J. Neurosci.* **30**, 2480–2489 (2010).
139. Horresh, I. *et al.* Multiple molecular interactions determine the clustering of Caspr2 and Kv1

channels in myelinated axons. *J. Neurosci.* **28**, 14213–14222 (2008).
140. Rubio-Marrero, E. N. *et al.* Structural Characterization of the Extracellular Domain of CASPR2 and Insights into Its Association with the Novel Ligand Contactin1. *J. Biol. Chem.* **291**, 5788–5802 (2016).
141. Lu, Z. *et al.* Molecular Architecture of Contactin-associated Protein-like 2 (CNTNAP2) and Its Interaction with Contactin 2 (CNTN2). *J. Biol. Chem.* **291**, 24133–24147 (2016).
142. Gordon, A. *et al.* Expression of Cntnap2 (Caspr2) in multiple levels of sensory systems. *Mol. Cell. Neurosci.* **70**, 42–53 (2016).
143. Pinatel, D. *et al.* The Kv1-associated molecules TAG-1 and Caspr2 are selectively targeted to the axon initial segment in hippocampal neurons. *J. Cell Sci.* **130**, 2209–2220 (2017).
144. Inda, M. C., DeFelipe, J. & Muñoz, A. Voltage-gated ion channels in the axon initial segment of human cortical pyramidal cells and their relationship with chandelier cells. *Proc. Natl. Acad. Sci.* **103**, 2920–2925 (2006).
145. Duflocq, A., Chareyre, F., Giovannini, M., Couraud, F. & Davenne, M. Characterization of the axon initial segment (AIS) of motor neurons and identification of a para-AIS and a juxtapara-AIS, organized by protein 4.1B. *BMC Biol.* **9**, 66 (2011).
146. Varea, O. *et al.* Synaptic abnormalities and cytoplasmic glutamate receptor aggregates in contactin associated protein-like 2/Caspr2 knockout neurons. *Proc. Natl. Acad. Sci.* **112**, 6176–6181 (2015).
147. Pinatel, D. *et al.* Inhibitory axons are targeted in hippocampal cell culture by anti-Caspr2 autoantibodies associated with limbic encephalitis. *Front. Cell. Neurosci.* **9**, 265 (2015).
148. Vogt, D. *et al.* Mouse Cntnap2 and Human CNTNAP2 ASD Alleles Cell Autonomously Regulate PV+ Cortical Interneurons. *Cereb. Cortex* **28**, 3868–3879 (2018).
149. Ogawa, Y. *et al.* Postsynaptic density-93 clusters Kv1 channels at axon initial segments independently of Caspr2. *J. Neurosci.* **28**, 5731–5739 (2008).
150. Ogawa, Y. *et al.* ADAM22, A Kv1 Channel-Interacting Protein, Recruits Membrane-Associated Guanylate Kinases to Juxtaparanodes of Myelinated Axons. *J. Neurosci.* **30**, 1038–1048 (2010).
151. Chen, N. *et al.* Interaction proteomics of canonical Caspr2 (CNTNAP2) reveals the presence of two Caspr2 isoforms with overlapping interactomes. *Biochim. Biophys. Acta - Proteins Proteomics* **1854**, 827–833 (2015).
152. Poliak, S. *et al.* Juxtaparanodal clustering of Shaker-like K+ channels in myelinated axons depends on Caspr2 and TAG-1. *J. Cell Biol.* **162**, 1149–1160 (2003).
153. Traka, M. *et al.* Association of TAG-1 with Caspr2 is essential for the molecular organization of juxtaparanodal regions of myelinated fibers. *J. Cell Biol.* **162**, 1161–1172 (2003).
154. Pathak, D., Guan, D. & Foehring, R. C. Roles of specific Kv channel types in repolarization of the action potential in genetically identified subclasses of pyramidal neurons in mouse neocortex. *J. Neurophysiol.* **115**, 2317–2329 (2016).
155. Scott, R. *et al.* Loss of Cntnap2 Causes Axonal Excitability Deficits, Developmental Delay in Cortical Myelination, and Abnormal Stereotyped Motor Behavior. *Cereb. Cortex* **29**, 586–597 (2017).
156. Bakkaloglu, B. *et al.* Molecular cytogenetic analysis and resequencing of contactin associated protein-like 2 in autism spectrum disorders. *Am. J. Hum. Genet.* **82**, 165–173 (2008).
157. Bonetto, G. *et al.* Selective Axonal Expression of the Kv1 Channel Complex in Pre-

myelinated GABAergic Hippocampal Neurons. *Front. Cell. Neurosci.* **13**, 222 (2019).
158. Anderson, G. R. *et al.* Candidate autism gene screen identifies critical role for cell-adhesion molecule CASPR2 in dendritic arborization and spine development. *Proc. Natl. Acad. Sci. U. S. A.* **109**, 18120–18125 (2012).
159. Canali, G. *et al.* Genetic variants in autism-related CNTNAP2 impair axonal growth of cortical neurons. *Hum. Mol. Genet.* **27**, 1941–1954 (2018).
160. Peñagarikano, O. *et al.* Absence of CNTNAP2 leads to epilepsy, neuronal migration abnormalities, and core autism-related deficits. *Cell* **147**, 235–246 (2011).
161. Selimbeyoglu, A. *et al.* Modulation of prefrontal cortex excitation/inhibition balance rescues social behavior in CNTNAP2-deficient mice. *Sci. Transl. Med.* **9**, (2017).
162. Saint-Martin, M. *et al.* Contactin-associated protein-like 2, a protein of the neurexin family involved in several human diseases. *Eur. J. Neurosci.* **48**, 1906–1923 (2018).
163. Meffre, E. & O'Connor, K. C. Impaired B-cell tolerance checkpoints promote the development of autoimmune diseases and pathogenic autoantibodies. *Immunol. Rev.* **292**, 90–101 (2019).
164. Lu, R. M. *et al.* Development of therapeutic antibodies for the treatment of diseases. *J. Biomed. Sci.* **27**, 1–30 (2020).
165. Kreer, C., Gruell, H., Mora, T., Walczak, A. M. & Klein, F. Exploiting B Cell Receptor Analyses to Inform on HIV-1 Vaccination Strategies. *Vaccines* **8**, (2020).
166. Zenzo, G. Di *et al.* Pemphigus autoantibodies generated through somatic mutations target the desmoglein-3 cis-interface. *J. Clin. Invest.* **122**, 3781–3790 (2012).
167. Su, K.-Y., Nojima, T., Kuraoka, M., Moody, M. A. & Kelsoe, G. An in vitro culture system for studying the human B cell repertoire (P1459). *J. Immunol.* **190**, 174.12--174.12 (2013).
168. Nojima, T., Reynolds, A. E., Kitamura, D., Kelsoe, G. & Kuraoka, M. Tracing Self-Reactive B Cells in Normal Mice. *J. Immunol.* **205**, 90–101 (2020).
169. Irani, S. R. *et al.* Antibodies to Kv1 potassium channel-complex proteins leucine-rich, glioma inactivated 1 protein and contactin-associated protein-2 in limbic encephalitis, Morvan's syndrome and acquired neuromyotonia. *Brain* **133**, 2734–2748 (2010).
170. Ahern, D. J. *et al.* A blood atlas of COVID-19 defines hallmarks of disease severity and specificity. *medRxiv* (2021). doi:10.1101/2021.05.11.21256877
171. DeWitt, W. S. *et al.* A Public Database of Memory and Naive B-Cell Receptor Sequences. *PLoS One* **11**, 1–18 (2016).
172. Yaari, G. & Kleinstein, S. H. Practical guidelines for B-cell receptor repertoire sequencing analysis. *Genome Med.* **7**, 121 (2015).
173. Fu, L., Niu, B., Zhu, Z., Wu, S. & Li, W. CD-HIT: accelerated for clustering the next-generation sequencing data. *Bioinformatics* **28**, 3150–3152 (2012).
174. McCarthy, K. R. *et al.* Memory B Cells that Cross-React with Group 1 and Group 2 Influenza A Viruses Are Abundant in Adult Human Repertoires. *Immunity* **48**, 174-184.e9 (2018).
175. Handlogten, M. W. *et al.* Prevention of Fab-arm exchange and antibody reduction via stabilization of the IgG4 hinge region. *MAbs* **12**, 1779974 (2020).
176. Briney, B., Inderbitzin, A., Joyce, C. & Burton, D. R. Commonality despite exceptional diversity in the baseline human antibody repertoire. *Nature* **566**, 393–397 (2019).
177. Wu, Y.-C. B., Kipling, D. & Dunn-Walters, D. K. The relationship between CD27 negative and positive B cell populations in human peripheral blood. *Front. Immunol.* **2**, 81 (2011).

178. Wu, Y.-C. *et al.* High-throughput immunoglobulin repertoire analysis distinguishes between human IgM memory and switched memory B-cell populations. *Blood* **116**, 1070–1078 (2010).
179. Akbar, R. *et al.* A compact vocabulary of paratope-epitope interactions enables predictability of antibody-antigen binding. *Cell Rep.* **34**, 108856 (2021).
180. Meffre, E. The establishment of early B cell tolerance in humans: lessons from primary immunodeficiency diseases. *Ann. N. Y. Acad. Sci.* **1246**, 1–10 (2011).
181. Cornec, D. *et al.* Identification and phenotyping of circulating autoreactive proteinase 3-specific B cells in patients with PR3-ANCA associated vasculitis and healthy controls. *J. Autoimmun.* **84**, 122–131 (2017).
182. Pollmann, R. *et al.* Identification of Autoreactive B Cell Subpopulations in Peripheral Blood of Autoimmune Patients With Pemphigus Vulgaris. *Front. Immunol.* **10**, 1375 (2019).
183. Lu, D. R. *et al.* T Cell-Dependent Affinity Maturation and Innate Immune Pathways Differentially Drive Autoreactive B Cell Responses in Rheumatoid Arthritis. *Arthritis Rheumatol. (Hoboken, N.J.)* **70**, 1732–1744 (2018).
184. Wu, X. *et al.* Single-cell sequencing of immune cells from anticitrullinated peptide antibody positive and negative rheumatoid arthritis. *Nat. Commun.* **12**, 4977 (2021).
185. Cho, A. *et al.* Single-Cell Analysis Suggests that Ongoing Affinity Maturation Drives the Emergence of Pemphigus Vulgaris Autoimmune Disease. *Cell Rep.* **28**, 909-922.e6 (2019).
186. Binks, S. *et al.* Distinct HLA associations of LGI1 and CASPR2-antibody diseases. *Brain* **141**, 2263–2271 (2018).
187. Wangriatisak, K. *et al.* The expansion of activated naive DNA autoreactive B cells and its association with disease activity in systemic lupus erythematosus patients. *Arthritis Res. Ther.* **23**, 179 (2021).
188. Malkiel, S. *et al.* Checkpoints for Autoreactive B Cells in the Peripheral Blood of Lupus Patients Assessed by Flow Cytometry. *Arthritis Rheumatol. (Hoboken, N.J.)* **68**, 2210–2220 (2016).
189. Tipton, C. M. *et al.* Diversity, cellular origin and autoreactivity of antibody-secreting cell population expansions in acute systemic lupus erythematosus. *Nat. Immunol.* **16**, 755–765 (2015).
190. Yaniv, G. *et al.* A volcanic explosion of autoantibodies in systemic lupus erythematosus: a diversity of 180 different antibodies found in SLE patients. *Autoimmun. Rev.* **14**, 75–79 (2015).
191. Harvey, W. T. *et al.* SARS-CoV-2 variants, spike mutations and immune escape. *Nat. Rev. Microbiol.* **19**, 409–424 (2021).
192. Starr, T. N. *et al.* Prospective mapping of viral mutations that escape antibodies used to treat COVID-19. *Science* **371**, 850–854 (2021).
193. Weisblum, Y. *et al.* Escape from neutralizing antibodies by SARS-CoV-2 spike protein variants. *Elife* **9**, (2020).
194. Katoh, K., Misawa, K., Kuma, K. & Miyata, T. MAFFT: a novel method for rapid multiple sequence alignment based on fast Fourier transform. *Nucleic Acids Res.* **30**, 3059–3066 (2002).
195. Fairhead, M. & Howarth, M. Site-specific biotinylation of purified proteins using BirA. *Methods Mol. Biol.* **1266**, 171–184 (2015).
196. Jumper, J. *et al.* Highly accurate protein structure prediction with AlphaFold. *Nature* **596**,

583–589 (2021).
197. Zhang, Y. & Skolnick, J. TM-align: a protein structure alignment algorithm based on the TM-score. *Nucleic Acids Res.* **33**, 2302–2309 (2005).
198. Kufareva, I. & Abagyan, R. Methods of protein structure comparison. *Methods Mol. Biol.* **857**, 231–257 (2012).
199. Liang, W. *et al.* Structural mapping of hot spots within human CASPR2 discoidin domain for autoantibody recognition. *J. Autoimmun.* **96**, 168–177 (2019).
200. Ruiz-García, R., Martínez-Hernández, E., Saiz, A., Dalmau, J. & Graus, F. The Diagnostic Value of Onconeural Antibodies Depends on How They Are Tested. *Front. Immunol.* **11**, 1482 (2020).
201. Höftberger, R. *et al.* An optimized immunohistochemistry technique improves NMO-IgG detection: study comparison with cell-based assays. *PLoS One* **8**, e79083 (2013).
202. van Sonderen, A. *et al.* Anti-LGI1 encephalitis is strongly associated with HLA-DR7 and HLA-DRB4. *Ann. Neurol.* **81**, 193–198 (2017).
203. Machiels, B. *et al.* Antibody Evasion by a Gammaherpesvirus O-Glycan Shield. *PLOS Pathog.* **7**, 1–15 (2011).
204. Lavie, M., Hanoulle, X. & Dubuisson, J. Glycan Shielding and Modulation of Hepatitis C Virus Neutralizing Antibodies. *Front. Immunol.* **9**, 910 (2018).
205. Dawes, J. M. *et al.* Immune or Genetic-Mediated Disruption of CASPR2 Causes Pain Hypersensitivity Due to Enhanced Primary Afferent Excitability. *Neuron* **97**, 806-822.e10 (2018).
206. Wang, S. *et al.* Spatially Adaptive Colocalization Analysis in Dual-Color Fluorescence Microscopy. *IEEE Trans. Image Process.* **28**, 4471–4485 (2019).
207. Raybould, M. I. J. *et al.* Thera-SAbDab: the Therapeutic Structural Antibody Database. *Nucleic Acids Res.* **48**, D383–D388 (2020).
208. Olatunde, A. C., Abell, L. P., Landuyt, A. E. & Hiltbold Schwartz, E. Development of endocytosis, degradative activity, and antigen processing capacity during GM-CSF driven differentiation of murine bone marrow. *PLoS One* **13**, e0196591 (2018).
209. Velmurugan, R., Ramakrishnan, S., Kim, M., Ober, R. J. & Ward, E. S. Phagocytosis of antibody-opsonized tumor cells leads to the formation of a discrete vacuolar compartment in macrophages. *Traffic* **19**, 273–284 (2018).
210. Opaliński, Ł. *et al.* High Affinity Promotes Internalization of Engineered Antibodies Targeting FGFR1. *Int. J. Mol. Sci.* **19**, (2018).
211. Shinoda, H. *et al.* Acid-Tolerant Monomeric GFP from Olindias formosa. *Cell Chem. Biol.* **25**, 330-338.e7 (2018).
212. Casey, J. R., Grinstein, S. & Orlowski, J. Sensors and regulators of intracellular pH. *Nat. Rev. Mol. Cell Biol.* **11**, 50–61 (2010).
213. Delva, E. *et al.* Pemphigus vulgaris IgG-induced desmoglein-3 endocytosis and desmosomal disassembly are mediated by a clathrin- and dynamin-independent mechanism. *J. Biol. Chem.* **283**, 18303–18313 (2008).
214. Ruggiero, F. M., Vilcaes, A. A., Yuki, N. & Daniotti, J. L. Membrane binding, endocytic trafficking and intracellular fate of high-affinity antibodies to gangliosides GD1a and GM1. *Biochim. Biophys. Acta - Biomembr.* **1859**, 80–93 (2017).
215. Bian, J. *et al.* Limited AT1 Receptor Internalization Is a Novel Mechanism Underlying Sustained Vasoconstriction Induced by AT1 Receptor Autoantibody From Preeclampsia. *J.*

Am. Heart Assoc. **8**, (2019).
216. Kumari, S. *et al.* Nicotinic acetylcholine receptor is internalized via a Rac-dependent, dynamin-independent endocytic pathway. *J. Cell Biol.* **181**, 1179–1193 (2008).
217. Vergoossen, D. L. E. *et al.* Functional monovalency amplifies the pathogenicity of anti-MuSK IgG4 in myasthenia gravis. *Proc. Natl. Acad. Sci.* **118**, (2021).
218. Fichtner, M. L. *et al.* Affinity maturation is required for pathogenic monovalent IgG4 autoantibody development in myasthenia gravis. *J. Exp. Med.* **217**, (2020).
219. Silva, J. P., Vetterlein, O., Jose, J., Peters, S. & Kirby, H. The S228P mutation prevents in vivo and in vitro IgG4 Fab-arm exchange as demonstrated using a combination of novel quantitative immunoassays and physiological matrix preparation. *J. Biol. Chem.* **290**, 5462–5469 (2015).
220. da, P., Gabriele Vincelli, D. & Chiarmo Santi Mario Spampinato Santi Mario Spampinato Correlatore Davide Comoletti, C. Characterization of the Caspr2 and NLGN2 ligands: a proteomic and biochemical approach Coordinatore Dottorato Relatore. (2013).
221. Avnir, Y. *et al.* IGHV1-69 polymorphism modulates anti-influenza antibody repertoires, correlates with IGHV utilization shifts and varies by ethnicity. *Sci. Rep.* **6**, (2016).
222. Acharya, P. *et al.* CD4-binding-Site Recognition by VH1-46 Germline-derived HIV-1 Neutralizers. *AIDS Research and Human Retroviruses* **30**, A120-1 (2014).
223. Wec, A. Z. *et al.* Longitudinal dynamics of the human B cell response to the yellow fever 17D vaccine. *Proc. Natl. Acad. Sci.* **117**, 6675–6685 (2020).
224. Rosenfeld, A. M. *et al.* Computational Evaluation of B-Cell Clone Sizes in Bulk Populations. *Front. Immunol.* **9**, 1472 (2018).
225. Barak, M., Zuckerman, N. S., Edelman, H., Unger, R. & Mehr, R. IgTree: creating Immunoglobulin variable region gene lineage trees. *J. Immunol. Methods* **338**, 67–74 (2008).
226. Hoehn, K. B. *et al.* Repertoire-wide phylogenetic models of B cell molecular evolution reveal evolutionary signatures of aging and vaccination. *Proc. Natl. Acad. Sci.* **116**, 22664–22672 (2019).
227. Yaari, G. *et al.* Models of Somatic Hypermutation Targeting and Substitution Based on Synonymous Mutations from High-Throughput Immunoglobulin Sequencing Data. *Front. Immunol.* **4**, 358 (2013).
228. Viant, C. *et al.* Antibody Affinity Shapes the Choice between Memory and Germinal Center B Cell Fates. *Cell* **183**, 1298-1311.e11 (2020).
229. Burnett, D. L. *et al.* Germinal center antibody mutation trajectories are determined by rapid self/foreign discrimination. *Science* **360**, 223–226 (2018).
230. Wellmann, U. *et al.* The evolution of human anti-double-stranded DNA autoantibodies. *Proc. Natl. Acad. Sci.* **102**, 9258–9263 (2005).
231. Meyer, S. *et al.* AIRE-Deficient Patients Harbor Unique High-Affinity Disease-Ameliorating Autoantibodies. *Cell* **166**, 582–595 (2016).
232. Kreye, J. *et al.* Human cerebrospinal fluid monoclonal N-methyl-D-aspartate receptor autoantibodies are sufficient for encephalitis pathogenesis. *Brain* **139**, 2641–2652 (2016).
233. Wenke, N. K. *et al.* N-methyl-D-aspartate receptor dysfunction by unmutated human antibodies against the NR1 subunit. *Ann. Neurol.* **85**, 771–776 (2019).
234. Tsuiji, M. *et al.* A checkpoint for autoreactivity in human IgM+ memory B cell development. *J. Exp. Med.* **203**, 393–400 (2006).
235. Altman, M. O., Angeletti, D. & Yewdell, J. W. Antibody Immunodominance: The Key to

Understanding Influenza Virus Antigenic Drift. *Viral Immunol.* **31**, 142–149 (2018).
236. Dugan, H. L. *et al.* Profiling B cell immunodominance after SARS-CoV-2 infection reveals antibody evolution to non-neutralizing viral targets. *Immunity* **54**, 1290-1303.e7 (2021).
237. Bruner, B. F., Vista, E. S., Wynn, D. M. & James, J. A. Epitope specificity of myeloperoxidase antibodies: Identification of candidate human immunodominant epitopes. *Clin. Exp. Immunol.* **164**, 330–336 (2011).
238. Kao, L., Lam, V., Waldman, M., Glassock, R. J. & Zhu, Q. Identification of the immunodominant epitope region in phospholipase A2 receptor-mediating autoantibody binding in idiopathic membranous nephropathy. *J. Am. Soc. Nephrol.* **26**, 291–301 (2015).
239. Gleichman, A. J., Spruce, L. A., Dalmau, J., Seeholzer, S. H. & Lynch, D. R. Anti-NMDA receptor encephalitis antibody binding is dependent on amino acid identity of a small region within the GluN1 amino terminal domain. *J. Neurosci.* **32**, 11082–11094 (2012).
240. Wisnovsky, S. *et al.* Genome-wide CRISPR screens reveal a specific ligand for the glycan-binding immune checkpoint receptor Siglec-7. *Proc. Natl. Acad. Sci. U. S. A.* **118**, (2021).
241. Chong, Z. S., Ohnishi, S., Yusa, K. & Wright, G. J. Pooled extracellular receptor-ligand interaction screening using CRISPR activation. *Genome Biol.* **19**, 1–16 (2018).